



**Aalto University
School of Chemical
Technology**

**School of Chemical Technology
Degree Programme of Chemical Technology**

Lauri Kirveskari

**DESIGN OF HORIZONTAL PHASE-SEPARATORS USING COMPUTATIONAL
FLUID DYNAMICS**

**Master's thesis for the degree of Master of Science in Technology submitted
for inspection, Espoo, 22 August, 2016.**

Supervisor **Professor Ville Alopaeus**

Instructors **D. Sc. (Tech) Johanna Vaittinen
Lic. Sc. (Tech) Veli-Matti Purola**

Author Lauri Kirveskari

Title of thesis Design of horizontal phase-separators using computational fluid dynamics

Department Chemical Engineering

Professorship Processes and products**Code of professorship** Kem-42

Thesis supervisor Professor Ville Alopaeus

Thesis advisor(s) / Thesis examiner(s) D.Sc. (Tech.) Johanna Vaittinen, Lic.Sc. (Tech.) Veli-Matti Purola

Date 22.08.2016**Number of pages**
94+16**Language** English

Abstract

Horizontal phase separator units are commonly used in the process engineering. The horizontal phase separators are based on the gravity; external force is not used to boost the separation. In the process industry, the separation of multiphase fluids is important to protect the other process equipment (e.g. pumps and compressors). Mixtures between immiscible multiphase fluids are usually found from the turbulent processes, where flow velocities are high. Gravitational separators are used to provide low enough velocities to separate these immiscible liquid-liquid or gas-liquid mixtures.

The design of the gravitational phase separators is usually based on the design engineer's know-how and simple empiric correlations. Computational fluid dynamics (CFD) offer tools to model different geometries and perform more extensive study to the flow phenomena. This gives the opportunity to simulate and evaluate the behaviour of different geometries and vessel orientations.

In the literature part of this thesis the phenomena affecting to the gravitational separation is reviewed. In addition, the most important design parameters are presented. Furthermore, the CFD modelling of separation process is discussed, and a few example cases from the literature are reviewed.

In the experimental part of this thesis two-phase gas-liquid separation is studied by CFD. Effect of several parameters, like the compression term, liquid droplet size, and the effect of turbulence model used were analysed. Additionally, several inlet distributor geometries were studied and analysed. The used model was found out to be sensitive for the studied parameters. Especially droplet size was found out to affect drastically to the results. When effect of different inlet distributors were studied, it was found out that the curved pipe distributors perform better than the impact plates. In addition, a small comparison between the single phase and two-phase model was performed. The similarities in flow patterns indicated that single phase modelling could provide accurate enough data to help compare designs. However, this is problem dependent and requires further studies.

Keywords Two-phase, Separation, Horizontal, CFD, Computational fluid dynamics, liquid-liquid, gas-liquid

Tekijä	Lauri Kirveskari
Työn nimi	Vaakaerotussäiliöiden suunnitteluperusteiden tarkastelu laskennallisen virtausdynamiikan (CFD) avulla
Laitos	Kemian tekniikka
Professuuri	Prosessit ja tuotteet
Professuurikoodi	Kem-42
Työn valvoja	Professori Ville Alopaeus
Työn ohjaaja(t)/Työn tarkastaja(t)	D.Sc. (Tech.) Johanna Vaitinen, TkL Veli-Matti Purola
Päivämäärä	22.08.2016
Sivumäärä	94+16
Kieli	Englanti

Tiivistelmä

Vaakaerotussäiliöitä käytetään laajalti painovoimaiseen faasierotukseen prosessiteollisuudessa. Painovoimaisessa faasierotuksessa faasien erottamiseen ei käytetä ulkoista voimaa, vaan erotus tapahtuu säiliössä painovoiman avulla. Faasierotus on prosessiteollisuudessa erityisen tärkeää, sillä useampaa faasia sisältävät virtaukset saattavat aiheuttaa ongelmia muussa laitteistoissa (esim. pumpput). Monifaasivirtauksia esiintyy erityisesti kovissa nopeuksissa ja turbulenteissa olosuhteissa, jolloin toisiinsa liukenemattomien faasien sekoittuminen mahdollistuu.

Vaakaerotussäiliöiden suunnittelu perustuu usein suunnittelijan kokemukseen ja yksinkertaisiin empiirisiin korrelaatioihin. Laskennallinen virtausdynamiikka (CFD) tarjoaa työkalut mallintaa ja simuloida virtauksia esimerkiksi erilaisten syötönjakajien tai säiliögeometrioiden kanssa. Tämä tarjoaa suunnittelijalle lisää tietoa mahdollisesta virtauskäyttäytymisestä ja ongelmakohdista.

Tämän työn kirjallisuusosassa käsitellään vaakaerotukseen liittyviä ilmiöitä sekä suunnitteluperusteita. Lisäksi esitellään CFD laskennan kaksifaasimallinnusperusteita ja kirjallisuudesta löytyneitä neste-neste erotustapauksia.

Työn soveltavassa osassa esitellään työssä simulointiin käytetty CFD kaksifaasimalli, esitellään tutkittu tapaus ja simuloinnit. Työssä tutkittiin erilaisten malliparametrien (kuten turbulenssimallin ja nesteen pisarakoon) vaikutusta. Havaittiin, että käytetty kaksifaasimalli oli erittäin herkkä ja jo pienet malliasettelun muutokset johtivat suhteellisen isoihin muutoksiin tuloksissa. Lisäksi tutkittiin erilaisten syötönjakajien vaikutusta erotustehokkuuteen. Käyräputkien havaittiin parantavan erotustehokkuutta enemmän kuin törmäyslevyjien. Kuitenkin kaikki testatut syötönjakajat paransivat erotusta. Lisäksi havaittiin yksifaasimallinnuksen ennustavan kaasuvirtauksen käyttäytymistä hyvin. Tulevissa tutkimuksissa onkin tärkeää havainnoida voidaanko ongelmaa mallintaa yksinkertaisemman ja helppokäyttöisemmän yksifaasimallinnuksen kautta ja tuoko monifaasimallinnus tarvittavaa lisäarvoa ongelmanratkaisuun. Mallin valinta on kuitenkin aina ongelmasidonnainen ja vaatii ymmärrystä sekä olemassa olevista työkaluista, että mallinnettavasta ongelmasta.

Avainsanat Vaakaerotus, Kaksifaasi, neste-neste, kaasu-neste, CFD, computational fluid dynamics

Preface

The work for this thesis was performed in the Technology and Product Development department of Neste Jacobs OY between January and June 2016.

I would like to thank my instructors, Johanna Vaittinen, Veli-Matti Purola and Mika Kettunen for their precise feedback and guidance. I want to also thank Tuomo Keskitalo for helping with cluster issues and invaluable help with two-phase modeling. Thanks for the whole NJ CFD team Johanna, Tuomo, Denis and Niina. I would also like to express my gratitude for Professor Ville Alopaeus for supervising and commenting.

Finally, thanks to the friends and family, especially Mai, for listening and providing thoughts and ideas. This was a great opportunity to combine my previous knowledge and tools, and to learn a lot of new things. I thank you all for supporting me in my efforts.

In Porvoo, July 14th, 2016

Lauri Kirveskari

SYMBOLS AND ABBREVIATIONS

Symbols

A	Area, m ²
C_α	Binary coefficient for interface sharpening by Wardle & Weller (2013), -
C_D	Drag coefficient, -
c	Droplet constant by Zhou and Kresta (1997), -
c_p	Specific heat capacity, kJ/kgK
d	Diameter, m
d_{32}	Sauter mean diameter, m
D_h	Hydraulic diameter, m
F	Force, N
F_D	Drag force, N
g	Gravitational constant, 9.81 m/s ²
m	Mass, kg
p	Perimeter, m
Q	Volumetric flow rate, m ³ /s
s	Standard deviation, -
t	Time, s
Δt	Time step, s
u	Velocity, m/s
V	Volume, m ³
\bar{v}	Mean velocity, m/s
Δx	Local cell length, m

Greek symbols

α	Volume fraction, -
η	Separation efficiency, -
θ	Dispersion correlation coefficient, -
μ	Dynamic viscosity, cP
ρ	Density, kg/m ³
σ	Interfacial tension, kg/s ²
τ	Surface stress, N/m ²
φ	Flow flux, m/s

Dimensionless numbers

<i>Cr</i>	Courant number, -
<i>Re</i>	Reynolds number, -
<i>We</i>	Weber number, -

Subscripts

<i>acc</i>	Accumulating
<i>area, avg</i>	Area averaged value
<i>avg</i>	Average
<i>c</i>	Continuous phase
<i>cell, avg</i>	Average cell value from the specific data set
<i>crit</i>	Critical
<i>d</i>	Droplet or dispersed phase
<i>D</i>	Drag
<i>H</i>	Heavy phase
<i>i</i>	Data point i
<i>in</i>	Inlet
<i>magnitude</i>	Vector magnitude
<i>max</i>	Maximum value
<i>min</i>	Minimum value
<i>k</i>	Phase k
<i>L</i>	Light phase
<i>L</i>	Light
<i>out</i>	Outlet
<i>t</i>	Terminal
<i>vol, avg</i>	Volume averaged value
<i>x, y, z</i>	Coordinates x, y, z, respectively

Abbreviations

<i>CFD</i>	Computational fluid dynamics
<i>DSD</i>	Droplet size distribution
<i>DN</i>	<i>Diamètre nominal</i> (Nominal diameter)
<i>DNS</i>	Direct numerical simulation
<i>E – E</i>	Euler-Euler or Eulerian-Eulerian
<i>E – L</i>	Euler-Lagrange or Euler-Lagrangian
<i>GUI</i>	Graphical user interface
<i>ID</i>	Inlet distributor
<i>LES</i>	Large eddy simulations
<i>OD</i>	Outlet distributor
<i>PBM</i>	Population balance method
<i>PISO</i>	Pressure-Implicit with Splitting of Operators
<i>RAM</i>	Random access memory
<i>RANS</i>	Reynolds averaged Navier-Stokes
<i>RNG</i>	Re-normalization group
<i>SIMPLE</i>	Semi-Implicit Method for Pressure-Linked Equations
<i>SST</i>	Shear stress transport
<i>VOF</i>	Volume of fluid

Table of Contents

1 Introduction	1
1.1 Background	1
1.2 Objectives	1
1.3 Scope	2
LITERATURE PART	3
2 Phase separation in horizontal vessels.....	3
2.1 Liquid-liquid separation.....	3
2.1.1 Phase dispersion and separation.....	4
2.1.2 Coalescence.....	5
2.1.3 Turbulence	6
2.1.4 Droplet size distribution	8
2.1.5 Emulsions	10
2.2 The design of liquid-liquid separator.....	11
2.2.1 Terminal settling velocity.....	12
2.2.2 Design droplet size and settling rate	14
2.2.3 Separator geometry.....	15
2.2.4 Coalescing media.....	16
2.3 Other modelling approaches for liquid-liquid separation	17
2.4 Gas-liquid separation.....	19
2.4.1 Mist eliminators	20
2.4.2 Foaming	21
3 Computational fluid dynamics.....	21
3.1 Multiphase models.....	22
3.2 Turbulence models.....	24
4 CFD modeling of liquid-liquid separators	25
4.1 Two-model CFD approaches to model liquid-liquid systems.....	26

4.1.1 Three-phase separator with VOF and Lagrangian approach	26
4.1.2 Collapsing liquid test using Eulerian and VOF approaches	29
4.1.3 Studies of CFD solvers with population balances.....	31
4.2 Industrial scale studies of liquid-liquid separation with CFD.....	33
4.2.1 Study of inclined water-oil separator	33
4.2.2 Study of water level effect on oil-water separation efficiency	35
EXPERIMENTAL PART	38
5 Used software and computers.....	38
5.1 Geometry.....	38
5.2 CFD calculations	38
5.3 Visualization.....	39
5.4 Computers	39
6 Case setup	40
6.1 Simulated vessel geometry.....	41
6.2 Inlet and outlet configurations	43
6.3 Fluid characteristics.....	45
6.4 Two-phase model.....	45
6.5 Transient time step	46
6.6 Boundary conditions	48
6.7 Data averaging procedure	48
6.8 Mesh dependency tests.....	50
7 Evaluation criteria	52
7.1 Surface reports and liquid accumulation.....	52
7.2 Velocity profiles.....	53
7.3 Wall shear stress	55
8 Simulation results	55
8.1 Model testing and optimization process	56

8.1.1 The effect of liquid droplet size.....	57
8.1.2 The effect of compression term	58
8.1.3 The effect of turbulence modeling.....	59
8.1.4 Modeling the liquid level as a wall	60
8.2 Studied inlet and outlet configurations.....	61
8.2.1 NOID (No inlet distributor).....	63
8.2.2 ID1 (Sloped impact plate).....	65
8.2.3 ID2 (Impact plate).....	66
8.2.4 ID3 (Curved pipe type 1)	68
8.2.5 ID4 (Curved pipe type 2)	69
8.2.6 ID5 (Curved pipe type 3)	71
8.2.7 Outlet distributors	72
8.3 Comparison of inlet configurations.....	74
8.3.1 Separation efficiency	74
8.3.2 Gas flow profiles.....	80
8.4 Comparison of outlet configurations	85
8.5 Single phase simulations.....	87
9 Conclusions.....	89
9.1 Results	89
9.2 Error sources and reliability.....	90
10 Further studies.....	92
11 Bibliography.....	90
12 Appendices	94

1 Introduction

1.1 Background

Phase separation is a crucial part of chemical engineering. In the process industry, the separation of multiphase fluids is important to protect the other process equipment (e.g. pumps and compressors). Separation also enhances the performance of downstream equipment, since certain equipment handle multiphase streams poorly. Vessels and containers are used to provide the separation between immiscible liquid-liquid or gas-liquid mixtures. These separators are based on the gravity; external force is not used to boost the separation.

Design of the separation vessels has been mainly based on the simple empirical correlations and designers empirical know-how. The Computational Fluid Dynamics (CFD) can provide more information to design and troubleshoot equipment and designs. It also allows the designer to test the effect of different geometrics with relatively low amount of work. The use of reliable CFD modelling at early stage of design process can help prevent flaws in design, or to analyze the performance of the design in advance.

1.2 Objectives

The objective of this thesis was to study the two-phase modeling of horizontal phase separation using CFD. The main purpose was to study and select a two-phase CFD model for horizontal separation vessel. To achieve this, liquid-liquid and gas-liquid separation principles were studied, and published CFD modeling cases for separation vessels were reviewed. The other objectives of this work were to study the effects of different vessel configurations (e.g. distributors), and to develop and analyze possible evaluation criteria for CFD simulations to measure the successfulness of separation efficiency.

1.3 Scope

In the literature part of this work the main focus is on the liquid-liquid gravitational separation in horizontal vessels. Different phenomena influencing to the separation process are discussed. A design principle of the horizontal liquid-liquid separation vessel is presented. CFD models developed and used to model the liquid-liquid separation are reviewed.

In the experimental part, an Euler-Euler CFD model is utilized to study different configurations for gas-liquid separation in horizontal vessel. Then the different configurations are tested and evaluated. Finally, conclusions of the performance are drawn, and suggestions for further studies are presented.

LITERATURE PART

2 Phase separation in horizontal vessels

This chapter presents the principles of phase separation in horizontal vessels with main focus on the liquid-liquid separation. Additionally, a gas-liquid separation is reviewed. First, the phenomena affecting liquid-liquid separation are introduced. Then the design of the liquid-liquid vessel and the most important parameters influencing to the design are discussed. At the third section, the alternative modelling approaches are reviewed. At the final part of the chapter, the comparison of gas-liquid and liquid-liquid separation is made.

2.1 Liquid-liquid separation

Separation of two dispersed liquid phases is a common unit operation in process industry. However, separation is complex phenomenon and it consists of multiple different interactions between liquid phases. In Figure 1, a schematic view of these interactions is presented. (Kopriva, et al., 2012)

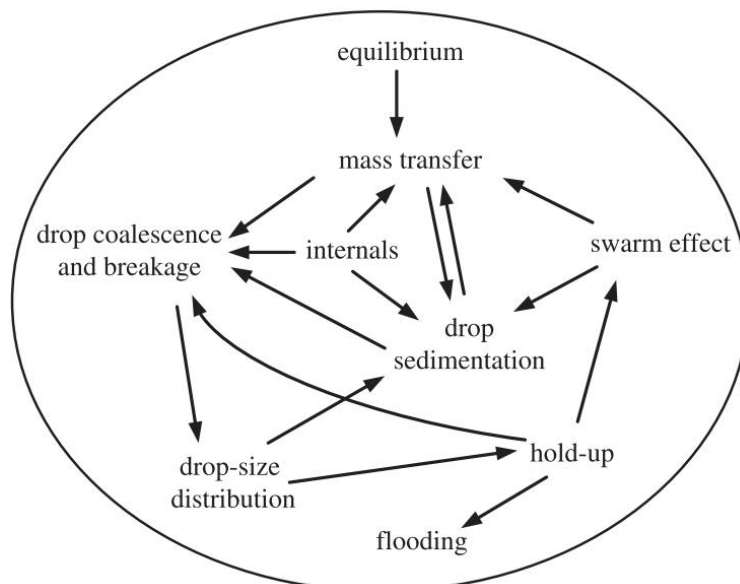


Figure 1. The interactions and phenomena taking place between liquid-liquid systems. (Modified from Kopriva, et al., 2012)

Figure 1 illustrates the complexity of liquid-liquid interactions. There are many different phenomena that can effect towards each other. In this chapter, a few of the most important liquid-liquid interactions in gravitational separation are considered.

2.1.1 Phase dispersion and separation

Dispersions are formed when two or more fluids contact and mix, causing one fluid to disperse into the continuous phase as small droplets. This is a common phenomenon, and dispersions are found especially after processes with high velocities. Actually, in some processes like liquid-liquid extraction the phases are first introduced in a way to improve contact area and facilitate mass transfer. In these kinds of processes the dispersions are unavoidable. However, if the liquid phases are immiscible, or partially immiscible, they will eventually form two separate phases, if left to settle.

These developing liquid-liquid dispersions are characterized by droplets. The common way is to use the terms water-in-oil, oil-in-water or emulsion. For example, a water-in-oil dispersion means that a water phase is dispersed into an oil phase as small droplets. In this case, the oil phase would be considered as a continuous phase, and the water phase as a dispersed phase. In some systems, dispersed and continuous phases are not easily determined. The continuous phase can also be present in the dispersed phase as smaller droplets, or a stable emulsion can be formed. These kinds of systems are called dual emulsions or liquid-membrane systems. (Perry, 1997)

The stability of a dispersion can be described with the droplet diameter; unstable dispersions have a droplet diameter of 1 mm or larger, while stable dispersions generally have droplet diameter of 1 μm or smaller. In the oil industry, the dispersions between different water and oil phases are usually unstable, thus relatively easy to separate. Reported average droplet diameter varies from 100 to 1000 μm . For design purposes the recommended values to use are 140 μm for a two-phase separator and a higher value of 500 μm for flare or vent scrubbers. (Perry, 1997; Laleh, 2010.) The effect of the droplet size when designing a liquid-liquid separator is further discussed in the Section 2.1.4.

Overall, the phase separation is affected by multiple variables and conditions. According to Frising et al. (2006) there are two major mechanisms that are fundamental to the separation process: droplet coalescence and droplet sedimentation. Sedimentation is defined by dispersed droplets falling or rising through the continuous phase due to gravity and buoyancy affecting the droplet. Coalescence is a phenomenon, where two droplets collide with each other, or a droplet collides with the phase interface, to form one uniform phase. Coalescence is further discussed in the next section. (Frising, et al., 2006)

The other relevant factors influencing the separation of dispersed phases are droplet size distribution, dispersed phase concentration, continuous phase viscosity and surface reactions (possible reactants or impurities). (Frising, et al., 2006) Additionally, temperature and pressure have effect on both viscosity and density of the fluids, thus having effect on the separation process. Furthermore, larger density differences and low viscosity of the continuous phase have been observed to boost the settling process. (Perry, 1997)

2.1.2 Coalescence

Generally, smaller dispersed droplets form more stable emulsion. In order to separate smaller dispersed droplets from the mixed phase, the dispersed droplets must grow in size. The phenomenon is known as coalescence. (Frising, et al., 2006) There are different theories for the coalescence process. The so called film drainage model is the most popular, and agreed in many different publications (For example Frising, et al., 2006; Saboni, et al., 2002; Gebauer, et al., 2015). In the film drainage theory, the coalescence takes place in several steps:

1. Approach and collision of two droplets, or a collision between a droplet and its bulk phase (binary and interfacial coalescence).
2. Drainage of the interfacial film.
3. Destabilization of the interfacial film by intermolecular forces (e.g. van der Waals forces)
4. Rupture of the film and combination of two droplets.

Coalescence does not always occur when two droplets collide. Droplets can also rebound from each other. This phenomenon is explained by the required interaction time, for too low interaction time, the drainage of the interaction film will not happen to the rupture point. (Liao & Lucas, 2010) In Figure 2, the film drainage theory of coalescence is schematically presented. Terms $h(r,t)$ and $h_{critical}$ describe the film thickness between droplets. According to the film drainage theory the coalescence can occur only when film thickness reaches a critical point and ruptures. Otherwise, droplets will rebound from each other.

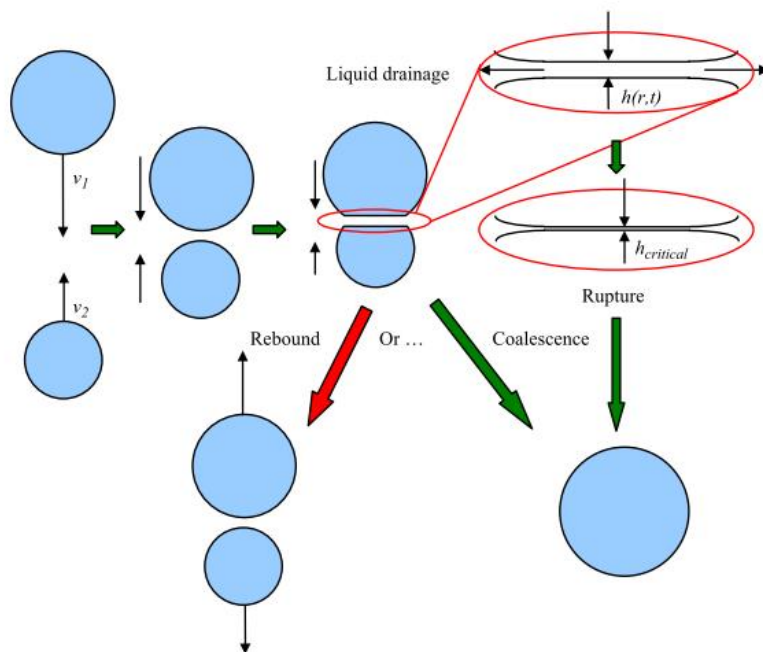


Figure 2. Collision of two droplets either leading to coalescence or to rebound. (Chen, et al., 2005)

Key factors of coalescence are collision frequency between two droplets, time of the collision contact and mobility of the droplet surface. There are several models, both empirical and physical, for coalescence frequency presented by Liao & Lucas (2010).

2.1.3 Turbulence

Turbulence is a chaotic motion of fluid, when fluid moves seemingly randomly forming different sized eddies and swirls. In horizontal separation, turbulence is caused by the

lateral movement of the continuous phase, which is perpendicular to the movement of the settling droplets. Reynolds number (Re) describes the ratio between inertial and viscous forces, thus it can be used to estimate the transition between laminar and turbulent behavior. (Equation 1) (Hooper & Jacobs, 1996)

$$Re = \frac{d\rho u}{\mu} \quad (1)$$

Where

d	characteristic measure of flow (m)
ρ	density of flow (kg/m ³)
u	velocity of flow (m/s)
μ	viscosity of flow (Pas)

Turbulence can cause undesired re-entrainment or emulsification in liquid-liquid separation. Therefore, its effect should be minimized, e.g., by baffle plates, inlet diverters and small design velocities. Hooper & Jacobs (1996) present a method based on the Reynolds number to summarize turbulence behavior in horizontal liquid-liquid separation vessels. They state that a designer should use a hydraulic diameter (D_h) as a characteristic measure to calculate the Reynolds number. The hydraulic diameter can be calculated by using four times the flow area of phase in question divided by the perimeter of flow channel (Equation 2).

$$D_h = \frac{4A_{flow}}{p_{flow}} \quad (2)$$

Where

D_h	hydraulic diameter (m)
p_{flow}	perimeter of flow (m)
A_{flow}	area of flow (m ²)

Now the effect of turbulence can be estimated by using empirical information from successful decanters. Table 1 presents a guideline to give initial estimates of the effect of turbulence to a separation process.

Table 1. Effect of turbulence to separation. (Hooper & Jacobs, 1996)

<i>Reynolds number (Re)</i>	<i>Effect</i>
Less than 5000	Little problem
5000 - 20000	Some hindrance
20000 - 50000	Major problem may exist
Above 50000	Expect poor separation

Table 1 gives information of the successfulness of the gravitational separation at used conditions. It has to be noted, that Table 1 alone does not give enough information to make a final conclusion on the effect of turbulence, but it can be a guideline to start from.

2.1.4 Droplet size distribution

The droplet size and droplet size distribution (DSD) has a huge impact on the liquid-liquid separation, since smaller droplets disperse better and form more stable dispersions as described previously.

The simplest and most common approach is to find a mean droplet size and a maximum stable droplet size and estimate the DSD using mathematical or empirical distribution. There are multiple ways to find mean and maximum droplet sizes. One of the most used is Sauter mean diameter, d_{32} . It is used to describe the average droplet size and can be calculated from observations. There is also a strong correlation between the Sauter mean diameter and the maximum stable droplet diameter (Equation 3). (Zhou & Kresta, 1997)

$$d_{32} = cd_{max} \quad (3)$$

According to Zhou & Kresta (1998) the constant value differs depending on the system at use. They have observed that the value of c seems to increase while the mixing speed of the system is increased. Depending on the system, Zhou & Kresta (1998) have presented values of c between 0.38 and 0.7.

One other possible approach is to find a critical Weber number (We), which presents the ratio of forces that are caused towards the droplets surface. The Weber number is considered to be a presentation between the forces that are either resisting (surface tension) or breaking (stress at the surface) the droplet. At a critical value of Weber the breakup of a droplet occurs (Zhou & Kresta, 1997).

$$We_{crit} = \frac{\rho \bar{v}^2 d_{max}}{\sigma} \quad (4)$$

σ interfacial (surface) tension, kg/s²
 \bar{v} mean velocity, m/s
 d_{max} maximum stable droplet diameter, m

The model has been further developed by assuming that maximum stable droplet can be determined by the balance between internal and capillary pressure of the droplet (Laleh, 2010).

$$We'_{crit} = \frac{\rho \bar{v}^2 d_{max}}{\sigma} \left(\frac{\rho_d}{\rho_c} \right)^{1/3} \quad (5)$$

According to Laleh (2010) We'_{crit} should be about 1 for both liquid-liquid and liquid-vapor dispersions.

The more complex modelling is required, if evolution of the DSD is wanted to take into account. There are eventually two mechanisms for droplet size distribution to evolve: breakup and coalescence. Droplet breakup can be caused by various effects, for example collision of droplets with vessel internals or turbulent eddies and forces within the continuous phase. Coalescence is considered harder to model, since the phenomenon involves the hydrodynamics of the continuous phase and the interactions between droplets and a coalescing interface (bulk phase). (Oshinowo, et al., 2016; Kopriva, et al., 2012)

The population balance method (PBM) presents an opportunity to model the DSD even more accurately. Kopriva, *et al.* (2012) describes the population-balance equation as a powerful tool to model population behavior (i.e., DSD and evolution of DSD). The

population-balance equation is rather complex, as it characterizes droplets within a certain volume, and regards the density of droplets of volume. The Population-balance method takes all the changes in the DSD into account, meaning two separate terms for coalescence and breakage, and additionally terms for entering and leaving droplets. The schematic view of modelling the DSD with PBM can be seen from the Figure 3.

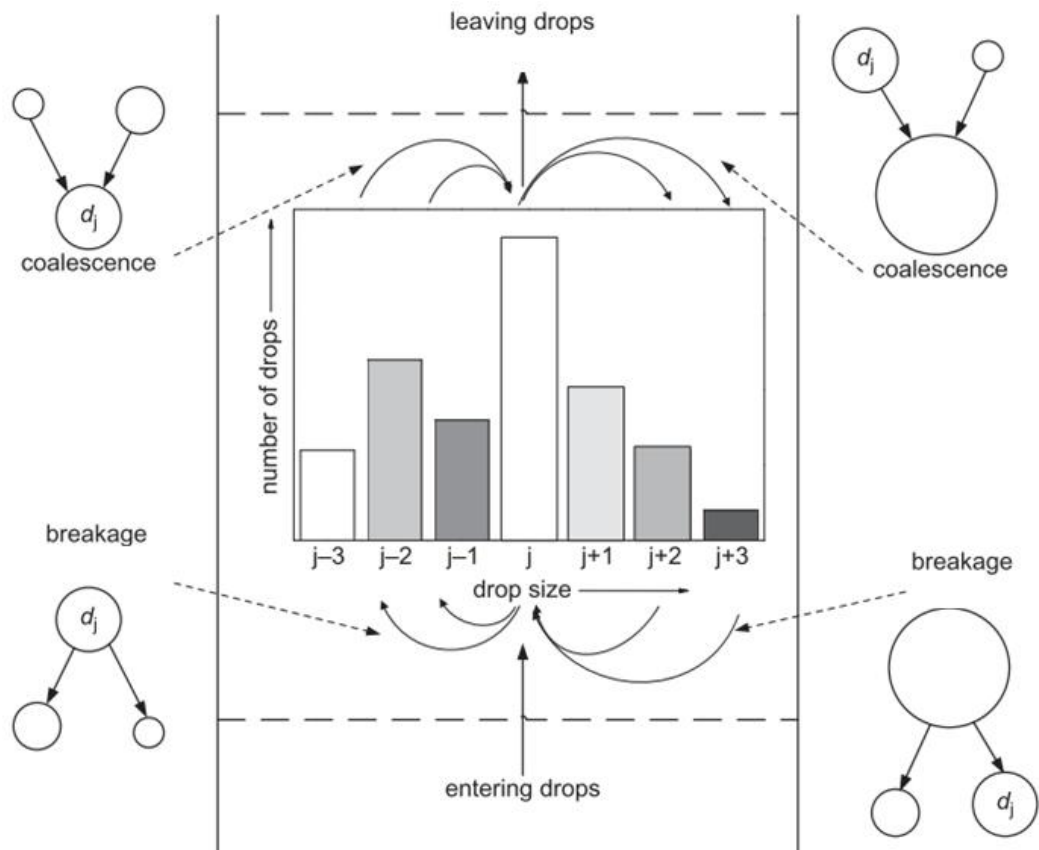


Figure 3. Different terms to model DSD with Population-Balances. (Kopriva, et al., 2012)

2.1.5 Emulsions

An emulsion can appear between two immiscible phases, and cause disturbances in the separation. Formation of emulsion requires sufficient agitation (e.g. turbulence caused by pressure drop), and an emulsifying agent (or stabilizer) for dispersed phase to emulsify into the continuous phase. There are multiple possible reactants or impurities that can act as an emulsifying agent. Without a stabilizer, e.g., in case of a pure oil-water mixture, no stable

emulsion will form. However, this is rarely the case in common process industry. (Stewart & Arnold, 2009)

There are multiple factors that have an effect on emulsion. The main factors are density of the phases, viscosity, size of dispersed droplets and interfacial tension forces. Additionally, the agitation and concentration of the emulsifying agents also have an effect on emulsion. Emulsions also become more stable the longer they age. Usually, emulsions have been reported between systems that have a low density difference and high viscosity. Furthermore, the smaller the dispersed droplet is, the more stable the emulsion or dispersion as explained before. (Stewart & Arnold, 2009)

Between two immiscible liquids, the mechanism for emulsifying is the emulsifying agent to affect towards the dispersed phase droplets to form a film with high surface tension. This prevents coalescence between droplets. (Stewart & Arnold, 2009)

Emulsion can be broken by either thermally or chemically. The thermal emulsion breakage is based on the deactivation of the emulsifying agent. This is done simply by rising the temperature. Chemical demulsifiers act to neutralize the effect of emulsifying agent. However, excessive use can cause problems, because it can decrease the surface tension of water and actually form even more stable emulsions. Additionally, demulsifiers for water-in-oil emulsions can promote oil-to-water emulsions, which can cause problems for water treating. (Stewart & Arnold, 2009)

2.2 The design of liquid-liquid separator

Liquid-liquid separator is used to separate immiscible or partially immiscible liquid phases from each other. Typical example would be oil-water separation. The simplest of liquid-liquid separators is the horizontal decanter without any internals or inlet diverting (See Figure 4). However, usually the separation is boosted by using vortex breakers, internal plates, dams, inlet diverters and/or coalescing media. (Towler & Sinnott, 2013; Perry, 1997)

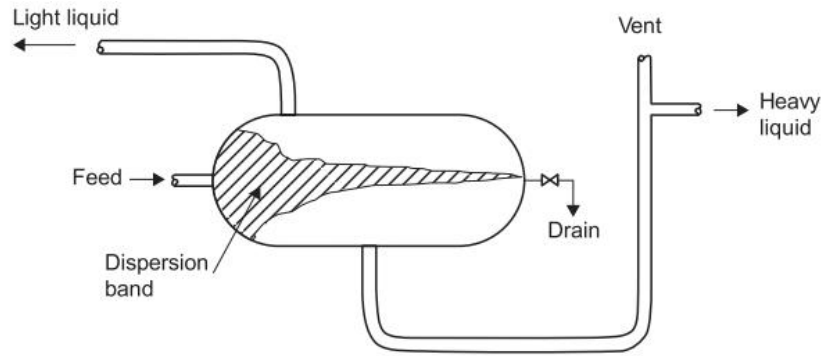


Figure 4. Simple design for horizontal decanter. (Towler & Sinnott, 2013)

As can be seen from Figure 4, the continuous feed usually causes dispersion band that settles along the separator. Heavy liquid is usually drawn from the bottom of the vessel and lighter from the top. There are multiple different configurations available and shown for example in Perry (1997), Towler & Sinnott (2013) and Laleh (2010).

In the following part of this Chapter, a common design process of the liquid-liquid separator is presented. The following design principle follows mainly theories and information from Perry (1997) and Hooper & Jacobs (1996).

2.2.1 Terminal settling velocity

When designing a separation vessel, one of the most used parameters is the terminal settling velocity. When a droplet moves in fluid and there is a relative motion between these phases, the fluid will exert a drag force to the droplet. Additionally, when a droplet is falling under gravitational field, the drag force will eventually balance the gravitational force. This constant velocity is called terminal settling velocity, and is described in Equation 6. (Perry, 1997)

$$u_t = \sqrt{\frac{2gm_d(\rho_d - \rho)}{\rho \rho_d A C_D}} \quad (6)$$

Where

- u_t terminal velocity (m/s)
- g gravitational acceleration (m/s²)

m_d	mass of the droplet (kg)
C_D	drag coefficient (-)
ρ_d, ρ	densities of the droplet and surrounding phase, respectively (kg/m ³)
A	projected droplet area in direction of motion (m ²)

For spherical particles Equation 6 becomes:

$$u_t = \sqrt{\frac{4gd_p(\rho_p - \rho)}{3\rho C_D}} \quad (7)$$

Where

d_p droplet diameter (m)

Drag coefficient for spherical particle is a function of the droplet Reynolds number. There are several empirical correlations for the drag coefficient. In Table 2 a few different correlations are presented.

Table 2. Several drag coefficient models.

Author	Correlation	Validity range
Stokes (Wegener, et al., 2014)	$C_D = \frac{24}{Re}$	$Re \ll 1$
Schiller and Naumann (Wegener, et al., 2014)	$C_D = \frac{24}{Re}(1 + 0.15Re^{0.687})$	$Re < 800$
Gas Processors Suppliers' Association (GPSA) approach (Laleh, 2010)	$C_D = \frac{5.0074}{\ln(x)} + \frac{40.927}{\sqrt{x}} + \frac{44.07}{x}$ $x = \frac{3.35 \cdot 10^{-9} \rho_c (\rho_d - \rho_c) d_p^3}{\mu_c^2}$	<i>Not given</i>
Clift and Gauvin (Wegener, et al., 2014)	$C_D = \frac{24}{Re}(1 + 0.15Re^{0.687})$ $+ \frac{0.42}{1 + 4.25 \cdot 10^4 Re^{-1.16}}$	$Re < 3 \cdot 10^5$

In Table 2, all the presented drag coefficient correlations are for rigid spheres. For more correlations see (Wegener, et al., 2014). When designing a gravitational separator, the most commonly used correlation is Stokes' law with laminar flow (From Table 2). When

combining Stokes' with Equations 6 and 7, the basic equation for calculating settling velocity can be calculated (Equation 8).

$$u_t = \frac{gd_p^2(\rho_p - \rho)}{18\mu} \quad (8)$$

Frising et al. (2006) criticize the use of Equation 8 by stating that it is only applicable for isolated spherical solid particles. Therefore it is not applicable for concentrated crude oil emulsions, where droplets are not isolated and moreover will probably even be in bigger diameter due to coalescence. They also add that Equation 8 contains two systematic errors:

1. It overestimates the sedimentation velocity of droplets and
2. It underestimates the mean droplet diameter.

These two errors are considered to balance each other somewhat. (Frising, et al., 2006)

In general process design the Stokes' law with assumption of rigid sphere is generally considered to be accurate enough to work on a simple design cases.

2.2.2 Design droplet size and settling rate

In the separator design literature the droplet size is usually assumed to be at certain ideal size. According to Hooper and Jacobs (1996) the mean droplet size is normally over 1000 μm and only a small portion of droplets are below 500 μm . They state that one would be expected to use a design droplet diameter of above 300 μm . However, because of other inadequacies in design equations 150 μm is recommended when designing a normal separation vessel. The aim is to design a separator that is able to remove larger droplets than the design value. (Hooper & Jacobs, 1996)

According to Perry (1997) droplets below 50 μm have low enough terminal velocity that the gravitational separation is not thought as an attractive way to separate phases. Laleh (2010) has presented several generally used droplet sizes that range from 140 to 500 μm , depending on the use of designed vessel.

From the assumption of ideal droplet size, settling velocity and dispersed phase, the droplet settling rate can be calculated using Equation 8. This requires knowledge of which phase is considered dispersed. This can be estimated using Equation 9 and Table 3.

$$\theta = \frac{Q_L}{Q_H} \left(\frac{\rho_L \mu_H}{\rho_H \mu_L} \right)^{0,3} \quad (9)$$

Where,

- Q_L, Q_H volumetric flow rate of light and heavy phase, respectively (m^3/s)
- ρ_L, ρ_H densities of light and heavy phase, respectively (kg/m^3)
- μ_L, μ_H viscosity of light and heavy phase, respectively (Pas)

Table 3. Correlation to theta in Equation 6. (Hooper & Jacobs, 1996)

Correlation, θ	Result
< 0.3	Light phase always dispersed
0.3 - 0.5	Light phase probably dispersed
0.5 - 2.0	Inversion possible, design for worst case
2.0 - 3.3	Heavy phase probably dispersed
> 3.3	Heavy phase always dispersed

2.2.3 Separator geometry

Separator geometry should be selected in a way that it is economical, efficient and safe. Normally, there are multiple restrictions that can affect to the optimal geometry (e.g. plant area space). Most decanters are cylindrical for economic reasons. (Hooper & Jacobs, 1996) According to Towler & Sinnott (2013) the most economical horizontal separator Length-to-diameter ratio will depend on operating pressure (see Table 4):

Table 4. The most economic length-to-diameter ratio per pressure. (Towler & Sinnott, 2013)

Design pressure, bar (a)	Length/Diameter, L/D
0-20	3
20-35	4
>35	5

Hooper and Jacobs (1996) are suggest that initial design should be measured in a way that flux, φ , is smaller than terminal velocity, u_t :

$$\varphi = \frac{Q}{A} < u_t \quad (10)$$

Here, φ is flux of the phase (m/s), Q is flow rate (m³/s) and is the cross-sectional area of flow (m²). Flux should be calculated for each phase and the measuring should be done in a way that flux is smaller than the terminal velocity calculated. (Hooper & Jacobs, 1996)

Additionally, when designing a separator, one should also consider the inlet and outlet arrangement. Hooper & Jacobs (1996) present a few good guidelines to follow:

1. Feed should be introduced uniformly across the cross section of the decanter
2. Feed should not cause residual jets or turbulence
3. Outlet velocity should be low enough to avoid formation of vortices and re-entrainment

2.2.4 Coalescing media

Coalescing media or coalescers are designed to collect small dispersed droplets and form or coalesce them into larger drops that will boost the separation process. This is usually achieved by passing these dispersed droplets through a dense fiber bed or filter mat. Dispersed droplets impinge onto these fibers while continuous phase on the fibers is thinned by displacement and viscous drag. Ultimately the continuous phase film ruptures and allows dispersed droplet to coalesce. The forming droplets are now continuing to grow in size until they are large enough to gravity and drag forces to drop them away from the fibers. Schematic view of the process is presented in Figure 5. (Sparks & Chase, 2016)

Three steps in coalescing

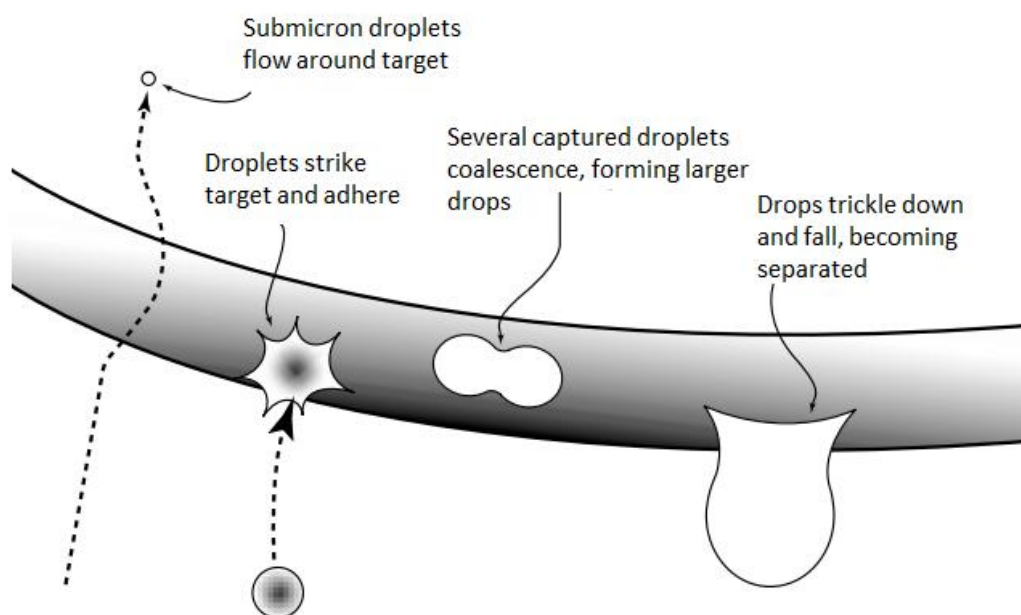


Figure 5. Coalescing process within coalescing media. (Modified from ACS Industries, LP, 2016)

Coalescing media is used to boost the coalescence of really small dispersed droplets, thus increasing the separation efficiency. This is especially used for hard separations, where small droplets and more stable emulsions are expected. (Sparks & Chase, 2016)

2.3 Other modelling approaches for liquid-liquid separation

Even though Stokes' law is known to model the gravitational separation with limitations and inaccuracies, it is still the most used model. There has been quite harsh critique towards it, as mentioned before in Section 2.1. Two different modelling approaches found from the literature are considered; separation and coalescence based models. Sedimentation based model is built on the assumption that sedimentation happens mainly by droplet falling or rising through the dispersed phase and coalescing to its bulk phase. The model has been acquired by investigating separation of two mixed immiscible liquid (e.g., water and oil) and observing positions of water/emulsion and emulsion/oil phase interfaces. (Frising, et al., 2006)

Sedimentation model is based on Jeelani, et al., (1999) observations that in the first state droplets settle to form a dense packed zone where they are in contact with each other. After time passes the height of this zone diminishes. Jeelani, et al. (1999) also state that coalescence happens only at the bottom of dense packed zone and that mean droplet diameter remains relatively constant as a function of time. Therefore, coalescence with bulk phase is preferred to coalescence between droplets. (Jeelani, et al., 1999)

Coalescence based model assumes that the dense packed zone does not diminish during the coalescence process; rather it remains at a same level. Coalescence based models assume that droplets mainly coalesce with each other until they are large enough to reach and join the bulk phase. (Frising, et al., 2006)

It has to be noted that both of these models are based on limited amount of research. Therefore, both models are only suited for limited case setups. For example, the sedimentation model requires very thorough understanding of the system at hand and it requires large droplet diameter (even over 1 mm) to work. Likewise, the coalescence based model has only been tested against water/hexadecane system, and thus it requires more testing. (Frising, et al., 2006)

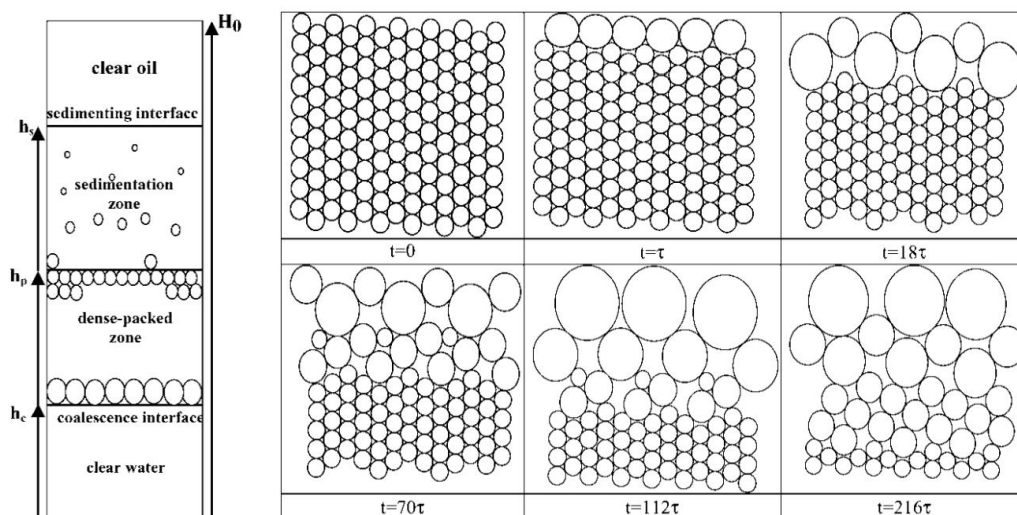


Figure 6. Schematic views of both sedimentation based (left) and coalescence based (right) models. (Modified from Frising, et al., 2006)

2.4 Gas-liquid separation

Gas-liquid separation can be considered rather similar to liquid-liquid separation. One of the largest differences between these is related to dispersion and density differences. First, the density differences of the phases are generally much larger with gas-liquid systems than with the liquid-liquid ones. As mentioned in Section 2.1 this makes the separation process easier. Therefore, it can be stated that it is generally easier to separate liquid from gas than two liquid phases. (Perry, 1997)

Impact plates or baffles are used to increase separation efficiency. Additionally, coalescing media, defoaming plates, mist eliminators, and vortex breakers are used. Typical horizontal gas-liquid separator with internals placed is presented in Figure 7.

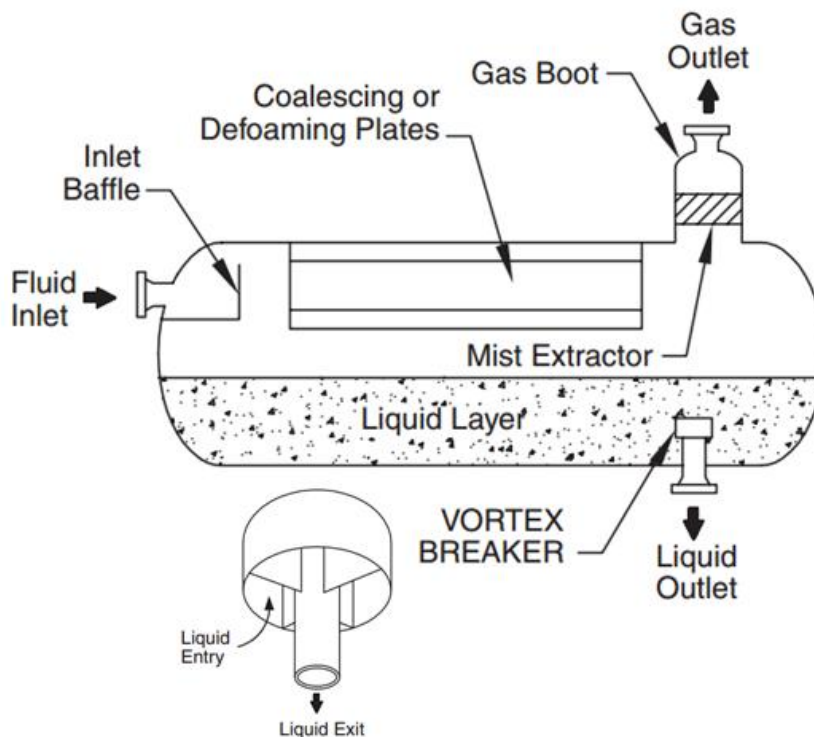


Figure 7. Horizontal gas-liquid separator with internals. (Modified from Stewart & Arnold, 2008)

Generally, the phenomena presented in Section 2.1 between liquid-liquid systems can be applied to a liquid-gas system with a few accommodations. In two-phase separators the liquid droplets are removed from the continuous gas phase. The effect of turbulence and

coalescence are similar to the liquid-liquid systems. For more specific research of the gas-liquid separation and sizing criteria see Huusari (2015).

2.4.1 Mist eliminators

Mist eliminators or demisters are used when separation with gravitational force is considered to be inadequate or the droplet size is small. They are used to boost gas-liquid separation. The mechanism can be based on multiple different phenomena, like coalescence, gravity separation, change of flow direction and velocity, filtering or centrifugal force. A few of the most common mist eliminators are demister pads and vane pack demisters (Figure 8). (Laleh, 2010; Couper, et al., 2012)

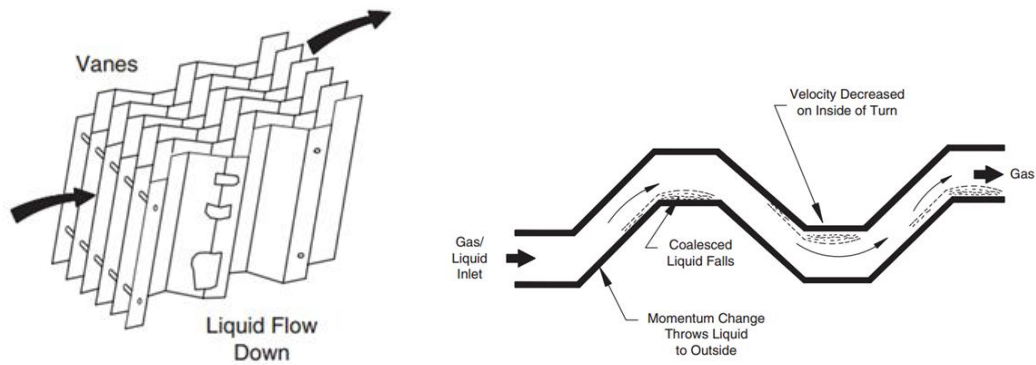


Figure 8. Typical vane pack demister. Left: a schematical view of vane packing. Right: the operating principle of vane packing. (Stewart & Arnold, 2008)

Demister pads are vessel internals that can be used in a variety of vessels. Demister pads are usually consisted of either fibers or wire mesh. The operating principle is following: continuous phase with small entrained droplets enters to the demister, which then separates droplets from vapor phase. This is due to coalescence assisted by the mesh, and then separation by gravity. The wire mesh demisters have been reported to remove droplets from 10 μm in diameter with relatively low pressure drop. (Laleh, 2010; Couper, et al., 2012)

2.4.2 Foaming

Foam consists of gas or vapor bubbles that remain at a stable suspension surrounded by liquid film. In this case liquid acts as a continuous phase, whereas gas or vapor are considered dispersed. Foaming requires gas to be dispersed into the liquid phase. Possibility of foam occurs at the interface of liquid and gas phase, if gas bubbles are liberating from the liquid. As in the case of emulsion (Section 2.1.5), foam will break without stabilizing mechanism. (Stewart & Arnold, 2008; Rosen & Dahanayake, 2000)

The most common way to deal with foaming is the usage of de-foaming chemicals. Usually, de-foaming chemicals act to prevent the stabilizing mechanism, which prevents foaming. However, excess use of de-foaming chemicals usually causes problems. Another possibility is to use de-foaming plates. De-foaming plates are closely spaced parallel plates or tubes that provide additional surface area, which causes the foam to break. (Stewart & Arnold, 2008; Rosen & Dahanayake, 2000)

3 Computational fluid dynamics

Computational Fluid Dynamics (CFD) is a combination of three traditionally different fields of science: computer science, fluid dynamics and mathematics. CFD deals with numerical analysis of fluid dynamic problems. The primary equations involved in CFD are called Navier-Stokes equations which consist on conservation of mass (continuity equation), conservation of momentum and energy equations. (Jamshed, 2015) CFD solving process can be seen from Figure 9.

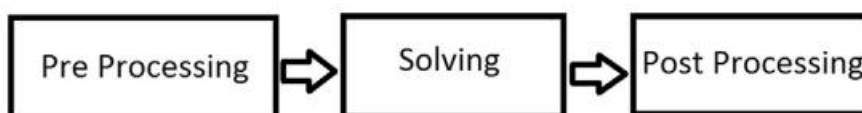


Figure 9. Solving process for CFD. (Jamshed, 2015)

Pre-processing consists on the meshing, *i.e.* defining the calculation volume and the boundary conditions. By meshing the calculated area is divided into smaller sections (cells)

where the conservation equations are solved in an iterative manner. The computational mesh is connected to the modeling problem and for example the mesh is required to be accurate enough to model the geometry used. Mesh size is also connected to the time that is required for solving the equations. Calculation time increases for larger number of cells. (Siikonen, 2014)

Second part consists iteratively solving the governing equations. There are multiple ways to solve these equations. The most common methods for solving are pressure based solving methods SIMPLE (Semi-implicit Method for Pressure-Linked Equations) and PISO (Pressure-Implicit with Splitting of Operators). In the SIMPLE method the finite difference equations are obtained from the governing equations. Then the pressure profile is estimated and with that the momentum equations are solved to form a velocity profile. With gotten results the pressure profile is updated with the continuity equations. Then velocity profile is iteratively solved with pressure until the satisfied solution has been found. PISO method is an improved version of the SIMPLE, but it is based on the same basics. (Laleh, 2010)

The final part is post-processing, where the analysis and visualization of the results is conducted. (Jamshed, 2015)

3.1 Multiphase models

Madhavan (2005) presents that there are four known approaches for multi-fluid flow modelling: Volume of Fluid (VOF), Eulerian-Lagrangian (E-L), Eulerian-Eulerian (E-E) and Mixture modelling. For immiscible or partially immiscible liquid-liquid system all of these approaches are possible to take and a more rational approach is required. The factors that are required to take into account are for example the computational load, resources, the scale of the work, and simulated substances.

The VOF method tracks the individual phase motion, thus helping it to trace the interface (Madhavan, 2005). It is best suited for stratified flows, where the phases form a clearly defined phase interface (Wardle & Weller, 2013). VOF allows tracking the dispersed phase surface, and in theory, it is possible to use it to model droplet coalescence behavior. However, in this case VOF method requires mesh that is much smaller than the droplet size

to be efficient in coalescence modeling. (Hlawitschka et al., 2012) This makes droplet coalescence modeling with VOF computationally impractical solution for industrial scale modeling. VOF has been used in a really small scale droplet coalescence modeling, e.g. Gebauer et al. (2015) performed CFD investigation on the single droplet coalescence with VOF, and when modeling outcome was compared to the high-speed camera images, the results indicated good modeling performance of the coalescence. VOF model is also been used in combination with some other model to simulate droplet behavior. For example Hlawitschka, et al. (2012) conducted a CFD simulation of DN32 extraction column using VOF with population balance modelling.

The Eulerian-Eulerian approach is the most used approach in liquid-liquid dispersion modelling. (Madhavan, 2005; Wardle & Weller, 2013) For example Walvekar, et al. (2009) have used it when modeling oil-water flow in a small pipe ($D=0,024\text{m}$, $L=9.7\text{m}$). The Eulerian-Eulerian approach is well suited to model systems which have substantial volume fractions of the dispersed phase, for example agitated tanks. (Madhavan, 2005)

The Eulerian-Lagrangian approach uses the Eulerian approach for the continuous phase and the Lagrangian approach for the dispersed phase. In multiple reviews, it is stated that the E-L approach can be used for small phase fractions (dispersed phase below 10 %). Laleh (2010) has used this approach when modelling pilot-plant-scale two-phase separator. Additionally, Laleh (2010) has implemented a VOF with E-L approach and used it to model a large-scale three-phase separator.

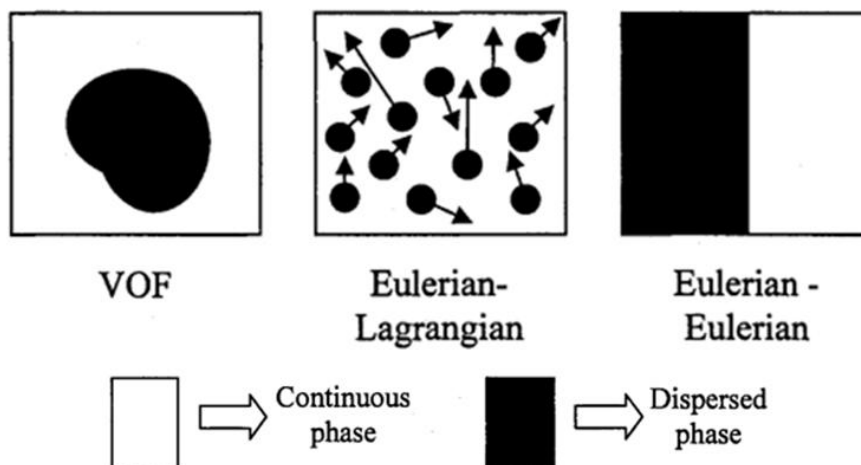


Figure 10. Different model approaches presented schematically. (Modified from Madhavan, 2005)

3.2 Turbulence models

Reynolds Averaged Navier-Stokes (RANS) is the most commonly used turbulence model in large scale. In RANS-based approach the values of flow variables are decomposed into a fluctuating component and a mean component, which are then time averaged over the time period of longest eddies. Typical RANS models have two additional transport equations, namely k - ϵ or k - ω models. Here k refers to kinetic energy equation and ϵ to the energy dissipation rate. The most common k - ϵ models are standard, realizable and re-normalization group (RNG) model. k - ω model is developed to solve for kinetic energy and specific dissipation. Carlson & Talseth (2009) describe that both of these models have their own advantages: k - ϵ is well defined in the boundary layer edge and free stream. On the other hand, k - ω model is accurate in the sublayer. Shear stress transport (SST) was developed based on combining the advantages in both the k - ω and k - ϵ -models. (Carlson & Talseth, 2009; Madhavan, 2005)

Shi (2015) has made a pressure gradient comparison with different turbulent schemes and experiments to see what kind of RANS model would be best suited for oil-water systems in horizontal pipe flow (Figure 11).






	Flow pattern	dp/dx (Pa/m)	Relative error for dp/dx
Run L-9-2, standard k - ϵ		582	+21%
Run L-9-3, RNG k - ϵ		575	+19%
Run L-9-4, SST k - ω (without turbulence damping treatment)		561	+16%
Run L-9, SST k - ω (with turbulence damping treatment)		427	-11%
Experiment		482	

Figure 11. Pressure gradient comparison between different RANS turbulence models and experimental results. Simulations were made using VOF. (Shi, 2015)

Theoretically, it is also possible to simulate three dimensional flow fields without resorting to any kind of modelling. This includes simulation of a turbulent flow field. This kind of modelling is called direct numerical simulation (DNS). However, this would require a computational mesh that is on the dissipation scale, i.e., mesh cell size must be smaller than the smallest eddy existing in the fluid. This would lead to a very large grid size. Additionally, in transient systems, time step required to simulate this kind of grid would be really small. Therefore, use of DNS as a turbulence model is currently not applicable on industrial scale. (Jamshed, 2015)

Large Eddy Simulation (LES) is an alternative approach to simulate turbulence. LES is based on the assumption that the large scale turbulence is problem-dependent, and thus, requires modelling. Small scale is considered as universal and isotropic; therefore it can be modelled easily. LES, while being less accurate than DNS (and thus requiring less computational capacity), is still considered to be too expensive to model process engineering work. (Jamshed, 2015)

4 CFD modeling of liquid-liquid separators

In this chapter a literature review about modeling the liquid-liquid systems with CFD is presented. All five cases discussed present a certain area of the liquid-liquid modeling. First section of this chapter presents three different modeling approaches that have been implemented to model the liquid-liquid separation process. In the second part two cases with two-phase liquid-liquid separation CFD models are reviewed. The presented cases and basic information are presented in a Table 5. Software and used multiphase models vary a lot. This is an indication of both the complex nature of liquid-liquid phenomena (multiple ways to approach the same problem), and the flexibility of the CFD as a modeling tool.

Table 5. Summary of reviewed cases.

Section	Modelled case (Phases modeled)	Author	Use (Scale)	Software	Multiphase model used
4.1.1	Three-phase separator (gas-liquid-liquid)	Laleh (2010)	Industrial (Large)	Fluent 6.3.26	VOF & Lagrangian
4.1.2	Collapsing dispersion test (liquid-liquid)	Wardle & Weller (2013)	Demo (Medium)	OpenFOAM 2.1	Eulerian & VOF
4.1.3	Emulsion breakage (liquid-liquid)	Oshinowo et al. (2016)	Laboratory (Very small)	ANSYS Fluent 14.5	Eulerian & PBM
4.2.1	Two-phase separator (liquid-liquid)	Chen et al. (2015)	Industrial (Large)	Fluent (version not specified)	Eulerian
4.2.2	Two-phase separator (liquid-liquid)	Behin & Azimi (2015)	Industrial (Medium)	Fluent 12.0.16	VOF

4.1 Two-model CFD approaches to model liquid-liquid systems

As discussed earlier, liquid-liquid dispersion is a complex phenomenon, thus describing the physical phenomena can often be difficult and require multiple models or approximations. This often leads to either unreliable results or heavier calculations, which are both expensive and undesired. In the following chapter three different approaches are presented. First is a study on a three phase separator, where Laleh (2010) has implemented a solver that uses both VOF and Lagrangian approaches to model the separator. Second study is by Wardle and Weller (2013) that illustrates the use of Eulerian based solver with coefficient to turn solver to work as a VOF approach. In the third part of this chapter, a few different approaches of CFD modeling with population balances are presented.

4.1.1 Three-phase separator with VOF and Lagrangian approach

Laleh (2010) implemented a VOF and Lagrangian particle tracking method and studied the model in both gas-liquid and three phase (gas-liquid-liquid) separators. VOF was used to catch interface behavior and Lagrangian to simulate droplet behavior. Coexisting phases,

both discrete phase (droplets) and continuous phase (gas and liquid), were solved simultaneously. Laleh (2010) used Fluent 6.3.26. Mesh was produced with Gambit.

Laleh (2010) had a separation of water-heavy oil-air as a three phase simulations. Heavy oil phase was simulated as a component mixture of heavy hydrocarbons (85 mol-% of n-C₂₇H₅₆ with 5 mol-% of each: n-C₂₈H₅₈, n-C₂₉H₆₀, n-C₃₀H₆₂). Using the mixture the estimated density and viscosity were 783.59 kg/m³ and 5.296 cP, respectively. Oil-water surface tension was estimated to be 0.0486 N/m. Simulated separator geometrics can be seen from Figure 12. It has to be noted that there are a demister pad and a square hole patterned perforated plates inside the separation vessel. The produced mesh was at a size of about 900 000 cells (see Figure 13). The assumed mean droplet size of 150 microns was used. Standard k-epsilon modelling for turbulence was used.

For discrete phase, it was assumed that 95 % of the normal momentum and 90 % of tangential momentum is lost when droplet contact with vessel walls.

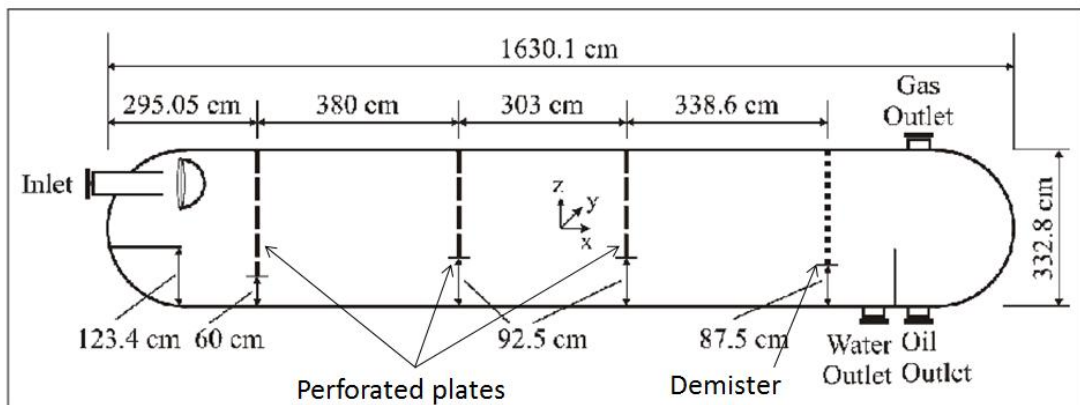


Figure 12. Geometry of studied three phase separator (Modified from Laleh, 2010).

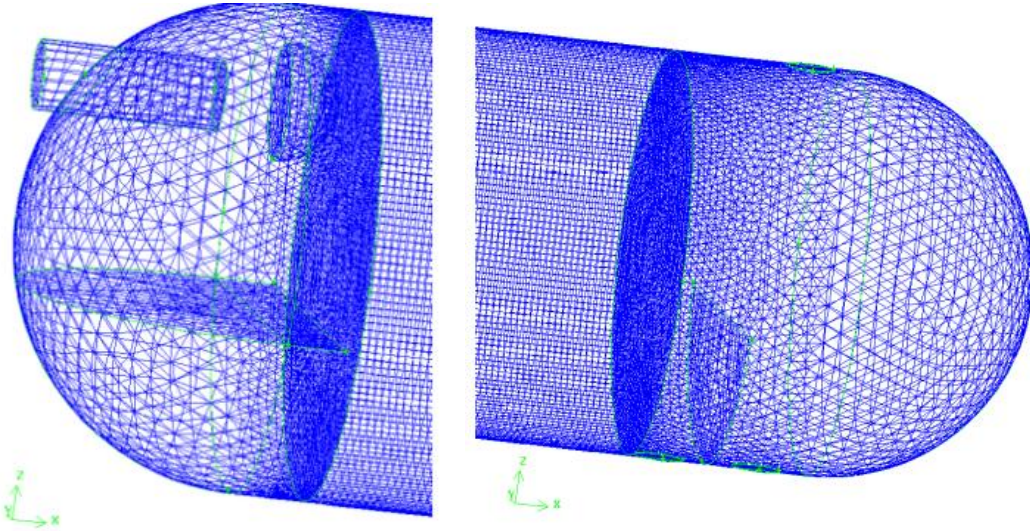


Figure 13. Produced mesh from study of Laleh (2010). Left is the front-end (inlet) part of the separator and right the back-end (outlet).

Laleh (2010) validated the results by incipient velocity, at which the minor fraction of the droplets (~1 wt-%) were carried over in the gas phase. The obtained incipient velocities were in most cases well aligned with the experimental data. Laleh (2010) concluded that the assumed mean diameter of 150 microns was an acceptable value for estimating separator incipient velocity. The second parameter that Laleh (2010) used to validate the results was separation efficiency versus gas velocity. Laleh (2010) found out that separation efficiency dropped beyond the incipient velocity rapidly while gas velocity was increased. This agreed with the experimental data.

However, Laleh (2010) also made simulations with solely Lagrangian solver and pilot-plant scale models. Here Laleh (2010) used only two-phase setting with gas and liquid. The results gathered from the experiment were not entirely in-line with the expected results. Incipient velocities gathered were close with the experimental ones, but separation efficiency did not drop to zero after reaching the characteristic incipient velocity as can be seen from Figure 14.

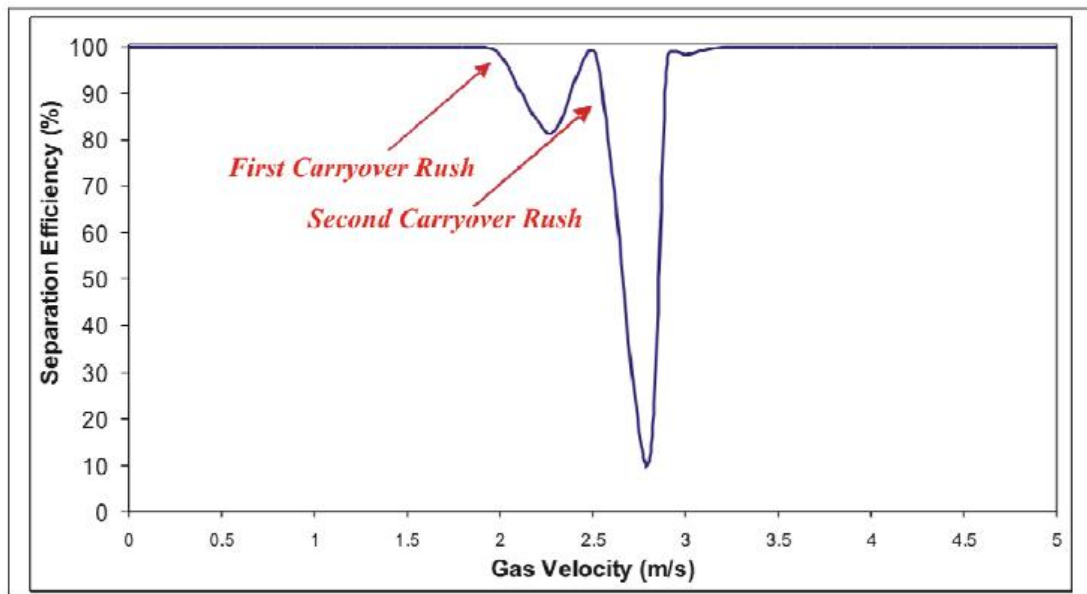


Figure 14. Separation efficiency as a function of the gas velocity by Laleh (2010). Pilot-plant scale gas-liquid separation modeled by Lagrangian scheme.

Laleh (2010) reports that with different simulations the carryover rushes (Figure 14) were occurring with all of the simulations that used solely Lagrangian model. He concludes that modeling only with one-way coupled Lagrangian framework does not give reliable results, since interactions between the liquid and the gas phase are neglected.

4.1.2 Collapsing liquid test using Eulerian and VOF approaches

Wardle & Weller (2013) conducted experiments to create a coupled multiphase solver to capture both multi-fluid and VOF methods. Their study emerged from the attempts to compile two different sets of CFD models (i.e., Eulerian approach and VOF) to model liquid-liquid extraction columns in a detailed way. They add that to accomplish this, methods which can adequately predict mixing and behavior of the small droplets are required.

To illustrate this Wardle & Weller (2013) used a multi-fluid-VOF coupling solver with binary coefficient (C_α) for interface sharpening. They state that with this coefficient the solvers multiphase model can be controlled switching it from VOF ($C_\alpha = 1$) to E-E ($C_\alpha = 0$). They also add that by dynamically switching the value of coefficient simulation of complex flows with any range from fully dispersed to fully segregated can be done with one unified solver. However, question of when flows are segregated and when dispersed arises. Wardle &

Weller (2013) suggest a use of predetermined flow regime or prediction of local droplet size based on the population balance or similar method.

Wardle & Weller (2013) used OpenFOAM 2.1 and multiphaseEulerFoam as a solver. Drag coefficient used was by Schiller and Naumann (presented in Table 2), with modification to larger Reynolds number. Cases were done at room temperature and pressure. Constant droplet sizes of 150 μm for the liquid phase and 1000 μm for the gas phase were used.

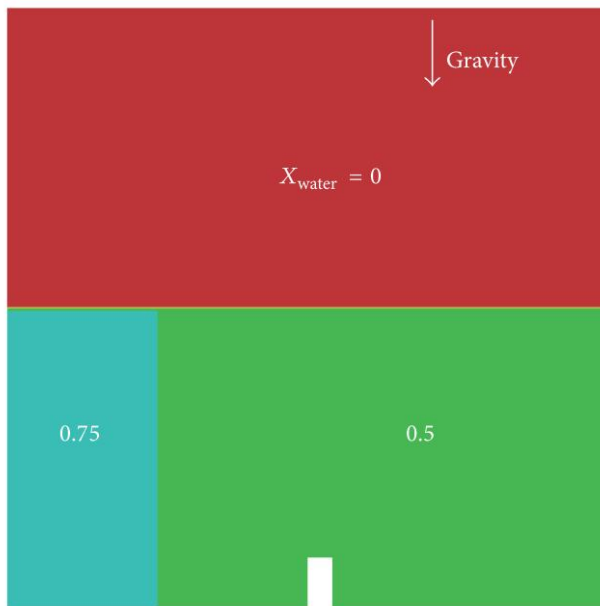


Figure 15. Initial condition for collapsing liquid-liquid dispersion test. (Wardle & Weller, 2013)

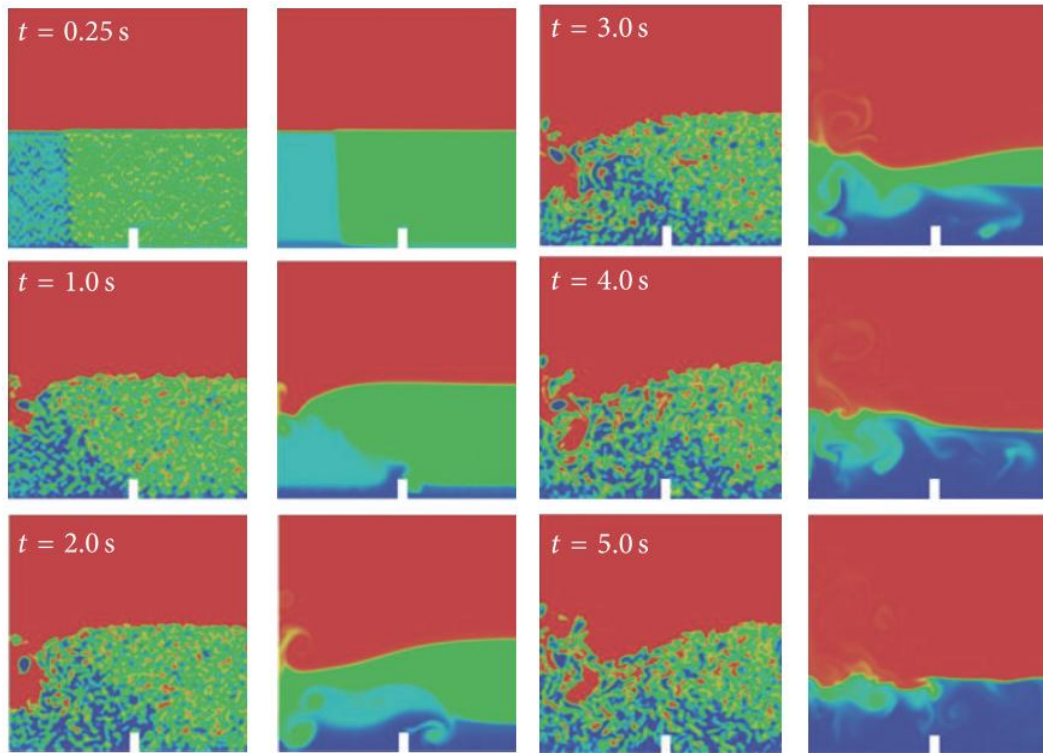


Figure 16. Comparison between Euler-Euler (left, $C_\alpha = 0$) and VOF (right, $C_\alpha = 1$) modelling with coupled solver. Blue is water and red is oil. (Modified from Wardle & Weller, 2013)

In Figures 15 & 16 are presented differences between Eulerian and VOF solvers. The VOF modelling shows sharp interface, while with the Eulerian solver interface between phases is much harder or even impossible to trace.

4.1.3 Studies of CFD solvers with population balances

Problem with the conventional multiphase solvers is the modeling of the breakage and the coalescence of dispersed droplets. There has been researches where single droplet coalescence has been modeled successfully with VOF (for example Gebauer, et al., 2015 and Villwock, et al., 2014), but mesh size in these researches has been smaller than droplet size. This would make the calculations too large and expensive from computational point of view. Alternative approach has been to model the dispersed droplet behaviour and evolution by population balance methods (PBM).

Oshinowo, et al. (2016) have modeled water-in-oil emulsion destabilization and separation in batch gravity separator. Experiments were carried in a small scale batch decantation cell

with internal diameter of 60 mm and height of 700 mm. Oshinowo et al. (2016) have used ANSYS FLUENT version 14.5. with in-house coding and user defined functions. Additionally, Oshinowo, et al. (2016) compared their data from CFD experiments to the experimental data. The CFD model used was based on Eulerian solver and coupled with PBM that was used to model coalescence and breakage. Schiller-Naumann correlation was used for drag coefficient with in-house modifications. The used mesh was small with only 1400 cells (grid spacing 3.2 mm). Oshinowo et. al. (2016) presented their results as development of the different fractions (height of the fractions in time, see Figure 17). The oil-water mixture is fully mixed at the start, and the evolution of separation is followed and compared between CFD calculations and experimental data.

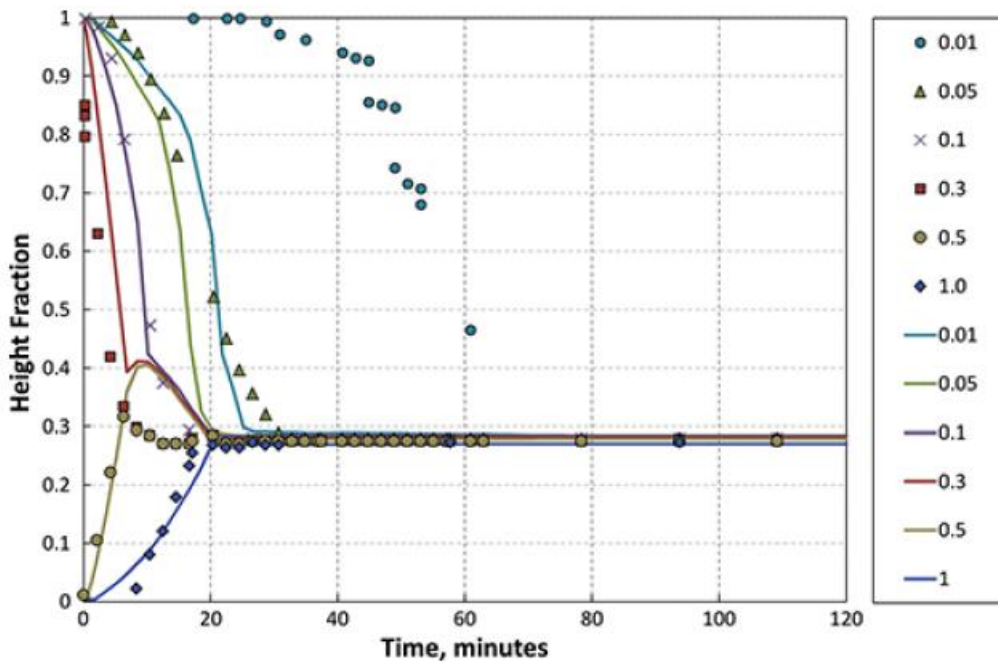


Figure 17. Fraction profiles for emulsion breakage test with water content of 28 vol-%. Points are experimental results and lines modeled results. Figure describes the evolution of certain volume fraction percentages as a function of time. (Oshinowo, et al., 2016)

The developed CFD-PBM model predicts the emulsion breakage behaviour quite well (Figure 17). However, the developed model clearly underestimates the time required for small water content to demulsify from the oil-water emulsion. Furthermore, Oshinowo et. al. (2016) state that more detailed analysis of the solver would require more information of

rheology and DSD at different locations in the separator. Also, the initial states at the test may not be as ideal as the CFD tests.

There are several other studies which couple CFD solvers with PBM. Examples of the work done are the articles from Silva & Lage (2011) and Buffo, et al. (2013) that describe implementing the coupled CFD-PBM solvers. Additionally, Gao, et al. (2016) made experiments with CFD-PBM solvers to model droplet breakage in turbulent liquid-liquid dispersions. Additionally, the CFD-PBM models are usually developed from mixing tank data, and may require further development, if and when used to model gravitational separation or other multi-phase separation problem.

4.2 Industrial scale studies of liquid-liquid separation with CFD

The second part of literature review consists on the larger scale liquid-liquid separation modelling studies. The primary objective is to find out what kind of models and assumptions have been used to model full scale separation processes. The other objective is to gather a review on what kinds of liquid-liquid separation processes have been modelled with CFD. Finally, the review on post-processing is made, how the results have been validated and what conclusions have been made.

4.2.1 Study of inclined water-oil separator

Chen, et al. (2015) studied the effect of inclination and residence time to oil-water separation efficiency. Schematics of used separator are presented in the Figure 18. They studied oil-water separation efficiency from the water content in oil outlet per inlet oil content. Additionally, Chen et al. (2015) set geometrical parameters to influence the geometry of the vessel and optimized them according their CFD results. They reported a 5 % increase in the separation efficiency after optimizing. Separation efficiency was based on the water content at the oil outlet and the oil content at the water outlet. The results can be seen from the Table 6.

Table 6. Result from the study of Chen, et al. (2015)

Item	Water content at the oil outlet	Oil content at the water outlet	Separation efficiency
Before the optimization	57,50 %	0,95 %	90,48 %
After the optimization	39,67 %	0,50 %	95,00 %

Chen et al. (2015) used an Eulerian approach to model the system. They also used standard k-epsilon turbulence model. The mesh was made with Gambit and mesh size was approximately 480 000 cells. The CFD simulations were conducted with Fluent. The used volume fraction of oil was 10 %. In their tests, Chen et al. (2015) varied inclination of the vessel from zero to 30 degrees. As a result they got an optimal inclination of 12 degrees. Additionally, when vessels inclination was increased from zero to 12 degrees separation efficiency increased. Furthermore, when inclination was over 15 degrees, the separation efficiency started to decrease. When inclination was set over 25 degrees and increased, the separation efficiency greatly decreased.

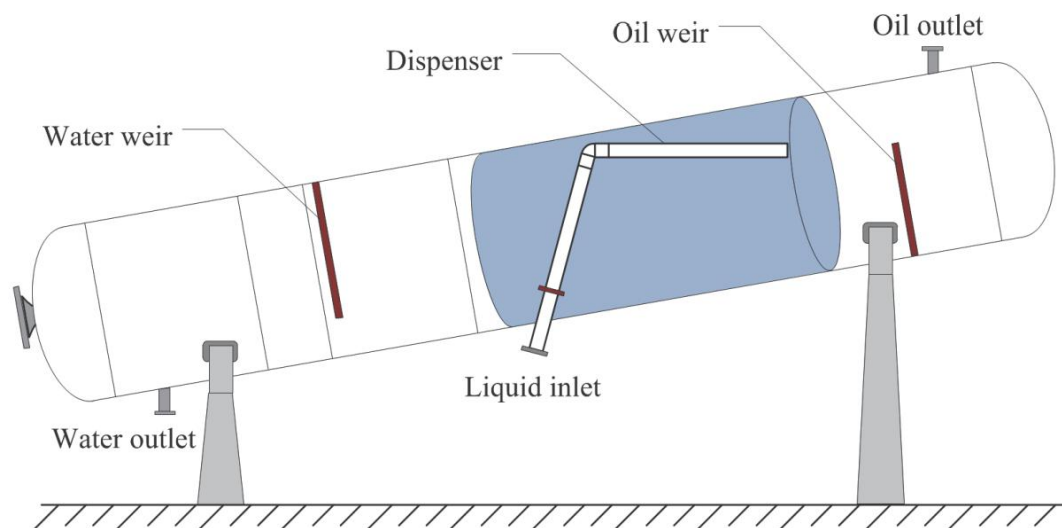


Figure 18. Oil-water separator used by Chen *et al.* (2015).

Besides the inclination, the other varied parameters were for example the weir positions and heights, length-to-diameter ration and oil outlet position. However, the inclined containers are still rare and the used optimal parameters quite far from the general recommendations (i.e. length-to-diameter ratio being much larger than 5 varying from 10 to 15).

4.2.2 Study of water level effect on oil-water separation efficiency

Behin & Azimi (2015) conducted both experimental and computational analysis on oil-water separation efficiency by altering the water level. They used a cylindrical horizontal separator (with measurements shown in Figure 19) and a 1/8th scale model of the main separator. Separator tank was designed for only oil-water separation.

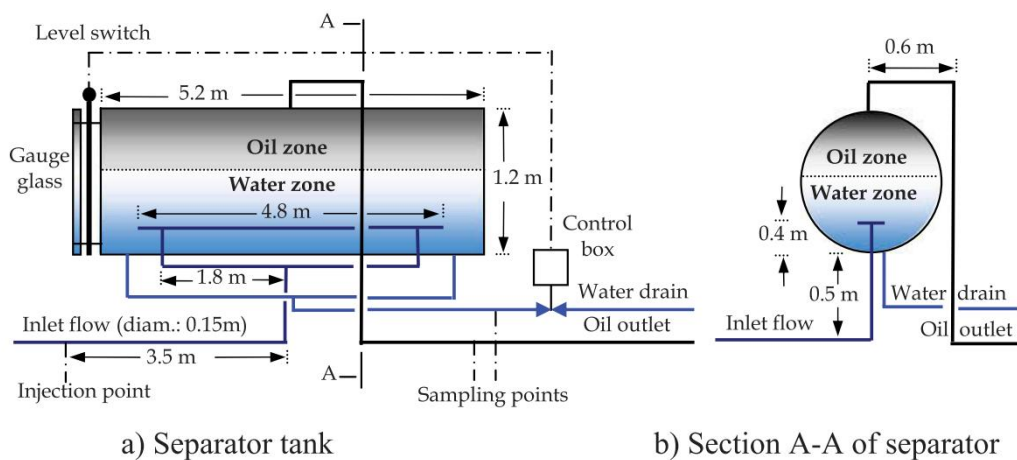


Figure 19. Cylindrical horizontal separator measurements simulated by (Behin & Azimi, 2015).

Behin & Azimi (2015) validated their results by measuring basic sediment and water as well as salt removal efficiency from the experimental vessel. Additionally, they used a water separation from oil as an indication of the performance level of the vessel. Water separation from oil was used to measure both experimental and CFD results. Water level alteration was between 0.5 and 0.9 meters from the bottom of the vessel. Initial condition given with CFD simulations was vessel filled with 0.5 volume fraction oil-water mixture. Behin & Azimi (2015) selected a VOF method to model their oil-water vessel. They used a commercial CFD package Fluent 12.0.16 and a mesh size of 150 000 cells. Mesh was created with Gambit, but not shown in their article.

Table 7. The CFD simulation results with different water levels. The $Q_{\text{water, in}}$ means water flow in the feed and $Q_{\text{water, out}}$ is the water flow amount in the oil outlet at the top of the vessel. (Behin & Azimi, 2015)

Water level (m)	$Q_{\text{water, in}}$ (m^3/s)	$Q_{\text{water, out}}$ (m^3/s)	η_{water} (%)
0.50	0.000993	0.000446	55.09
0.60	0.000993	0.000428	56.90
0.70	0.000993	0.000453	54.38
0.80	0.000993	0.000492	50.45
0.90	0.000993	0.000505	49.14

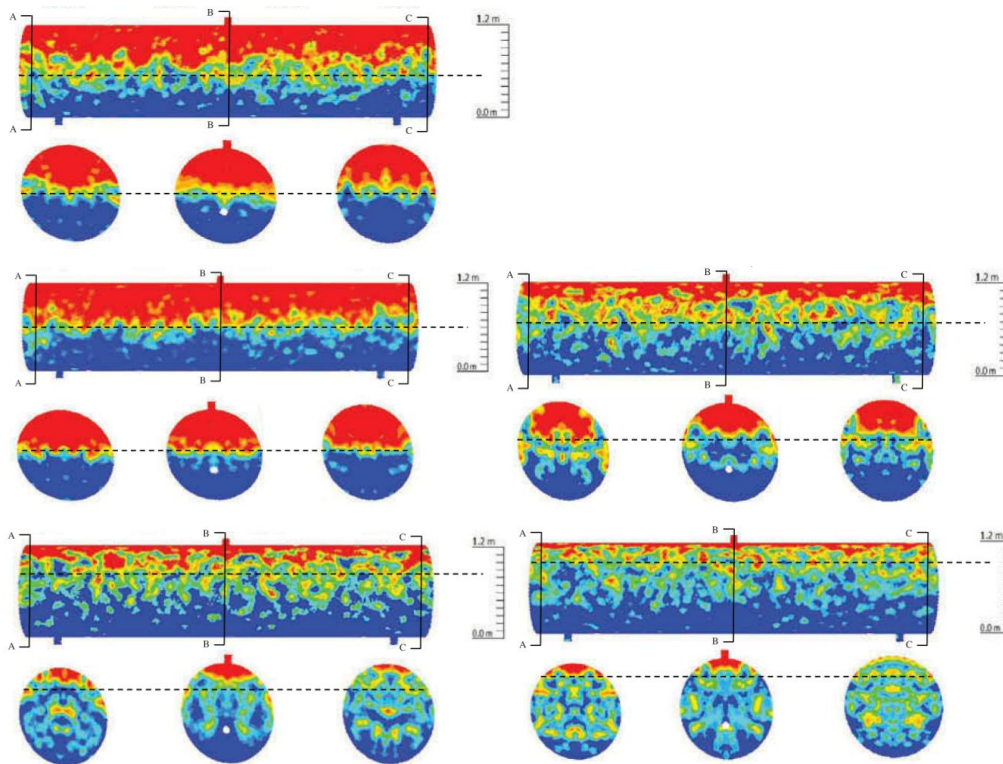


Figure 20. The CFD simulations. Oil volume fraction at different water levels. In the top figure the water level is 0.5 m. In the middle left, water level is kept at 0.6 m and in the right it is 0.7 m. In the bottom, the figures are with water levels 0.8 m and 0.9 m, left and right, respectively. (Behin & Azimi, 2015)

According to the authors water efficiency results (Table 7), the water levels between 0.5 and 0.7 m yield similar results, with a clear drop in efficiency after water level is over 0.7 m. When looking into the oil volume fraction figures (Figure 20), it is clear that the dispersion

band width grows when water level is over 0.6 m. Increasing dispersion band width could also be one of the reasons behind the weak performance in the higher water levels. Authors of the experiment have also speculated with this kind of increase in the dispersed level, and stated that the optimal water level according CFD simulations is 0.6 m.

Behin & Azimi (2015) also obtained empirical results from their experimental container that yield similar results. According to their basic sediment and water measurements, and salt removal measurements the most effective result is obtained when water level is 0.7 m. They state that their result is in agreement with the other obtained modelling. One other thing to consider is the inlet and its effect to the separation process. Inlet was introduced by dividing inlet feed equally into lower part of the container. The authors have not commented on the influence of the feed into the results, but it is rather obvious that some sort of influence could be found. For example, when Huusari (2015) carried out CFD simulations with different inlet distributors for vertical gas-liquid separation vessels, it was obvious that there was a huge difference in distribution of the fluid. Therefore, these results are applicable for this separator only, and there are no universalities that can be applied to overall design of the separators.

EXPERIMENTAL PART

The experimental part of the thesis studies gravitational separation in a horizontal vessel. This is conducted by using CFD tools in several different setups. First, the used software and computers are reviewed. After that the complete case setup is presented. The following chapters consider the principal evaluation criteria and the simulation results, respectively. In the final chapter of the experimental part conclusions on the topic are drawn, and follow-up experiments are suggested.

5 Used software and computers

Multiple software tools were utilized to calculate CFD cases. The tools were used to create geometry, do the actual CFD calculations, and to perform post processing and visualization of the results.

5.1 Geometry

Geometry was produced by using MicroStation V8i version 08.11. Geometry was made based on measurement drawings and then exported as STL-file. The STL file format essentially converts the geometry to triangles. Resolution was set to the level that the STL-files appeared round like visually. This was achieved using maximum angle of 10° and minimum triangle edge length possible.

5.2 CFD calculations

The CFD calculations were performed using OpenFOAM source code with commercial package of HELYX®. OpenFOAM is an open source free software package licensed and distributed by the OpenFOAM Foundation (<http://www.openfoam.org/>). HELYX is a commercial program based on OpenFOAM. It provides slightly modified CFD library based from OpenFOAM code, and a graphical user interface (GUI). This work was done with OpenFOAM-2.2_engysEdition-2.4, which is essentially HELYX® version 2.4.

5.3 Visualization

The visualization of the work was done by using open-source program ParaView 4.3.1 (<http://www.paraview.org/overview/>). ParaView is designed especially to analyze large datasets using distributed memory computing resources. ParaView allows user to visualize the large datasets for example by lines, colors and contours. ParaView also contains additional tools to modify and analyze different datasets. In this work the most used tools were streamlines of the flow, volume fractions of the different phases and velocity field of the container.

5.4 Computers

All of the CFD calculations were conducted with Neste Jacobs Linux cluster computers. The cluster was composed from two computers with Opteron 6172 processors (48 cores) and 128 GB RAM each, and from two other computers with Opteron 6380 processors (64 cores) and 512 GB RAM each. Most of the two phase calculations were simulated using amount of cores between 8 and 16. The rule of thumb used was not to exceed 20-30 thousand cells per core. However, the lowest amount of cells per core was tried to avoid falling below 10 thousand cells. By using this setup, typical transient two-phase 180 second simulation took between 55 and 202 hours of time, depending on the case and used geometry. Transient single phase simulation lasted 8 hours, whereas all the steady state simulations (2000 iterations) were calculated in less than one hour.

6 Case setup

In this chapter, the case setup of simulations is discussed. The topics reviewed are simulated geometry, geometry alterations, fluid characteristics, used model, and boundary conditions. Additionally, data processing and mesh dependency tests are described. Example of the complete case setup for HELYX® GUI can be found from Appendix 1. The simulated case setup was based on a real design case.

The simulated cases varied in between single and two-phase modeling. Additionally, steady state and transient simulations were both used. In Table 8 a summary of all the cases is made.

Table 8. Summary of simulated cases.

Section	Simulations	Phases	Simulation solver time type	Simulated vessel type
6.8	Mesh dependency	Single phase	Steady state	Upper half
8.1	Model testing	Two-phase	Transient	Upper half & Full
8.2	Inlet and outlet configurations	Two-phase	Transient	Upper half

The mesh dependency tests were done to test the effect of mesh towards the results. They are further discussed in the Section 6.8. The mesh dependency tests are the only steady state simulations done in the thesis. The steady state was seen as an easy way to start out the CFD simulations and was selected to familiarize the author to the CFD modeling tools. Rest of the simulations was transient. There were two alternative two-phase models that were considered; VOF which can model the phase interface, and Euler-Euler which was considered to be more robust. With VOF the calculations were tried, but constantly crashed, and with given timetable a solution to this issue was not found. With Euler-Euler -model similar problems did not occur, and it was used to simulate all the two-phase cases in this thesis. The two-phase model is further presented in the Section 6.5.

In the model testing part effect of liquid droplet size, compression term, and turbulence modeling were studied. Additionally, full vessel simulations were tested. Model testing cases are presented in the Section 8.1. In the inlet and outlet configuration simulations different inlet and outlet distributors were investigated. Inlet and outlet configuration cases are presented in the Section 8.2.

6.1 Simulated vessel geometry

The same vessel dimensions were used in all simulated cases. The simulated vessel is horizontal cylindrical vessel with internal diameter of 1 m. In the heads there are 2:1 half ellipsoids (500 mm x 500 mm x 250 mm). The inlet internal diameter is 203.2 mm (8"), the vapor outlet internal diameter is 10.2 mm (4"), and liquid outlet internal diameter is 76.2 mm (3"). Dimensions of the simulated container are presented in Figure 21.

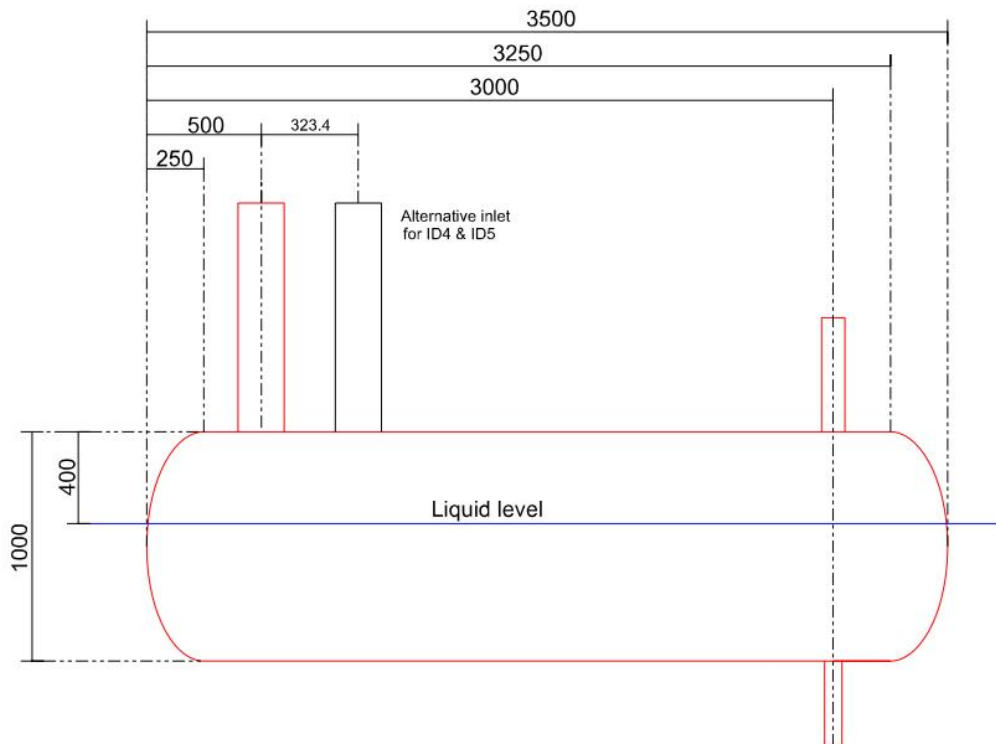


Figure 21. The dimensions of modelled horizontal container, side view. Measures are in millimeters.

In Figure 21 an alternative inlet is shown. This was used due to the tested inlet configurations, which required more space than the initial design. The length-to-diameter ratio used is well aligned with the ratio recommended in the design guidelines presented in Section 2.2. In Figure 22 a schematic view of the simulated vessel is presented.

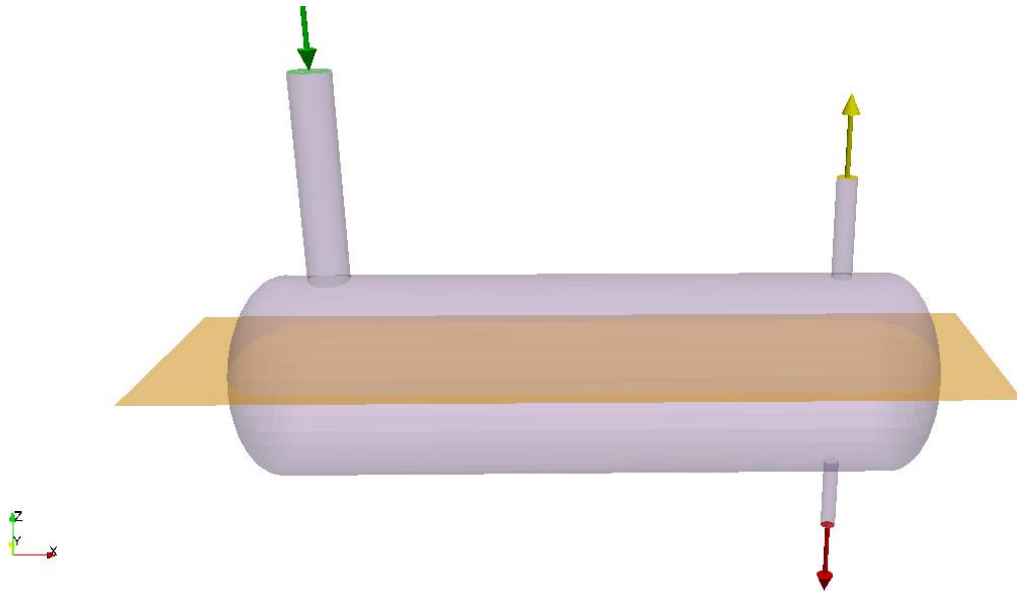


Figure 22. Schematic view of the simulated base geometry. The orange plane describes the liquid surface at the vessel. Inlet is marked as green, yellow is the gas outlet and red the liquid outlet.

With full vessel modeling the whole vessel was simulated with initial state of liquid level at the level presented in Figure 22. Also, both outlets were simulated. With upper half modeling the liquid level was simulated as an impermeable wall. The liquid outlet (red in the Figure 22) was not simulated in these cases. Liquid outlet was excluded after a non-physical phenomenon occurred in a few simulations. This is further discussed in Section 8.1.4.

6.2 Inlet and outlet configurations

Five different inlet distributors and two different outlet plates were simulated. The inlet distributors can be divided into two groups; pipes and impact plates. For the first three cases, the original container was used. For the last two cases, a modified inlet configuration was used as shown in Figure 21. The inlet distributors were connected to the inlet nozzle, at the top of the container. For the STL-pictures and dimensions of the used inlet distributors see Figures 23 and 24.

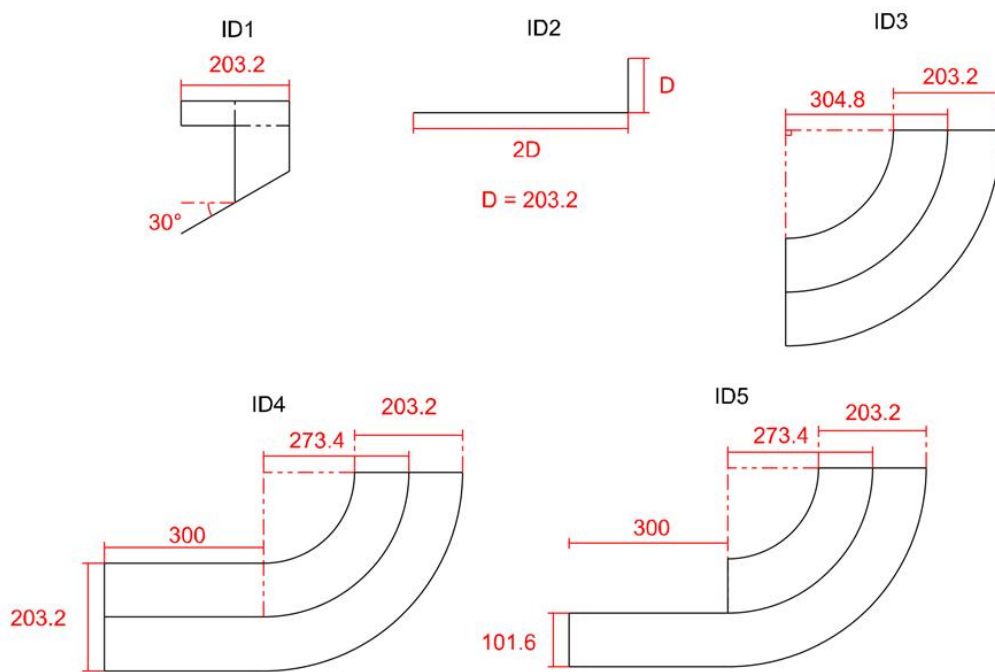


Figure 23. Dimensions of the tested inlet distributors, the measures are in mm.

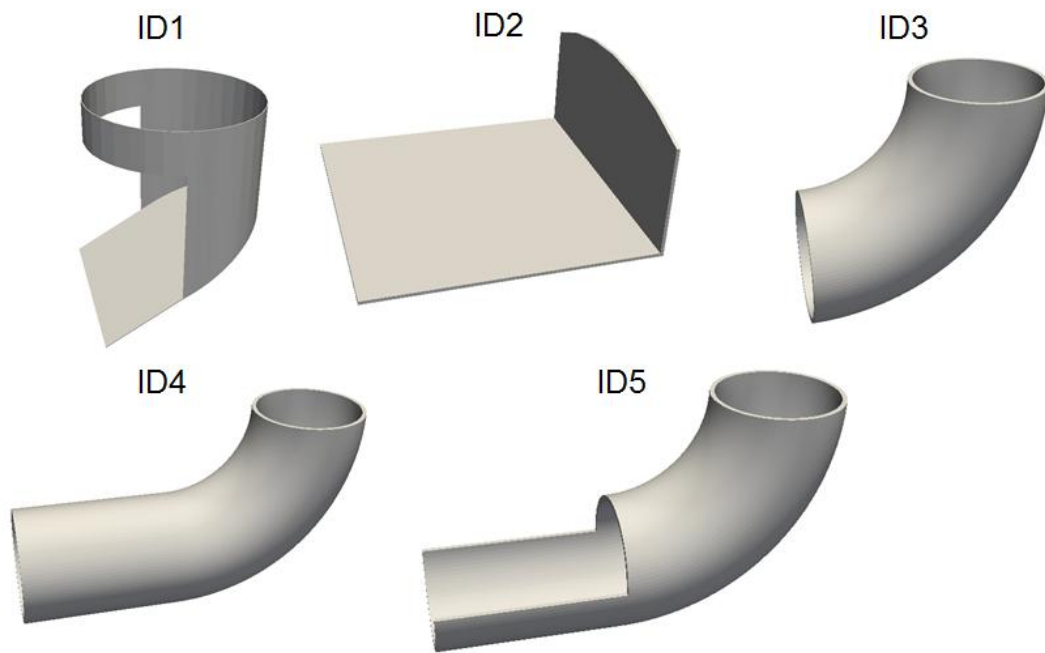


Figure 24. STL-images of the simulated inlet distributors.

In addition to the inlet configurations, two different outlet configurations (OD1 and OD2) were tested. Both outlet configurations were similar to the ID2 geometry. OD1 is a similar corner impact plate, but it is much smaller, since it follows the internal diameter measures of 4 inch vapor outlet. OD2 is essentially the same geometry without the end plate. Both plates in outlet geometries are 101.6 mm below the vapor outlet. Square bottom side length in outlet configurations is 101.6 mm. Both geometries are presented as STL-figures in Figure 25.



Figure 25. STL-images of tested outlet configurations. OD1 is left and OD2 is right.

6.3 Fluid characteristics

The simulations were conducted using two-phase gas-liquid mixture. The simulated mixture is a real design case of naphtha overhead drum. The fluid characteristics are acquired from the design case. The gas phase is named as gas and the liquid phase as light naphtha. Characteristics of the fluids are presented in Table 9.

Table 9. The fluid characteristics of gas and light naphtha compounds.

Fluid	gas	light naphtha
Density (kg/m ³)	21.96	555.3
Dynamic viscosity (cP)	0.01	0.2
Specific heat capacity (kJ/kgK)	1.8	2.5
Thermal conductivity (W/mK)	0.02	0.098

6.4 Two-phase model

The initial model selection was based on the previous tests performed by Huusari (2015). There are multiple solvers in Helyx that can be used for the two-phase gas-liquid case, each of them having both their advantages and disadvantages. Euler-Euler multiphase model was selected, mostly because of the robustness of the solver. The used solver was multiphaseEulerFoam. The solver contains multi-fluid model equations for incompressible and isothermal flow. The mass and momentum equations are given for each phase k , and are following (Equations 11 & 12). (Wardle & Weller, 2013)

$$\frac{\partial \alpha_K}{\partial t} + \vec{u}_K \cdot \nabla \alpha_K = 0 \quad (11)$$

$$\frac{\partial (\rho_K \alpha_K \vec{u}_K)}{\partial t} + (\rho_K \alpha_K \vec{u}_K \cdot \nabla) \vec{u}_K = -\alpha_K \nabla p + \nabla \cdot (\mu_K \alpha_K \vec{u}_K) + \rho_K \alpha_K \vec{g} + \overrightarrow{F_{D,k}} \quad (12)$$

Where $\overrightarrow{F_D}$ is the drag force. In this work, all of the simulations were conducted by using drag model from Schiller and Naumann. In this model, drag term is given by Equation (13). (Wardle & Weller, 2013)

$$\overrightarrow{F_{D,k}} = \frac{3}{4} \rho_c \alpha_c \alpha_d C_D \frac{|\overrightarrow{u_d} - \overrightarrow{u_c}| (\overrightarrow{u_d} - \overrightarrow{u_c})}{d_d} \quad (13)$$

Schiller and Naumann model defines drag coefficient as a function of Reynold's number (Equation 14):

$$C_D = \begin{cases} 24 (1 + 0.15 Re^{0.683}); & Re \leq 1000 \\ 0.44; & Re > 1000 \end{cases} \quad (14)$$

Where Reynold's number is calculated from (Equation 15):

$$Re = \frac{|\overrightarrow{u_d} - \overrightarrow{u_c}| d_d}{\mu_c} \quad (15)$$

The model requires a constant diameter for dispersed phase (gas bubble or liquid droplet). The dispersed phase is determined by the volume, and whichever phase is locally dominant is interpreted as the continuous phase. This means that both phases can act as a dispersed phase, therefore a droplet diameter must be determined for each phase. For liquid phase (light naphtha) constant droplet diameters of 10, 30, 50, and 150 μm were tested in separate cases. For gas phase (gas) the constant bubble diameter of 1000 μm was used in all of the simulations.

6.5 Transient time step

The Courant number (see Equation 16) limited transient time step was used in dynamic simulations. Different maximum Courant number values were tested, since the Courant number has a direct effect towards the time step, thus effecting to the calculation time as well. When Courant number was examined, it was noted that the Courant number was high only in a few cells close to the outlet nozzle (see Figure 26). However, substantial increase in maximum Courant led simulation to become unstable. The Courant number seemed to become unstable at values of 3 and more, therefore the maximum local Courant number used in the simulations was 2.

$$Cr = \frac{u\Delta t}{\Delta x} \quad (16)$$

Cr	Courant number (-)
u	Local velocity (m/s)
Δx	Local cell length (m)
Δt	Time step (s)

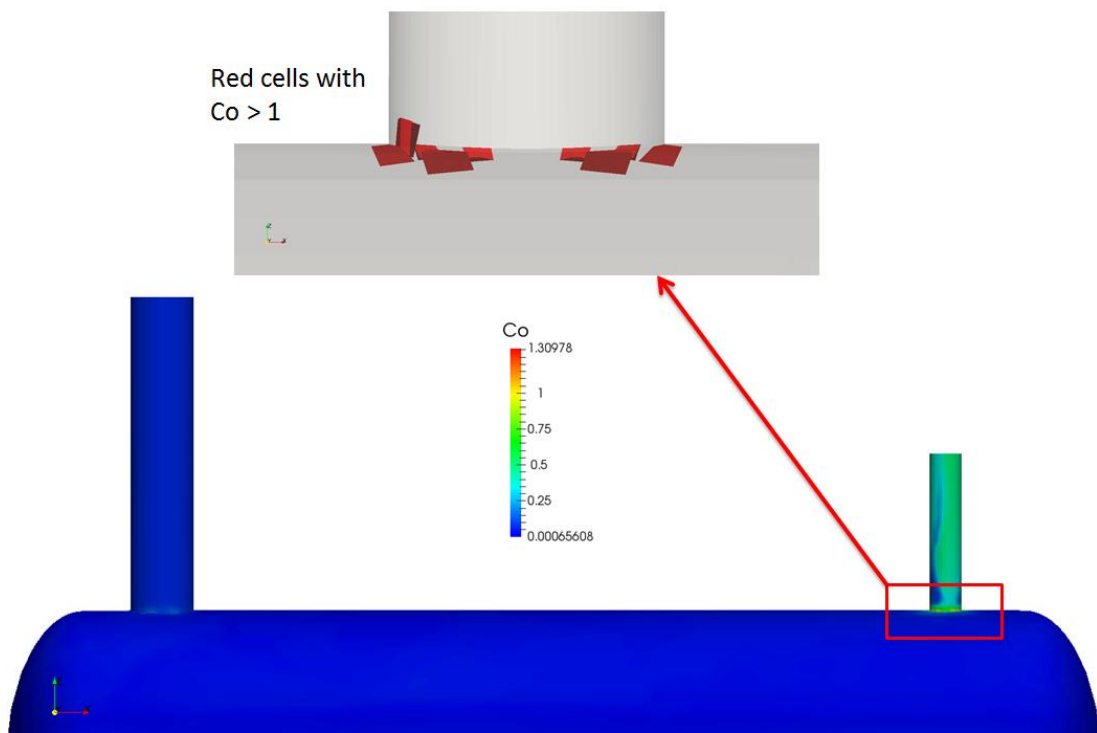


Figure 26. Limiting cells with the highest Courant number, when simulating the upper half of the vessel.

6.6 Boundary conditions

Two turbulence modeling approaches were used, and two others were tested during this thesis. The $k-\omega$ SST -model was selected as the initial approach, because of previous work done with the single phase flows by Huusari (2015). However, the turbulence model seemed to yield too dissipative results, which showed as all the chaotic motion disappearing especially near the phase interface, and an alternative approach was decided to use. Laminar flow model does not model the turbulence at all. Since there are no generally accepted turbulence models for two phase flow (Hiltunen, et al., 2009), and the aim of this thesis was not to test different turbulence models, laminar model was decided to use as the best alternative. This approach was used, when inlet and outlet configurations were tested. The effect of turbulence models is further discussed in Section 8.1.3.

Inlet was specified with the flow rate of 2.73 kg/s and volume fractions of 96.155 % for the gas phase and 3.845 % for the light naphtha phase. When turbulence model was used, the inlet turbulence was specified with mixing length of 0.2 m and turbulence intensity 5 %. All wall surfaces were simulated as a no-slip wall with zero surface roughness. The no-slip condition dictates the fluid movement as zero on the surface of the wall. Vapor outlet was specified with fixed relative mean pressure of 0 Pa (g). In the cases where full container was simulated, the liquid outlet was specified with liquid phase flow velocity of 0.543 m/s. The liquid outlet velocity was calculated in a way that the gas-liquid phase interface would remain at the same level for the entire time of simulation.

6.7 Data averaging procedure

The fluids and the flow of fluid have a natural tendency of instability. This causes every single solution to become unique, thus observations between different calculations and similarities in them are difficult to observe and evaluate. However, when the solutions are averaged these small seemingly random inaccuracies disappear and regularities are easier to observe. The Equation 17 was used to obtain average values of velocity field, when steady state simulations were used. The averaging procedure was also used similarly for transient calculations.

$$U_{AVG} = \frac{\sum_{i=1}^n U_i}{(n_n - n_i)} \quad (17)$$

U_{AVG}	Averaged velocity (m/s)
U_i	Velocity at iteration or time point i (m/s)
n_n, n_i	First and last points of iteration procedure

For steady state calculations the averaging procedure was conducted between iterations 1000 and 2000. For the transient calculations, the averaging procedure was more problem dependent. At the beginning of the simulations, especially when the upper half configuration was used, there is a major transient period. This is caused by the initial state, where the whole vessel is filled with gas. When the simulation starts, the gas space is expected to react more ideally at the beginning, since there are not yet liquid-gas interactions. Additionally, the entering liquid generates a liquid film that extends along the sides of the vessel and finally hits to the back-end of the vessel. This causes a liquid pile-up to the back-end of the vessel and leads to a poor separation efficiency. Similar behavior can be spotted consistently from all the simulations made with upper half configuration. However, there are no indications of similar behavior within the full vessel simulations. Therefore, this is not considered to present the normal behavior of the separator, rather it can be seen as a transient behavior.

From the averaging point of view, the upper half configuration presents also another problem. When the simulations are extended over a longer period of time, the accumulation of liquid begins to affect the results. Therefore, it is important to carefully select a period of time to be averaged, where neither of these effects, initial transient nor accumulation, are present.

6.8 Mesh dependency tests

The mesh creation is one of the demanding tasks of the CFD calculations. Mesh size affects the stability, robustness and the maximum accuracy at which the phenomenon can be modeled. Therefore, the mesh is required to be accurate enough at critical areas of the container. However, too accurate mesh can cause problems, for example in a high required calculation times and possible stability issues. (Siikonen, 2014)

To determine a suitable base mesh size, mesh dependency tests were conducted. In these tests mesh size was varied until mesh did not have an effect to the results. The mesh was refined using similar strategy in every case; the outlet and inlet pipes were more accurately refined and mesh was denser in the inlet and outlet pipes. Especially outlet pipe required higher refinement, because of the relatively small size of the outlet pipe. In Table 10 the base mesh sizes and sizes of the mesh are presented. Base mesh size means the size of the largest cells in the mesh. In the Figure 27 a sectional view of the meshes used is presented.

Table 10. Simulated cases for mesh dependency tests.

Case name	Coarse	Medium1	Medium2	Dense1	Dense2
Layers	Not used	Not used	Used	Used	Used
Base mesh size (mm)	100	55	55	20	15
Mesh size (Total number of cells)	4150	8470	15266	102971	178010

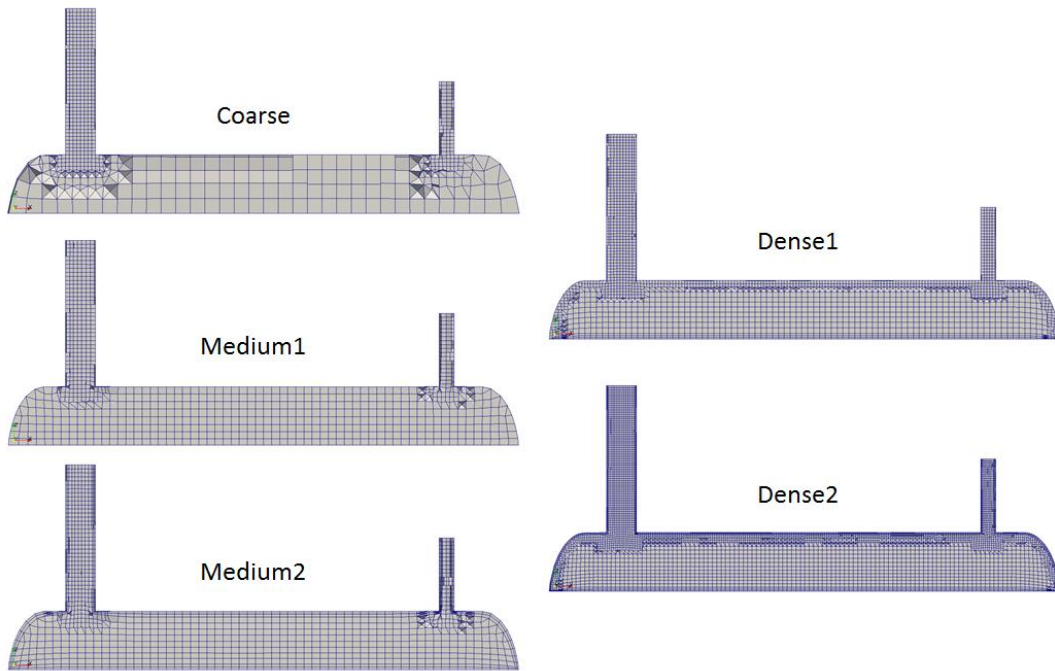


Figure 27. Sectional view of the meshes used in mesh dependency tests. From the top left down meshes are: Coarse, Medium1, Medium2. From the right side top: Dense1 and Dense2.

To determine an appropriate mesh size an analysis of the velocity profiles were made. The aim was to find a mesh with smallest number of cells that provided grid independent results. Data averaging procedure (presented in Section 6.5) was used between iterations 1000 and 2000. The average values of velocity were used, when the results were evaluated. The complete setup and boundary conditions can be seen from the Appendix 1. The evaluated velocity profiles can be found from Appendix 2.

Based on the simulated velocity profiles in the mesh dependency tests, a base mesh size was selected to be as 20 mm as in the case of Dense1. The Dense1-case presented good enough results with the gas phase, and when compared to denser case of Dense2, no remarkable differences between the results were found. However, in the two-phase simulations, bottom of the container contains mostly liquid. This phase was expected to have little effect to the case, and to make simulations more robust and quicker, a base mesh size of 40 mm was used when full size container was simulated. Furthermore, the upper half of container was always simulated by using a refinement box that would make a cell size to maximum of 20 mm.

Finer grid size was used for inlets and outlets. For example, in a case of Medium1, refinement level of 2 was used for both inlet and outlet. High refinement level was due to the small size of inlets and outlets, when compared to the container size.

7 Evaluation criteria

In this chapter, the evaluation criteria used to analyze the simulation results is discussed. The main parameters used to evaluate the results were monitoring area-averages of liquid volume fraction at the surface of the outlets, calculating the accumulation of liquid phase, and conducting an analysis of the velocity profiles at selected 2D cross-section in the computational domain. In addition a larger clip volume of data was analyzed. Additionally, wall shear stresses of the simulated vessels were calculated and evaluated.

7.1 Surface reports and liquid accumulation

Surface reports from the outlet were taken by using Helyx monitoring function feature. The used surface reports were written on 0.2 second intervals (simulation time). The monitored fields were flux and volume fractions of flow through the outlet patch. Liquid accumulation in the vessel can be calculated by integrating over the monitored outlet data and specifying the inlet flow constant (Equation 18).

$$V_{acc} = V_{in} - V_{out} = \varphi_{in} \cdot \alpha_{liquid,in} \cdot t - \int_{t=0}^{t=t} \varphi_{out} \cdot \alpha_{liquid,out} \quad (18)$$

Where φ is the volume flow (m^3/s), α is the volume fraction (-), t is time (s), and V the calculated volume (m^3).

With the accumulated volume of liquid, the separation efficiency can now be calculated (Equation 19).

$$\eta = \frac{m_{liquid,in} - m_{liquid,out}}{m_{liquid,in}} = \frac{V_{liquid,acc}}{V_{liquid,in}} \quad (19)$$

7.2 Velocity profiles

Velocity profiles are amongst the strongest indicators of the separators efficiency. However, since the calculations are transient, major variations between single time steps may exist. This might have an effect to the results, and thus averaging results is necessary. In the inlet and outlet configuration cases, all the used data is time averaged between 60 - 90 seconds simulation time. OpenFOAM gives an opportunity to analyze velocities in every 3D direction (x, y and z). In addition to this magnitude of the velocities was analyzed (Equation 20).

$$U_{magnitude} = \sqrt{U_X^2 + U_Y^2 + U_Z^2} \quad (20)$$

Cell size should also be taken into account. In CFD calculations there might be really small computational cells that may have unphysically high velocities. Additionally, when data is post-processed, the selection of certain 2D-slice may cause a cell area to become small. If there are multiple small cells with extreme velocity values, distortions may occur. Therefore, the cell size should also be considered when comparing the results. In this thesis the data cell size has been taken into account by either balancing the data cells with volume (Equation 21) or by area (Equation 22).

$$U_{x,vol,avg} = \frac{V_{cell,i}}{V_{cell,avg}} \cdot U_{x,i} \quad (21)$$

$$U_{x,area,avg} = \frac{A_{cell,i}}{A_{cell,avg}} \cdot U_{x,i} \quad (22)$$

Where $A_{cell,i}$ and $V_{cell,i}$ are the cell size (area or volume) of the measured data cell, $A_{cell,avg}$ and $V_{cell,avg}$ are the average cell size of the entire data series analyzed, $U_{x,i}$ is the x-directional velocity of the measured data point i.

In ideal case, the fluids travel with the ideal velocity from inlet to outlet. However, in reality, the instruments, or other geometry can cause local deviations from the ideal velocity. These deviations are expected to increase local velocity, which leads to worse

separation. For efficient separation the velocity profiles should be as equal as possible to prevent high gas velocities, especially near the liquid surface level. The hypothesis is that for more even flow profile, better separation efficiency is expected. The data was analyzed by using average (Arithmetic mean, Equation 23) and standard deviation values (Equation 24) from the datasets.

$$U_{AVG} = \frac{1}{n} \sum_{i=1}^n U_i \quad (23)$$

$$s = \sqrt{\frac{1}{n} \sum_{i=1}^n (U_i - U_{AVG})^2} \quad (24)$$

Two different types of movement analysis were performed. The first analysis was performed from different diagonal slices. The four slices were taken as illustrated in Figure 28. The second performed analysis was taken with larger volume of data. This was carried out by taking the data from cells limited by a clip. The clip placement is also presented in Figure 28. Data analysis of the gas flow profiles is made in Section 8.3.2.

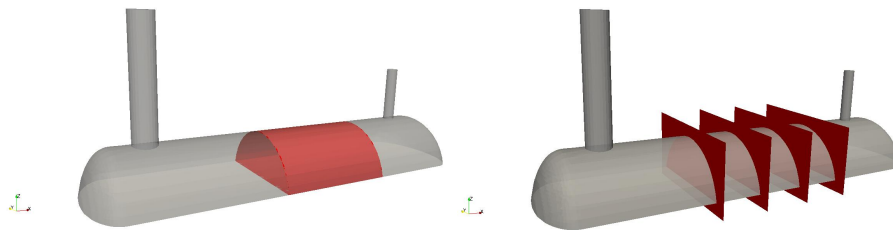


Figure 28. Analyzing the flow profiles of the vessel. Left: The clip of data that was analyzed is highlighted with red color. Right: Planes where the analyzed data is taken from.

The clip data has been selected in a way that it would describe the calmest area of the vessel. This was thought to be the volume, where an even flow profile would be the most critical for effective separation. The planes were selected in such a way that the evolution of the flow profile would be clearly shown, but the influence of inlet distributor and outlet suction would not be shown.

7.3 Wall shear stress

Wall shear stress describes the surface pressure caused to the wall by tangentially moving fluid. Essentially, a wall shear stress is the force that is caused to the wall by the surrounding fluid movement. Wall shear stress can be used to indicate the mechanical durability of design, since high shear stress enhances erosion or corrosion-erosion. However, one should be careful when assessing the wall shear stress values, since they are affected by transient nature of two phase calculations. Wall shear stress values are also mesh dependent, thus averaged values would be preferred when the shear forces are calculated.

In this work, the calculated wall shear stress values are much lower than real ones expected. The most likely reason is mesh, which should be denser near the walls to obtain more accurate results. Additionally, Helyx version of OpenFOAM currently does not have an alternative to directly depict wall shear stresses for two phase calculations. Wall shear stresses were calculated manually as a post-processing step for a single time-step, by using Swak4FOAM utility. Therefore, the used values are calculated by using transient values, which might have an effect to the results. The values presented in this thesis are from time step $t = 60$ s, unless otherwise stated. The time step was chosen for two reasons: behavior of the fluid flow pattern seems to be balanced, and the accumulation of liquid does not affect the fluid behavior at this state.

8 Simulation results

In this chapter the simulation results are presented. There were multiple cases that were studied during the simulations. The main focus was to model a gas-liquid phase separation vessel with Euler-Euler model. This required some model testing and simplifications due to the nature of multiphaseEulerFoam. The developed model was used to test different inlet and outlet distributors. The used geometry is presented in the Chapter 6.

Essentially, the simulations can be divided into two different groups. First is the development of the model; selection of boundary conditions and vessel geometry. The

second part is about simulating the different distributors and selecting a case that is the most suitable for gas-liquid separation with respect to liquid separation efficiency.

8.1 Model testing and optimization process

Three different schemes were tested: the effect of liquid phase droplet size, the effect of turbulence model, and the effect of compression term. Additionally, the effect of modeling liquid interface as a wall is discussed. All of the tested cases are presented in Table 11.

Table 11. Simulated cases for model testing and optimization.

	<u>Case name</u>	<u>Vessel type</u>	<u>Mesh size / Gas phase base mesh</u>	<u>What was tested</u>
Initial tests with full size vessel	EulerSM4	Full	67 000 / 35 mm	Initial test case with presented boundary conditions
	EulerLM4	Full	280 000 / 20 mm	Effect of larger mesh to simulation results
	EulerSM7	Full	79 000 / 35 mm	Minor tweaks to the base mesh, the effect of Courant Number, Inlet feed 200 %
Effect of droplet size	Euler_SD1	Full	67 000 / 35 mm	Liquid phase droplet size 50 microns
	Euler_SD2	Full	67 000 / 35 mm	Liquid phase droplet size 10 microns
	Euler_SD3	Full	67 000 / 35 mm	Liquid phase droplet size 30 microns
Effect of interface compression with large mesh	Euler_IFC	Full	511 000 / 10 mm	Interface compression term 1
	IFC_test1	Full	511 000 / 10 mm	Interface compression term 0.5
	IFC_test2	Full	511 000 / 10 mm	Interface compression term 0.25
	IFC_test3	Full	511 000 / 10 mm	Interface compression term 0
	IFC_test4	Full	511 000 / 10 mm	Interface compression term 0.5 with 50 micron liquid droplet size
Effect of turbulence modeling & simulating upper half of the vessel	Eulerwall2	Upper	109 000 / 17,5 mm	Simulating only upper half of the vessel
	Turbulence test1	Upper	101 000 / 20 mm	k-ε RNG turbulence model with upper half of the vessel
	Turbulence test2	Upper	101 000 / 20 mm	k-ε STD high Re turbulence model with upper half of the vessel
	Turbulence test4	Upper	101 000 / 20 mm	Laminar turbulence model with upper half of the vessel
	Turbulence test5	Full	536 000 / 12,5 mm	Laminar turbulence model with full vessel

8.1.1 The effect of liquid droplet size

The effect of liquid droplet size was found out to be crucial to the separation efficiency. When droplet size is decreased enough, liquid starts to drift with the gas phase. Solver reaches a state where separation of the liquid and gas phase no longer happens; liquid droplets are too small to be separated by gravitational force.

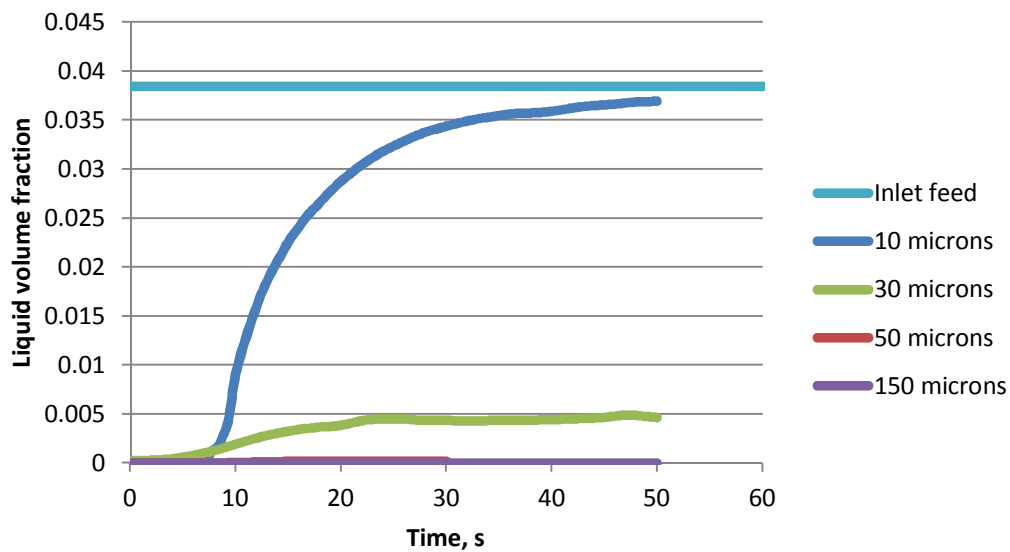


Figure 29. Liquid volume fraction in outlet from area-averaged surface reports.

As seen from Figure 29, the tests indicated that the separation efficiency in used CFD model was really sensitive to the liquid droplet size. Beginning of the simulations is similar in all cases; cause of this is the initial configuration (at the beginning the vessel is filled with gas). It takes about 9 seconds for gas to flow from inlet to outlet, and for the first liquid droplets to appear in the outlet. The initial test EulerSM4 with 150 μm droplet size yielded almost perfect separation (liquid outlet volume fraction stabilized at the level of $2 \cdot 10^{-5}$), EulerSD1 with 10 μm droplet showed no separation between liquid and gas, and all liquid droplets ended up to the gas outlet. However, even the 50 μm droplet size showed almost perfect separation with liquid outlet content of 0.0002. A 30 μm droplet size showed still effective separation, but with reasonable amount of liquid in the outlet as well. Therefore, a 30 μm liquid droplet was selected to be used in with the inlet and outlet configurations.

8.1.2 The effect of compression term

The Engys HELYX® user guide describes the compression term as a level of compression at the multiphase interface. User guide adds that it works as a $c\alpha$ correlation in the VOF solvers. The compression term can be set to a value between 0 and 1.5 or to the value of -1 (to switch off the compression term). As an example, the effect of compression is described as following: for values between 0 and 1 a conservative compression (increasing when higher values are used), and any value above 1 enhanced compression at the interface. (Engys Ltd, 2016) The demonstration of differences between Euler-Euler and VOF solver can be seen from the Section 4.1.2.

The effect of compression term was tested with five cases. Different values of 0, 0.25, 0.5 and 1 were tested. In addition, the effect of droplet size was tested. The case setup used was as described in Chapter 6. Liquid droplet size of 150 microns was used, but one test with 50 microns droplet size was also tested. The compression term worked as expected, compressing dispersed liquid droplets towards each other, and also trying to sharpen or create the interface at the phase interface level. Since inlet feed was specified as a fully dispersed liquid droplets with volume fraction of 0.03845 the effect was best shown in the inlet feed pipe (see Figure 30).

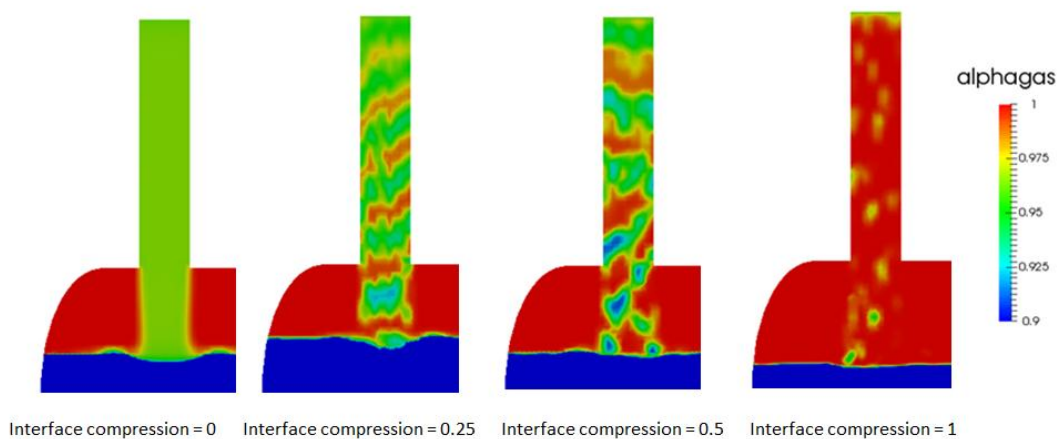


Figure 30. The effect of interface compression at the inlet. From left to right the cases are IFC_test3, IFC_test2, IFC_test1 and Euler_IFC. Alphagas is the volume fraction of gas.

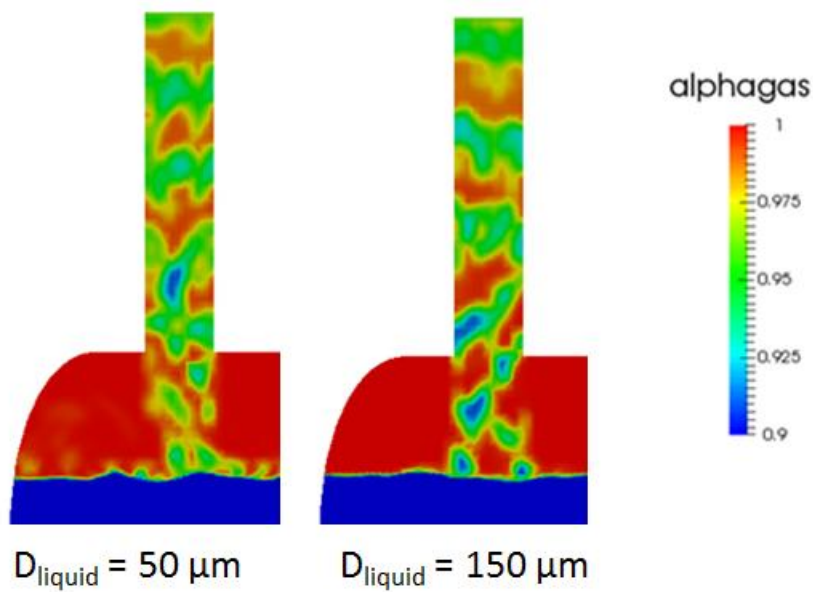


Figure 31. Effect of interface compression at inlet between different droplet sizes. The used interface compression value was 0.5. The α_{gas} is the volume fraction of gas.

At low interface compression values the effect was weaker than with the larger values. The compression also seems to be heavier with higher liquid droplet size (Figure 31). This is understandable since bigger droplet size means fewer droplets to compress with each other, the same amount of droplets compressing means smaller lumps with smaller droplet size. When interface compression term was increased to 1, mass balances were no longer feasible, *i.e.*, the compression term was compressing the liquid phase too much. The interface compression term seemed to work at lower values as expected, but it had only a small effect towards the results, and therefore it was decided not to be used in the further simulations.

8.1.3 The effect of turbulence modeling

Four turbulence models were tested: laminar (no turbulence modeling), $k-\omega$ SST, standard high Reynold $k-\epsilon$, and $k-\epsilon$ RNG. All of the used turbulence models were found very dissipative at the liquid surface level. Ultimately, this led to a really effective (over three times better than laminar model) separation of liquid phase from the gas phase (see Figure 32).

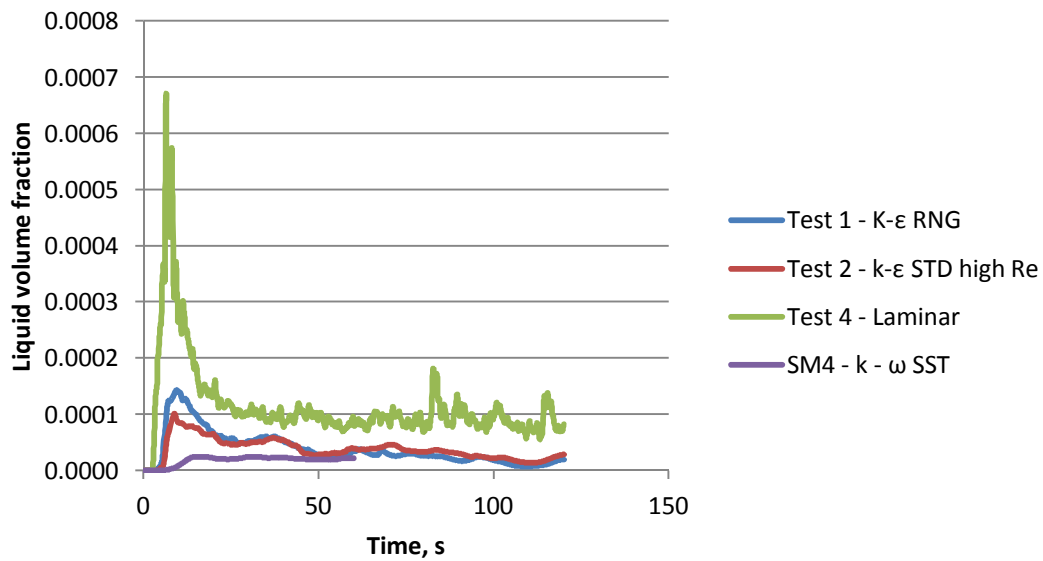


Figure 32. Liquid volume fractions in outlet. Turbulence tests.

Laminar modeling also seemed to have more transient behavior, both in the beginning and as the simulation continued. Turbulent multiphase flows are also very difficult to model and there are not any generally accepted turbulence model found from the literature (Hiltunen, et al., 2009). Since the behavior of turbulence model seemed to be too dissipative, and there were no other recommendations available, the laminar modeling was decided to be used when inlet and outlet configurations were studied.

8.1.4 Modeling the liquid level as a wall

The full vessel simulations featured a phenomenon, where inside the liquid outlet pipe, a small swirl was formed. In some cases this swirl caused really unexpected non-physical behavior when swirl intensified, and effectively caused the gas phase to be sucked inside the swirl. This caused a huge explosion-like mixing of the liquid and gas phase. Behavior seemed to appear randomly and fast, it did not appear in all cases, and when case was restarted from time step previous to the phenomenon; the event could not be reproduced. There were a few options that were studied to prevent the phenomenon. First the modeling of vortex breaker was considered. Other alternatives included the alteration of the geometry in a way that this swirl phenomenon could be prevented. Finally, it was decided that modeling the liquid level as a wall was the best alternative.

There are a few drawbacks from modeling the liquid level as a wall. Firstly, the accumulation of liquid would have an effect to the gas flow profile. Nevertheless, the liquid accumulation was assumed to be rather similar in all of the modeled cases, and thus the effect could be controllable. Minor deviations between distributors were expected. The second drawback is obviously the loss of the bottom of the vessel. However, the full vessel simulations showed that the liquid phase below the interface remained calm, and the gas flow was not penetrating the liquid surface, nor it was causing sizable waves. Therefore, modeling the liquid level as a wall was considered as the best alternative for the full vessel simulations, and it was selected for the rest of the cases.

8.2 Studied inlet and outlet configurations

Five different inlet distributors (ID) and two outlet distributors (OD) were studied. This chapter presents all of the inlet and outlet configurations cases as case by case. Comparison between different inlet and outlet configurations is presented in the Section 8.3. The complete geometrics used are presented in the Section 6.1.2. The inlet and outlet simulations were 180 s long. All of the tested cases are presented in the Table 12.

Table 12. Simulated cases for inlet and outlet configurations.

	<u>Case name</u>	<u>Vessel type</u>	<u>Number of cells / Gas phase base mesh</u>	<u>What was tested</u>
Inlet distributors	NOID	Upper	84 000 / 20 mm	Reference case
	ID1	Upper	113 000 / 20 mm	Inlet distributor 1
	ID2	Upper	174 000 / 20 mm	Inlet distributor 2
	ID3	Upper	170 000 / 20 mm	Inlet distributor 3
	ID4	Upper	217 000 / 20 mm	Inlet distributor 4
	ID5	Upper	214 000 / 20 mm	Inlet distributor 5
Outlet distributors	OD1	Upper	91 000 / 20 mm	Outlet configuration 1
	OD2	Upper	91 000 / 20 mm	Outlet configuration 2
	ID4_OD1	Upper	226 000 / 20 mm	ID4 with OD1
	ID4_OD2	Upper	226 000 / 20 mm	ID4 with OD2
Inlet feed	SP200	Upper	84 000 / 20 mm	Inlet feed 200 %
Droplet size	50_ID4	Upper	217 000 / 20 mm	Liquid droplet size 50 microns
Single phase simulations	SP_ID4	Upper	217 000 / 20 mm	Single phase with ID4

The gas phase simulation (SP_ID4) was simulated using pisoFoam -solver. Other cases were simulated using the setup presented in Chapter 6. Tests made with increase of inlet feed (SP200) and larger droplet size (50_ID4, 50 microns vs. 30 microns) showed that the used model is really sensitive for the initial conditions. The increase in inlet feed flow rate caused separation efficiency to drop to practically zero, whereas the larger droplet size caused separation to become almost perfect (See Figure 33).

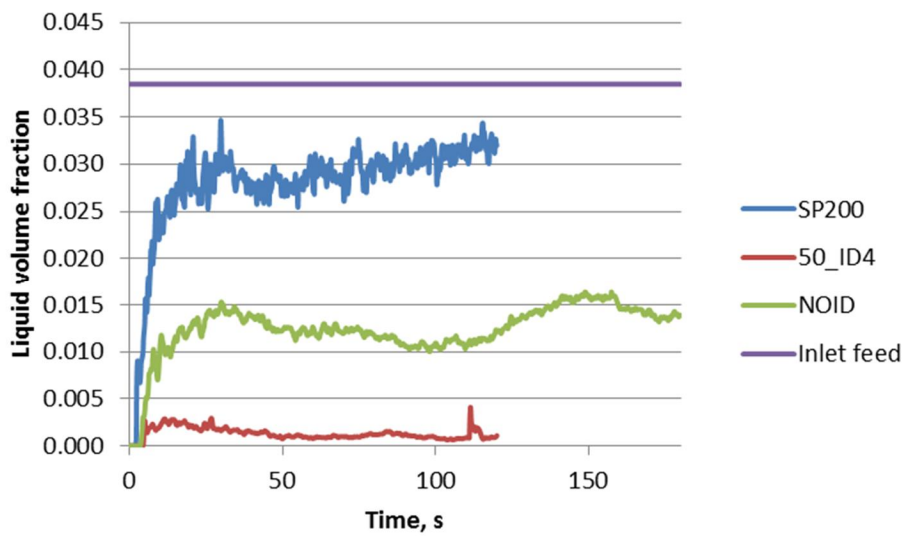


Figure 33. Liquid volume fraction in outlet measured with surface report.

The sensitivity of the model (as presented in Figure 33) was expected after the initial tests with the model, which showed that the increase in liquid droplet size effects heavily to the separation efficiency. The increased feed seems to effect to the model really heavily too. Behavior seems to be in-line with the expectations based on the droplet settling theory (discussed in Chapter 2), the increases in gas velocity cause liquid droplets to carry out with the gas flow.

8.2.1 NOID (No inlet distributor)

No inlet distributor case was studied as a reference case. The geometry with stream tracers to track flow patterns are presented in Figure 34. Figures of stream tracers in different camera angles are presented in Appendix 3.

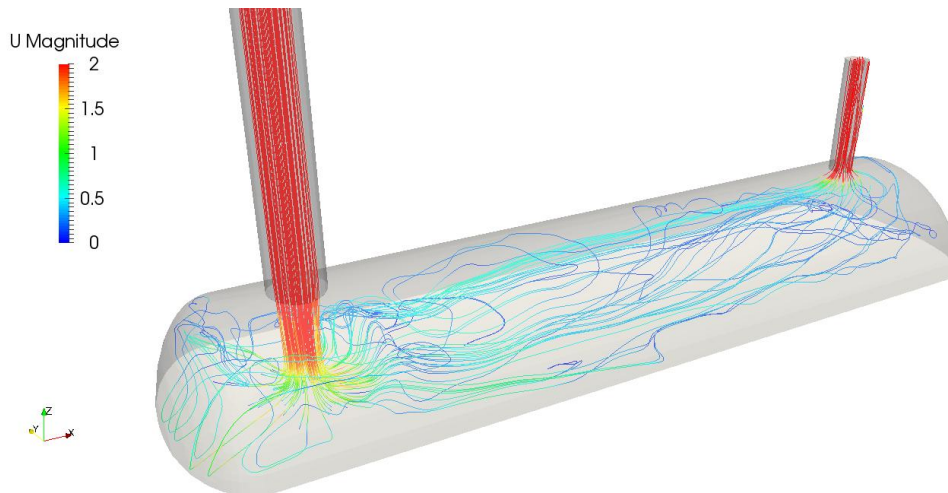


Figure 34. No inlet distributor case with stream tracers to describe a flow orientation from inlet pipe. The U magnitude scale is in m/s.

With no inlet distributor the inlet flow hits straight towards the liquid plane below the inlet. This causes flow to distribute in every direction along the surface level. In front of the feed a small swirl is created. Also a front end of the vessel has a small swirl. The flow profile seems to even out along the vessel. The highest gas velocities are right above the liquid level near the vessel side edges, while the top of the vessel features a backward flow (in x-direction).

Wall shear stress seems to have only a minor effect at the vessel (Figure 35). The outlet pipe seems to be under the most stress. The velocities are also much higher around the outlet. In addition, wall shear stress figures are largely affected by the mesh and thus the values are probably quite much lower than actual ones. Mesh is actually quite much denser at the outlet pipe than within the large area of vessel, and this might also have an effect on the wall shear stress values. Nevertheless, the front end values are comparable with other cases, and can give initial indications of the largest mechanical wear, or indicate possible corrosion areas.

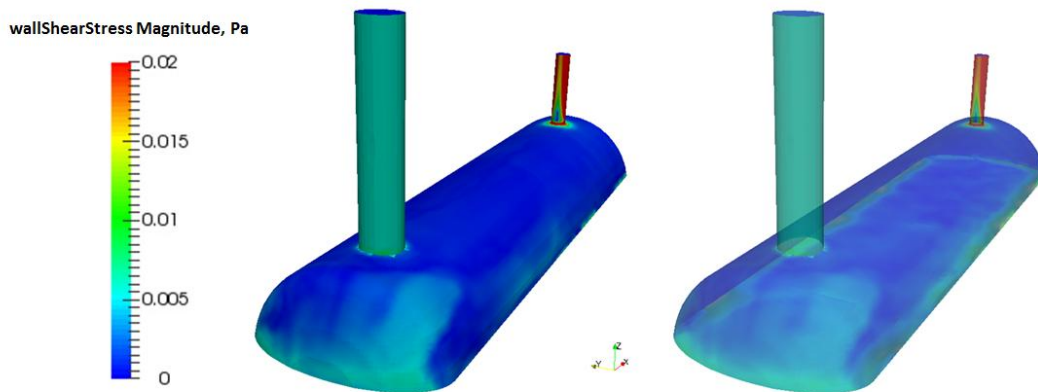


Figure 35. Wall shear stress in the NOID case.

8.2.2 ID1 (Sloped impact plate)

The sloped impact plate consists of a sloped cut pipe with impact plate at the bottom. The impact plate is at 60 degree angle towards the initial flow movement. The dimensions of the distributor can be found from section 6.1.2. The ID1 configuration turns the flow towards to the front end of the vessel, and a quite large swirl is created to the front end. This swirl guides the flow towards the top of the vessel. The inlet distributor also causes a larger backward flow from the middle of the vessel towards the distributor. This flow path crosses with the swirl coming from the front end, and seems to cause the flow to be pushed downwards and more towards the vessel walls. The main flow path from the inlet can be seen with stream tracers in Figure 36.

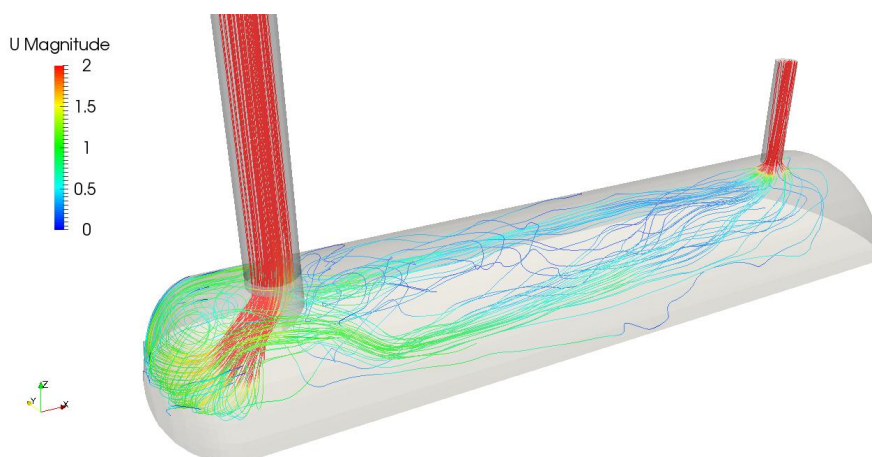


Figure 36. The sloped impact plate case with stream tracers to describe a flow orientation from inlet pipe. Coloring describes the velocity of flow in m/s.

Wall shear stress seems to be caused mainly towards the distributor's edge (see Figure 37). There is also an indication of small wear in the front end, but interestingly this geometry does not seem to cause high enough velocities to cause higher wall shear stress values.

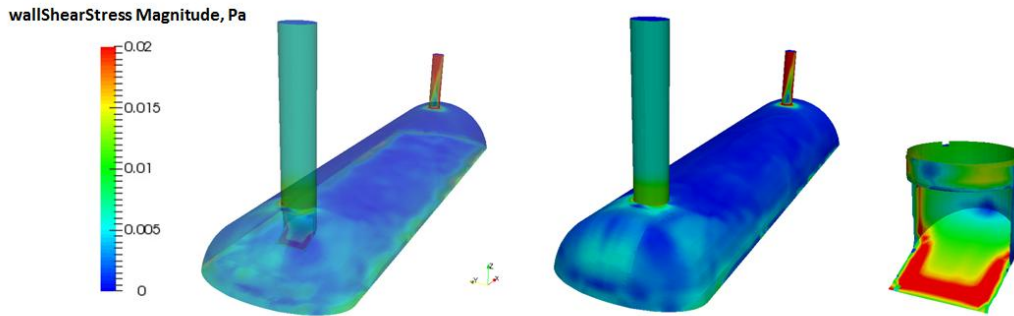


Figure 37. Wall shear stress in the ID1 case.

8.2.3 ID2 (Impact plate)

The corner impact plate is a square plate placed directly under the inlet pipe with a corner plate towards the outlet. The distributor is placed in one inlet feed pipe diameter length away from the pipe, and its side is two times the length of feed pipe diameter. The geometry with stream traces representing the flow path from the inlet can be seen in Figure 38.

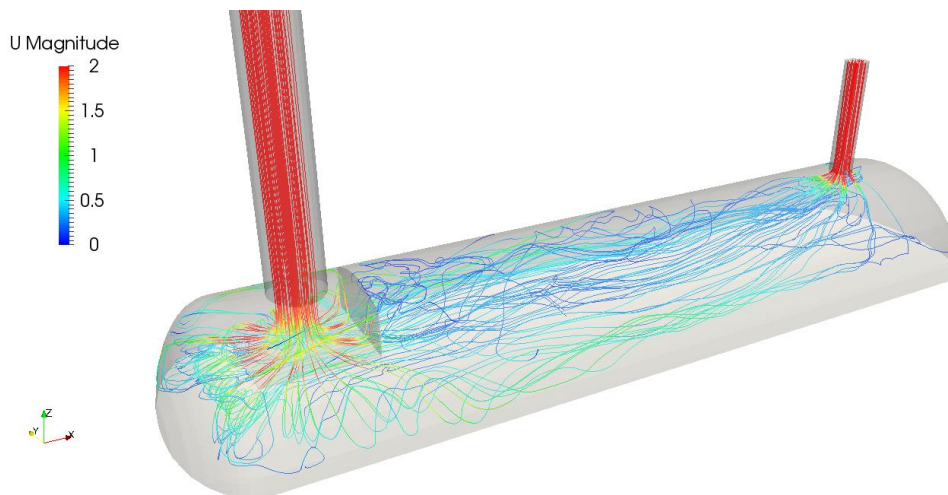


Figure 38. The corner impact plate case with stream tracers to describe a flow orientation from inlet pipe. Coloring describes the velocity of flow in m/s.

The corner impact plate distributes the flow quite evenly along the plate (Figure 38). The flow is mainly guided towards the sides and below the distributor. When ID2 is compared to the ID1, the ID2 does not guide the flow directly into the front wall, rather it distributes similar to the NOID case. This and the restrictions to the flow caused by the impact plate, lead to high gas velocities to develop below the distributor. This is a unique behavior; since there are no other distributors studied that have major flow profile pathing in the middle of the vessel or under the distributor.

With liquid accumulation, this flow orientation causes problems. The high velocity area under the distributor is particularly interesting, since it is highly dependent of the liquid surface level. Actually, it seems that when the liquid surface reaches a certain critical point and this path is almost filled with liquid, the entire flow profile changes. It seems that this change causes large swirl to form at the back of the vessel between 150 and 180 seconds. It is not entirely clear if this is the sole cause of the swirl, but in other simulations the effect is not nearly as powerful, even with the same or higher liquid accumulation levels. However, operating vessel with such a high liquid levels is not realistic nor it is used in the process industry. The forming swirl can be seen with the stream tracers in Figure 39.

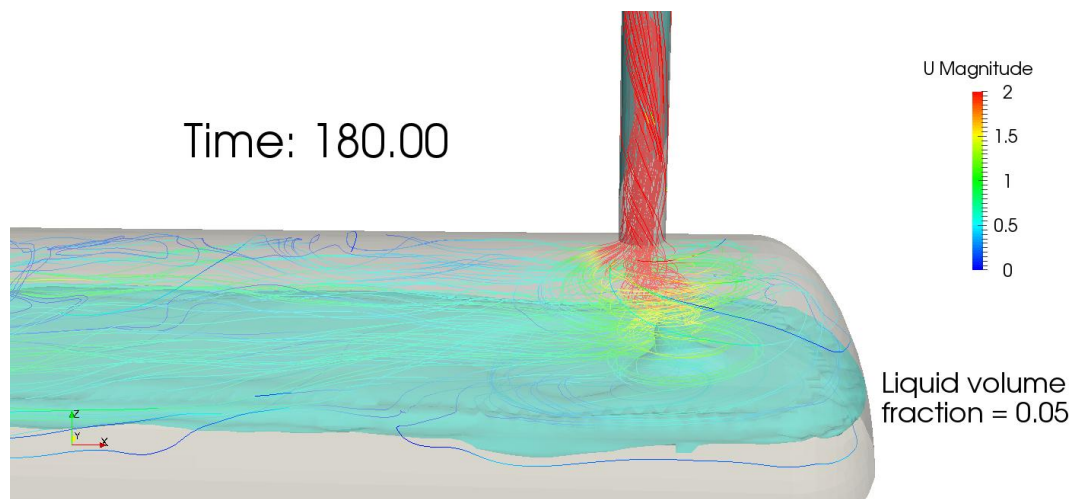


Figure 39. Forming back-end swirl with stream tracers and a contour to present the liquid volume fraction 0.05 interface. The stream tracer lines are colored representing the velocity of flow (m/s).

Wall shear stress seems to be caused mainly to the top vessel wall between inlet pipe and the edge of impact plate (Figure 40). Additionally, the distributor's edges have also high shear stress values, which increase almost symmetrically from the middle of the distributor toward edges.

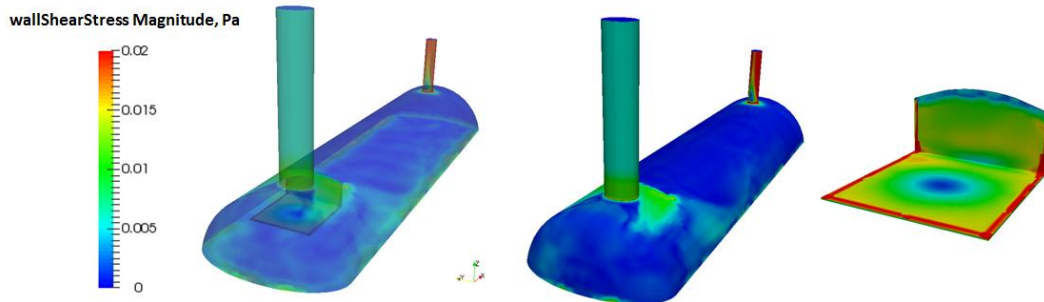


Figure 40. Wall shear stress in the ID2 case.

8.2.4 ID3 (Curved pipe type 1)

The curved pipe type 1 is an inlet distributor made from standardized 90 degree pipe angle. The pipe curve arc height is 304.8 mm. The geometry with stream tracers can be seen from Figure 41.

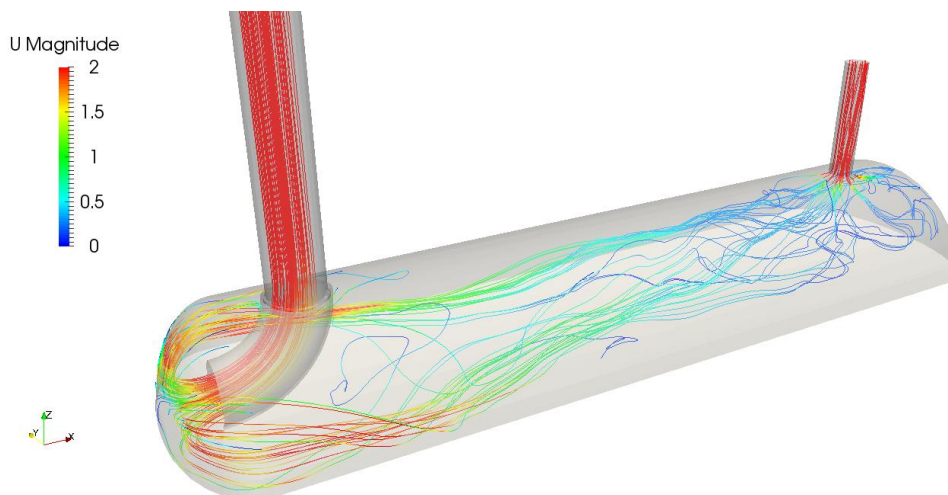


Figure 41. The ID3 case with stream tracers to describe a flow orientation from inlet pipe. Coloring describes the velocity of flow in m/s.

The curved pipe distributor guides the flow directly towards the f end of the vessel, where it splits towards the sides and top of the vessel. This causes the backward flow to become more intensive in the middle of the vessel than with the impact plate cases. Furthermore, this causes the vessel to have two forward moving zones (in both sides, near the liquid level) and one backward zone (middle, top). The profile evens out towards the outlet.

The shear stress values seem to be highest at the bottom of the distributor pipe (Figure 42). Additionally, shear stress values are higher right above the distributor pipe and at the sides. These are the areas that would probably require wear plates to provide protection against corrosion.

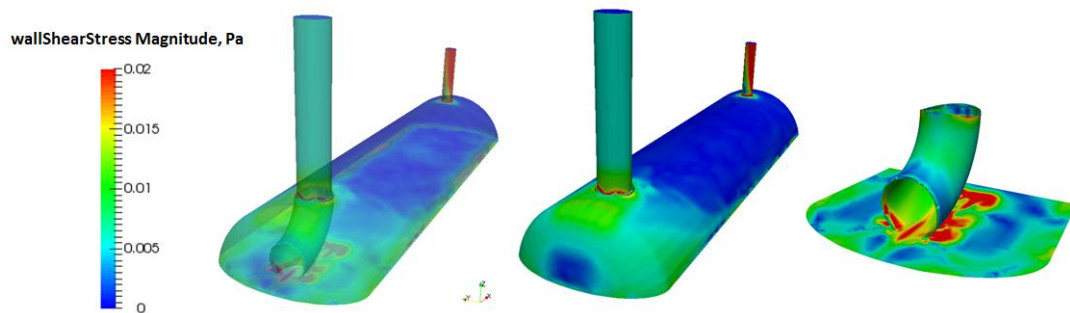


Figure 42. Wall shear stress in the ID3 case.

8.2.5 ID4 (Curved pipe type 2)

The second type of curved pipe was fixed in a way that it fits inside the vessel, *i.e.* the inlet nozzle was moved along the vessel towards the outlet by 323.4 mm. Additionally, 300 mm extension pipe was installed after the 90 degree bend. This guides the flow to the front end of the vessel. The geometry with stream tracer can be seen in Figure 43.

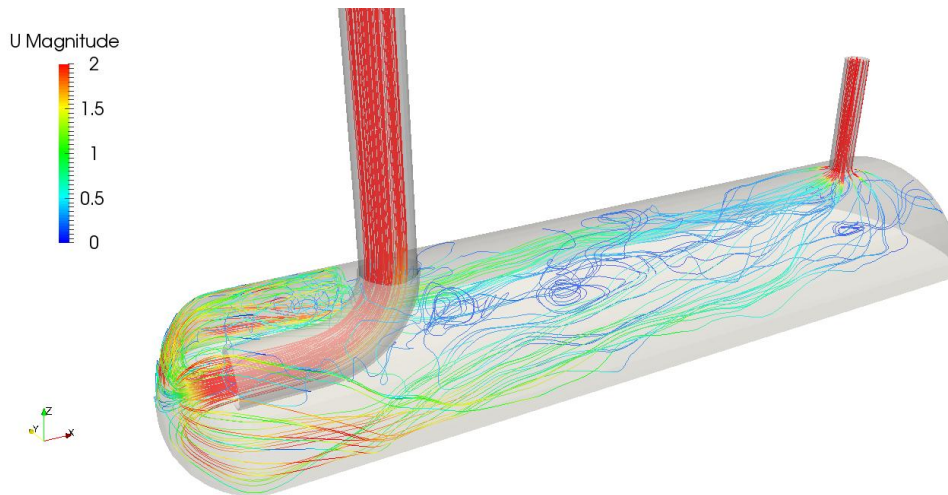


Figure 43. The ID4 case with stream tracers to describe a flow orientation from inlet pipe. Coloring describes the velocity of flow in m/s.

The ID4 distributes the flow quite like ID3; the flow is guided to the back end of the vessel. The main flow pathing (as in Figure 44) goes to the vessel side walls and slowly returns towards the middle, when flow profile develops further. The upper part behind the distributor features again the backward flow phenomenon.

Wall shear stresses seem to be caused similarly than with the ID3 case. However, the bottom of the distributor pipe has a little bit increased values, as well as the top of the front end of the vessel (see Figure 44).

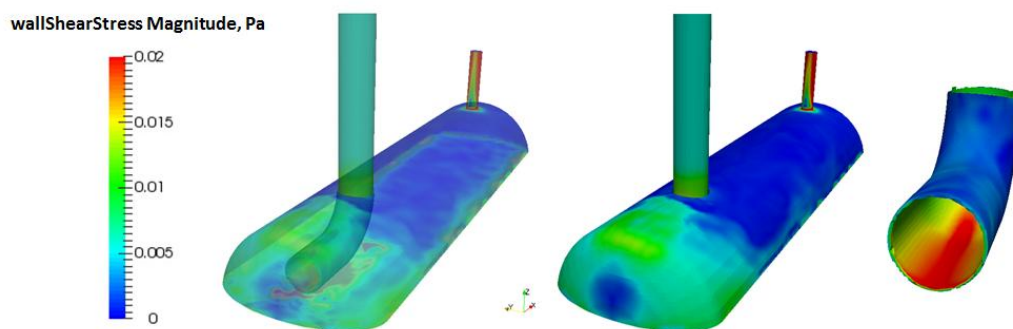


Figure 44. Wall shear stress in the ID4 case.

8.2.6 ID5 (Curved pipe type 3)

The curved pipe type 3 follows the same geometry than with type 2. The only alteration is with the extension pipe; it is only a half-pipe (top open). This allows flow to bounce towards the top of the vessel a little bit earlier than with the ID4 case. However, this does not seem to have a huge effect towards the flow profile. The ID5 case geometry with stream tracers from the inlet can be seen from Figure 45.

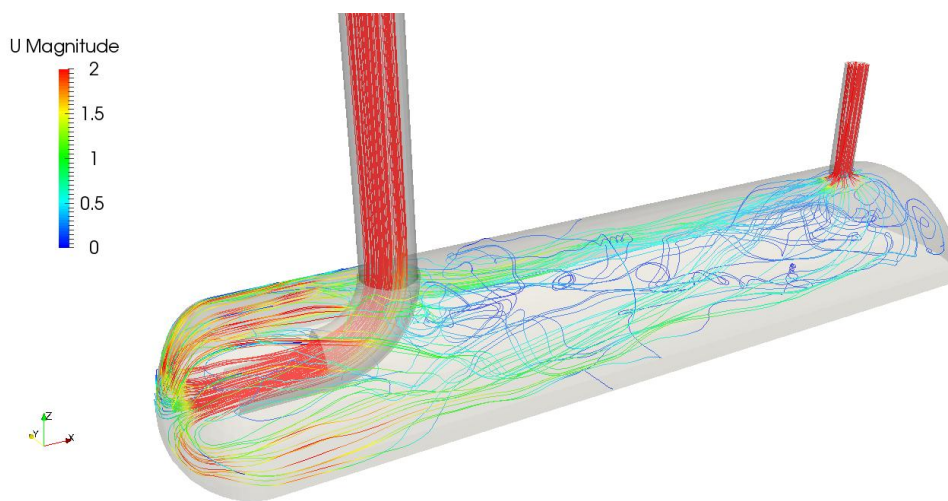


Figure 45. The ID5 case with stream tracers to describe a flow orientation from inlet pipe. Coloring describes the velocity of flow in m/s.

Interestingly, the ID5 wall shear stresses seem to differ from ID3 & ID4 cases (Figure 46). The shear stress values at top of the vessel wall are clearly higher, whereas at the sides of the vessel the shear stress values are lower. The difference is probably caused by the top of the distributor pipe being open. The distributor pipe seems to have similar shear stress values than with the ID4 case.

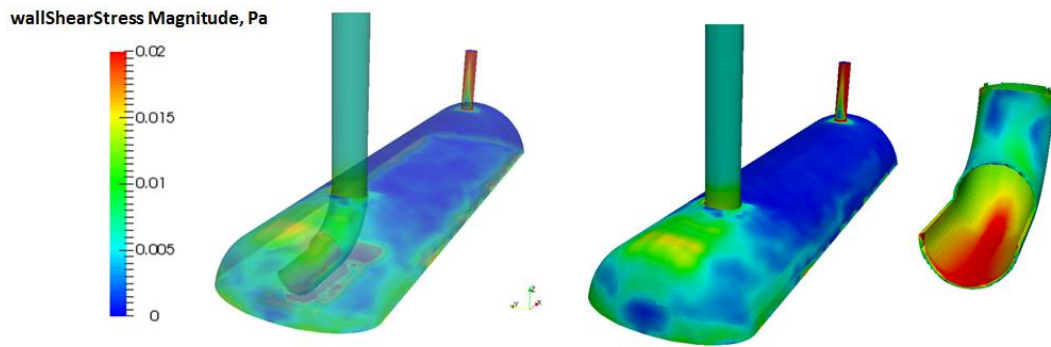


Figure 46. Wall shear stress in the ID5 case.

8.2.7 Outlet distributors

Two different outlet distributors were tested with ID4 and NOID cases. The stream tracers from NOID case with the both outlet configurations are presented in Figure 47 & Figure 48 (OD1 and OD2 cases, respectively).

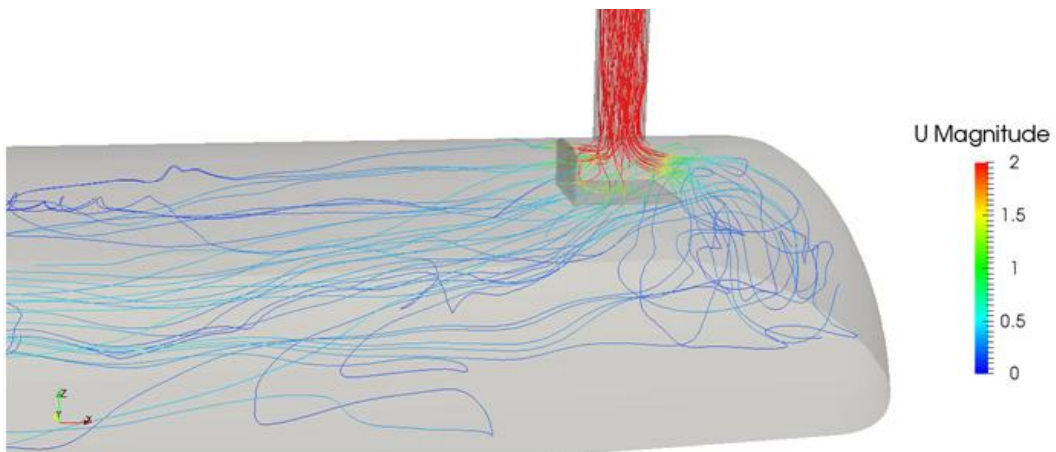


Figure 47. Stream tracers of OD1 near the outlet with NOID vessel configuration.

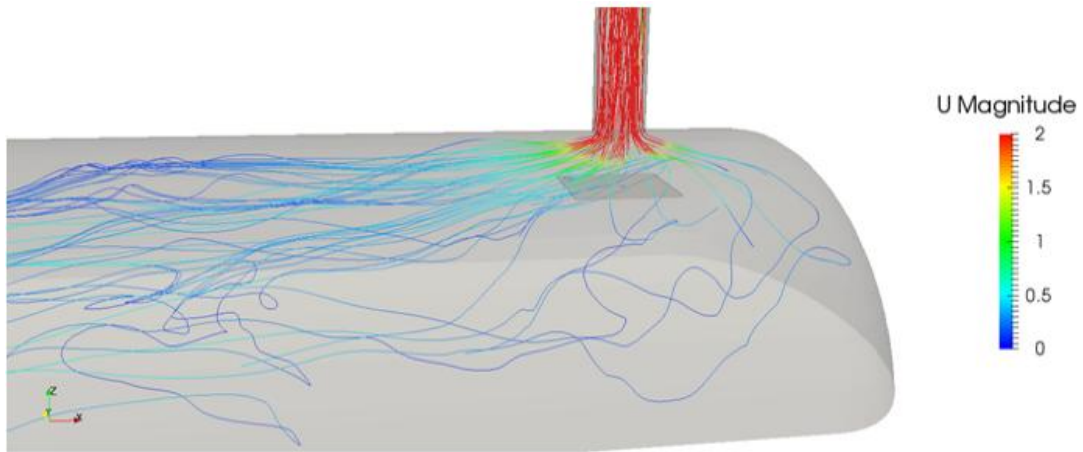


Figure 48. Stream tracers of OD2 near the outlet with NOID vessel configuration.

The outlet configurations had only minor effects to the flow field. OD1 forces flow to go around the corner end plate, but this does not seem to effect the separation efficiency much. OD2 blocks only the route directly below the plate, and seems to effect even less. In Figure 49 and Figure 50 the outlet configurations are presented with the ID4 configuration.

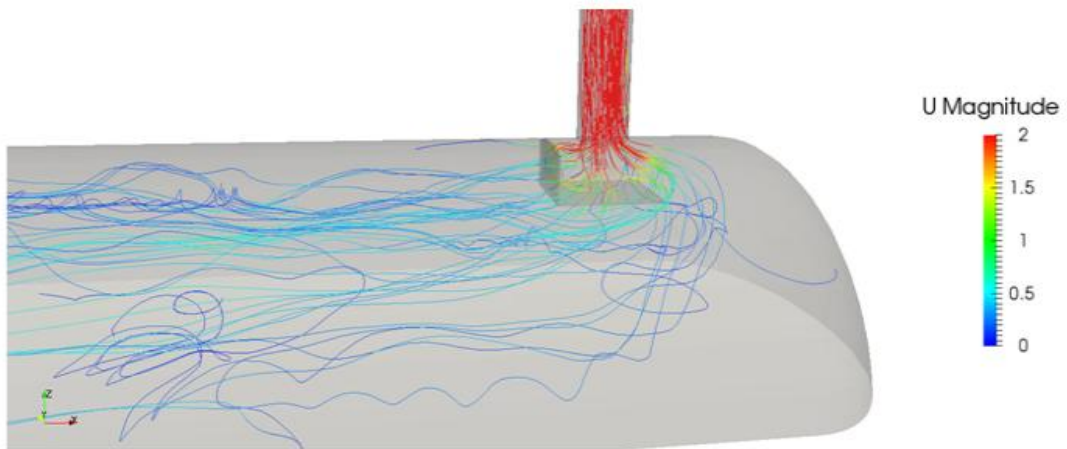


Figure 49. Stream tracers of OD1 near the outlet with ID4 vessel configuration.

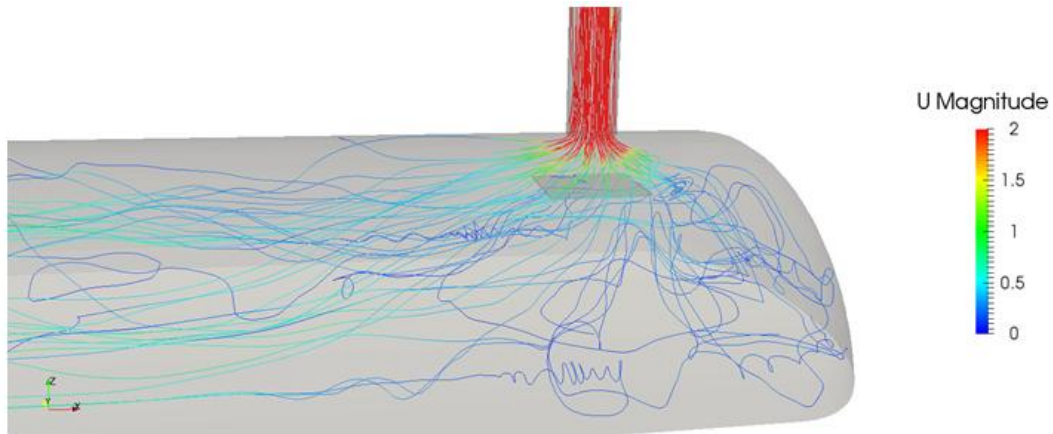


Figure 50. Stream tracers of OD2 near the outlet with ID4 vessel configuration.

Outlet distributors with ID4 are similar to the NOID cases. Outlet distributors do not seem to effect to the flow field in any significant way. The flow velocities seem to be really similar in all of the cases. Further comparison between outlet configurations is taken in Section 8.4.

8.3 Comparison of inlet configurations

In this section, a comparison between inlet configurations is made. The separation efficiency and gas flow profiles are discussed, respectively. The separation efficiency and gas flow profile were analyzed as presented in Chapter 7.

8.3.1 Separation efficiency

Separation efficiency was measured by analyzing velocity profiles and observing the outlet liquid content by monitoring the outlet with surface report. The surface report results for different inlet distributors can be seen from Figure 51.

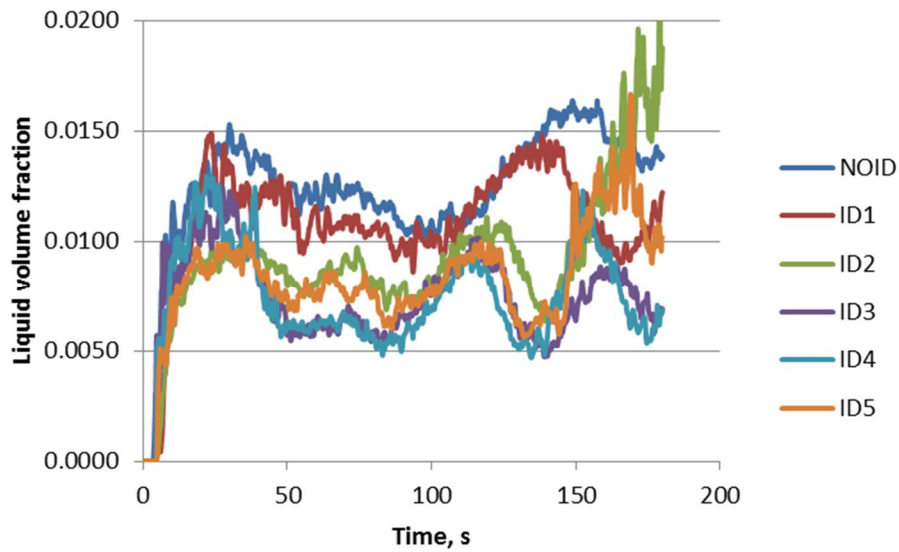


Figure 51. Effect of inlet configuration to liquid volume fraction in outlet.

There are two clear trends in the liquid outlet content (Figure 51). First is the transient period in the beginning of every case. This transient period is caused by the initial condition (whole vessel is filled with gas), and this takes between 30 and 40 seconds to even out. The second seen phenomenon is the transient behavior of the cases at later stage. The main cause of this behavior is the accumulation of liquid, and the rise of the gas-liquid phase interface. This seems to start after 100 s of simulation. However, this behavior is not equal between the cases. For example, ID2 liquid content stays almost the whole simulation below 0.01, but at the latter state (after 150 s) the liquid content rises higher than with any other case.

When the liquid volume fraction in outlet is integrated (as presented in Section 7.1 Equations 19 & 20), gathered data indicates the accumulation of liquid, and separation efficiency of the distributors can be calculated (Figure 52 & Figure 53).

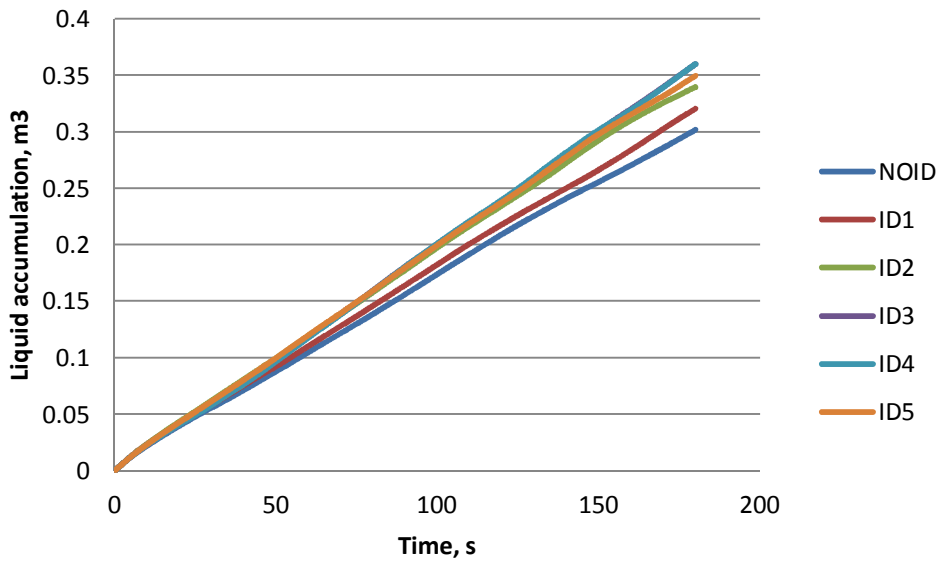


Figure 52. Accumulation of liquid between different inlet distributors as a function of time.

Liquid separation efficiency, 0 -180 s

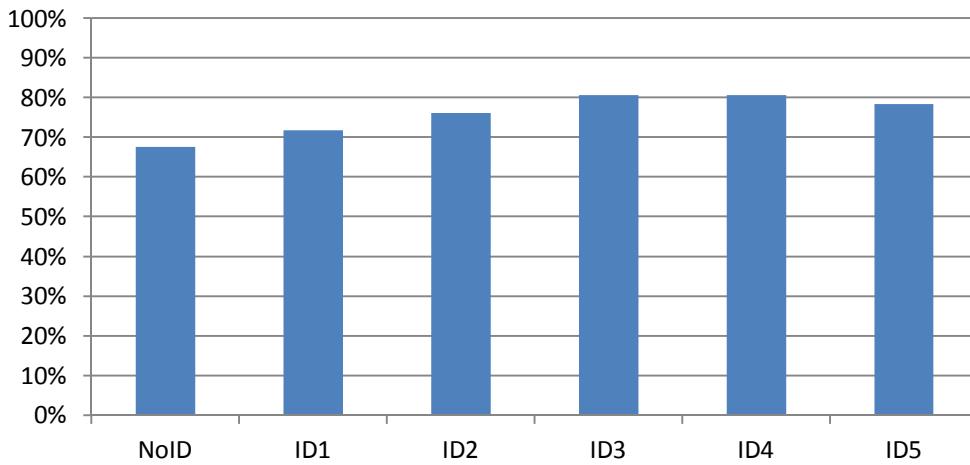


Figure 53. Liquid separation efficiency between 0 and 180 seconds.

When the total separation efficiencies over the entire simulation are compared (Figure 53), there are two distributors, ID3 and ID4, which seem to perform over the 80 % rate. The liquid accumulation (Figure 52) indicates that NOID and ID1 are clearly weaker than the other distributors, showing lack of separation efficiency already at the early stages. However, in other cases the differences are smaller and only occurring at the later stages of the simulation. The accumulation of liquid affects these results, and the effect seems to

differ between cases. In Table 13 the separation efficiency is presented in smaller time periods to give clearer indication of transient behavior and performance differences.

Table 13. Evolution of liquid separation efficiency at different time periods. Here green refers to relatively good separation efficiency and red for poor one.

Time period	NOID	ID1	ID2	ID3	ID4	ID5
0 - 20s	79.9 %	85.3 %	87.3 %	82.9 %	82.2 %	85.9 %
20 - 40s	64.1 %	66.9 %	75.7 %	72.4 %	71.8 %	75.9 %
40 - 60s	67.4 %	70.1 %	78.1 %	83.0 %	83.2 %	80.0 %
60 - 80s	68.3 %	72.2 %	77.4 %	83.9 %	84.1 %	79.6 %
80 - 100s	71.6 %	74.0 %	80.2 %	83.2 %	84.9 %	81.7 %
100 - 120s	71.1 %	71.5 %	75.1 %	76.8 %	78.2 %	76.8 %
120 - 140s	64.2 %	64.9 %	76.8 %	82.3 %	84.7 %	81.2 %
140 - 160s	59.1 %	68.1 %	75.5 %	82.0 %	76.0 %	75.3 %
160 - 180s	63.4 %	73.8 %	59.5 %	80.3 %	81.8 %	69.3 %

Table 13 gives a better view of the performance of distributors. The first 40 seconds can be considered to behave as transient, but actually there are quite large differences between the cases. The two best performing distributors (ID3 & ID4) are performing relatively weakly at the beginning of the simulations. This causes their separation efficiency to show weaker results over the entire simulation than they probably would if experimental tests were made. Nevertheless, they seem to outperform all the other at the most critical stage between 60 and 90 seconds. This is the time range that indicates the normal state behavior the best, since the beginning transient has stopped influencing, and the accumulation of liquid does not affect the results yet.

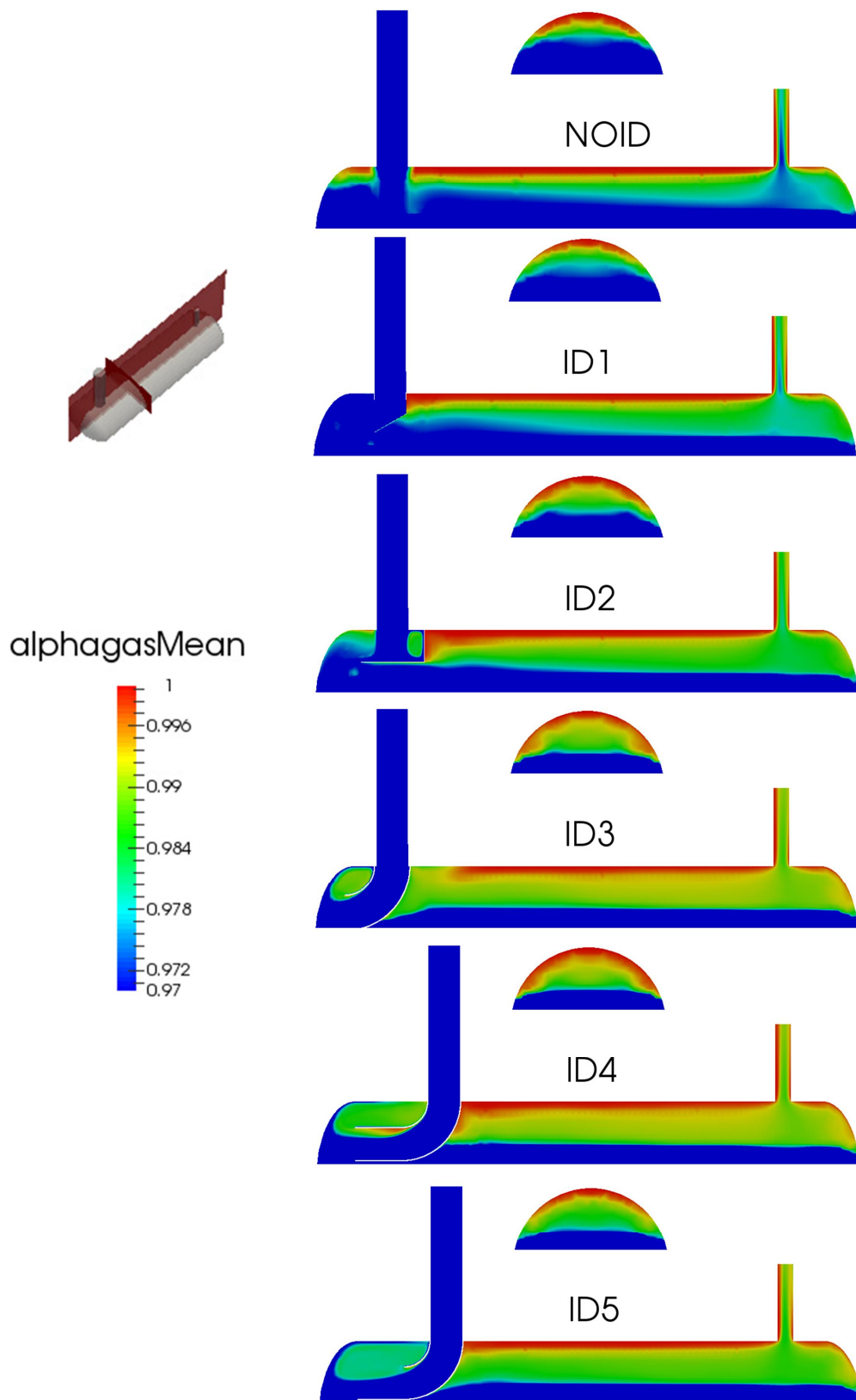


Figure 54. Gas volume fractions with different inlet distributors. Values are averages between time period of 60 and 90 seconds. The alphagasMean is the averaged volume fraction.

When Table 13 results are compared to the liquid content in gas space (Figure 54), the correlation between liquid separation efficiency and liquid content in gas space seems evident. The separation efficiency data would clearly indicate that the best performing distributors are ID3 and ID4, whereas ID1 seems to be the worst distributor. However, reference case NOID performs the worst. This indicates that usage of inlet distributor would always have a positive impact towards the separation efficiency. Additionally, it would seem that the impact plates perform weaker than the curved pipe configurations. One of the reasons could be separation effect caused pipe the pipe curve (Figure 55). In impact plates the effect is visible, but weaker (Figure 56).

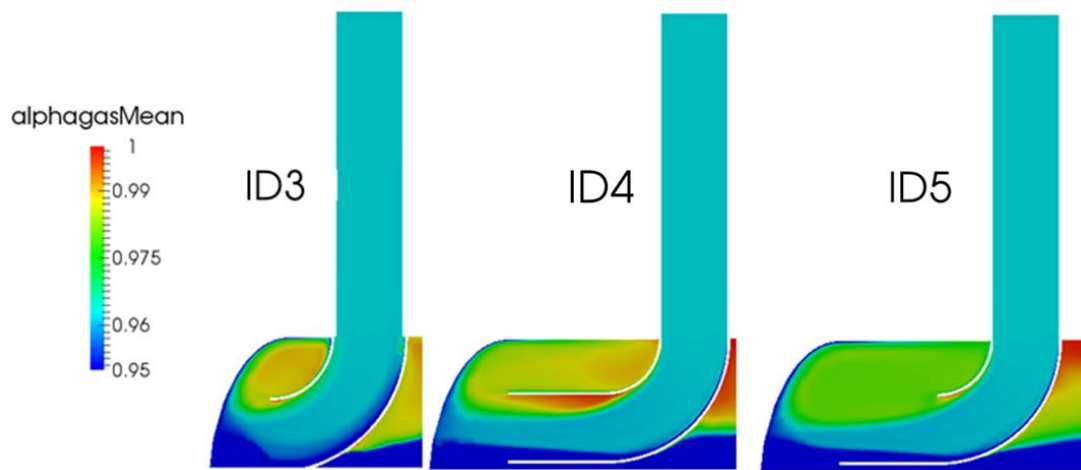


Figure 55. Separation effect within pipe curve in different pipe distributors. The alphagasMean is the averaged volume fraction.

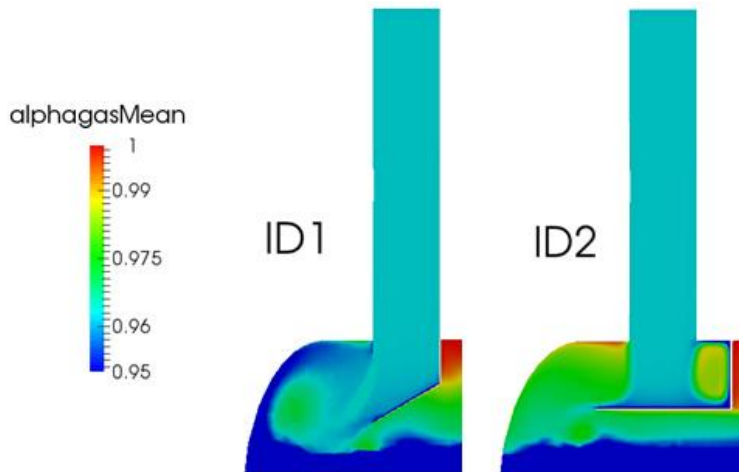


Figure 56. Separation effect in impact plates. The alphagasMean is the averaged volume fraction.

8.3.2 Gas flow profiles

A thorough investigation for gas flow profiles was performed to study if the gas flow profile data would support the separation efficiency. An ideal flow profile was expected to correlate with higher separation efficiency. The used values are averaged data between 60 and 90 seconds (see Section 6.6 for averaging procedure). The data was analyzed as a clip and as 4 slices (see Section 7.2). The diagonal slices with schematic view of flow profiles can be found from Appendices 4 & 5. All the figures from analyzed data can be found from Appendices 6 & 7 (for clip and slice data, respectively).

The lateral movement was found out to carry most of the magnitude of the flow. This behavior was expected and consistent in every case. The evenness of flow profiles were measured using standard deviation of gas flows (according to the Equation 24 in Section 7.2). The standard deviation was calculated for each slice separately. The standard deviations for slices are presented in Figure 57.

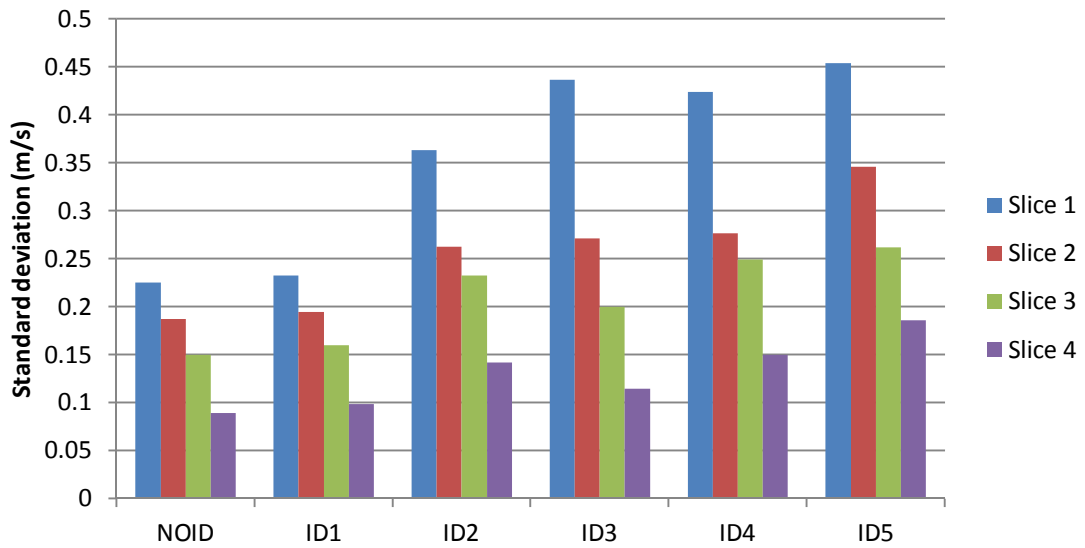


Figure 57. Standard deviations of horizontal gas velocities in slice data, case by case. Slice locations are shown in Figure 28.

Figure 57 shows that in every distributor case the gas flow profile evens out, when observation point is moved towards the outlet. Additionally, lowest observed deviations are with the NOID case, which would imply that the NOID case has the best, *i.e.* the most even flow profile. According to the data, it seems that there is no clear correlation between flow profile evenness and separation efficiency. However, the separation efficiency of NOID case was the worst, whereas ID4 and ID3 performed the best (Section 8.3.1, for example Table 13). This is inconsistent to the flow profile hypothesis (presented in Section 7.2.), which was that the evenness of flow profile increases the separation efficiency. When the larger volume based 3D clip data is analyzed (Figure 58), a same conclusion can be drawn.

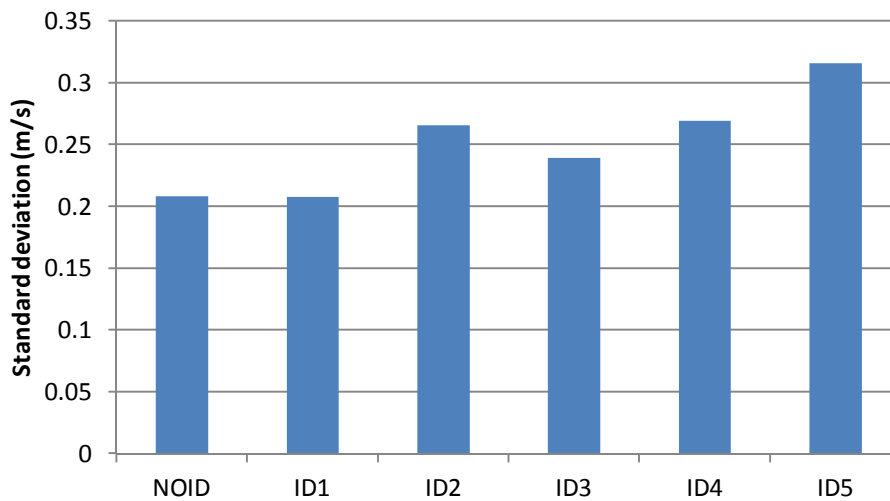


Figure 58. Standard deviations of horizontal gas velocities in clip data, case by case. Clip location is shown in Figure 28.

Figures 57 & 58 seem to correlate well, and data seems to be consistent between cases. Furthermore, when gas velocity histograms from clips (Appendix 8) are analyzed, the velocity profiles indeed seem to differ, for the benefit of the weaker performing distributors (for separation efficiency see Section 8.3.1). However, the liquid accumulation seems to cause some problems with the data-averaging. For example, the average horizontal velocities were thought to balance at a certain ideal level that would depend on the gas space available. When the averaged values were analyzed (see Appendices 6 & 7), it was found out that no such correlation could be found. When momentary values were analyzed the data showed correlations with the expected values. It was concluded that the averaged values were disturbed by the rising liquid level. This caused average gas velocity to behave ambiguously when the cells that were near the liquid surface were covered with liquid. Since the average values and standard deviation have direct effect toward each other, this may have an effect to the compared standard deviations. Unfortunately, effective way to remove this phenomenon from data averaging was not found.

When the distribution is looked schematically (Figure 59), an interesting phenomenon can be found. It seems that increase in backward flow right after the distributor correlates with better separation efficiency.

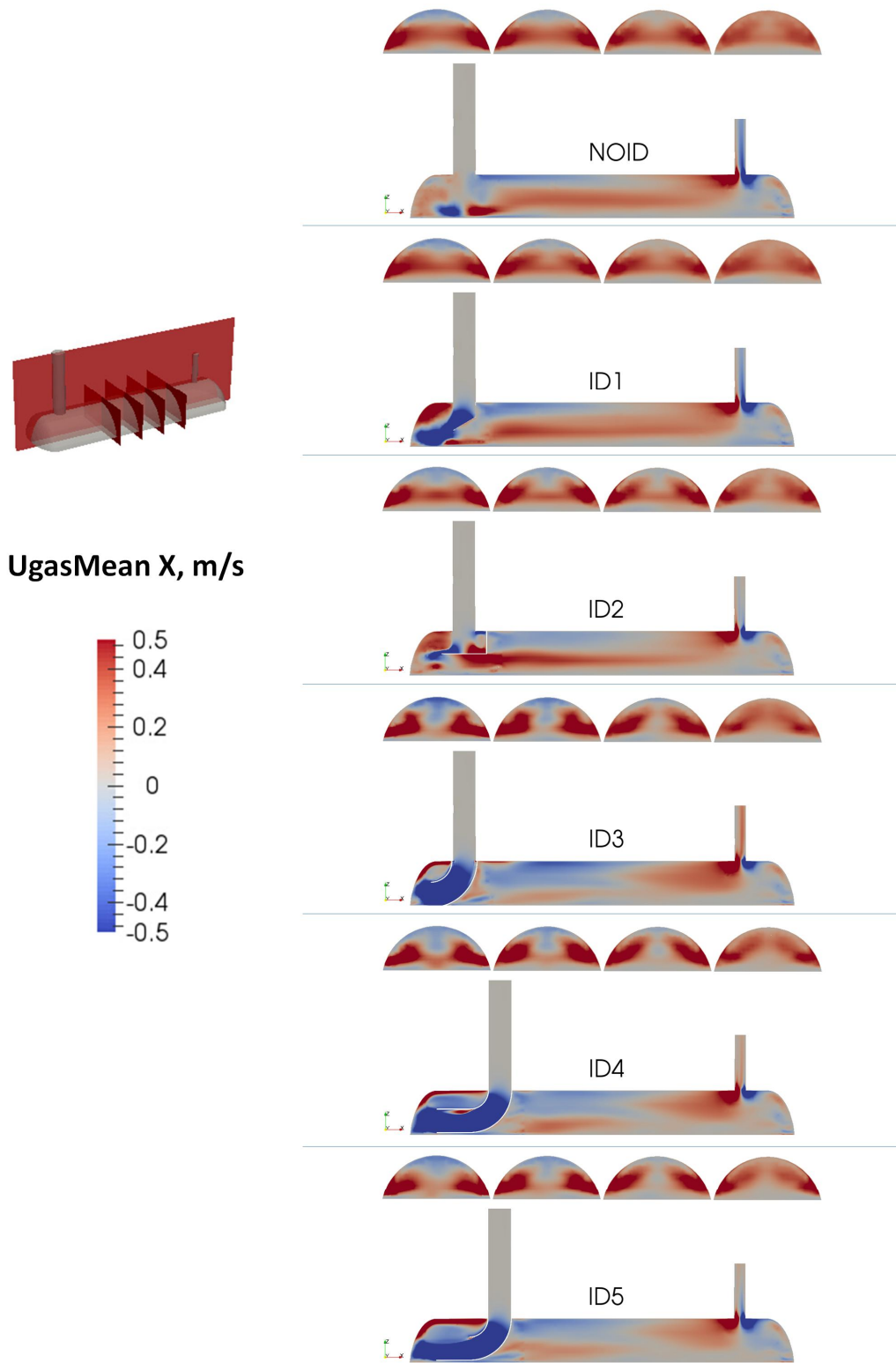


Figure 59. Schematic view of the horizontal movement in different cases. Red describes flow direction from inlet to outlet (i.e. forward movement), while blue is the opposite direction.

Figure 59 shows also that even though distributors are causing relatively large differences in flow profiles near the inlet in the first half of the vessel, the second half closer to the outlet seems much more equal between the cases. It might be possible that lateral flow distribution is even enough in all the cases near the outlet and the phenomenon affecting to the differences in separation efficiency can be found elsewhere.

One of the flow areas that might affect to the separation efficiency is right behind the inlet distributors. When lateral and horizontal movement are viewed at the same time near the inlet distributor In the case of ID3 (Figure 60), the areas that have high lateral movement towards the outlet are also the areas that have high downward movement. Whereas in the case of NOID (Figure 61), the flow profile seems to be almost the opposite; the same areas that are showing gas flows up are showing high lateral movement towards the outlet. This could explain why NOID would raise more droplets into the gas space, whereas ID3 features effective separation.

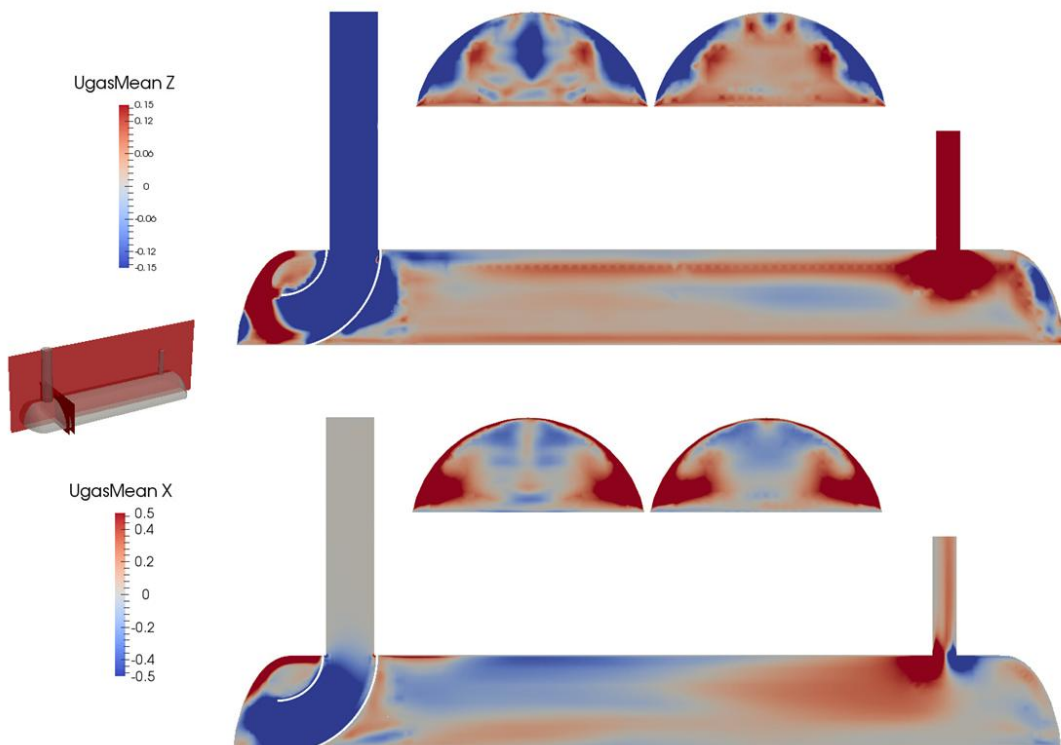


Figure 60. ID3 case. Lateral and vertical velocity (m/s) near the inlet distributor.

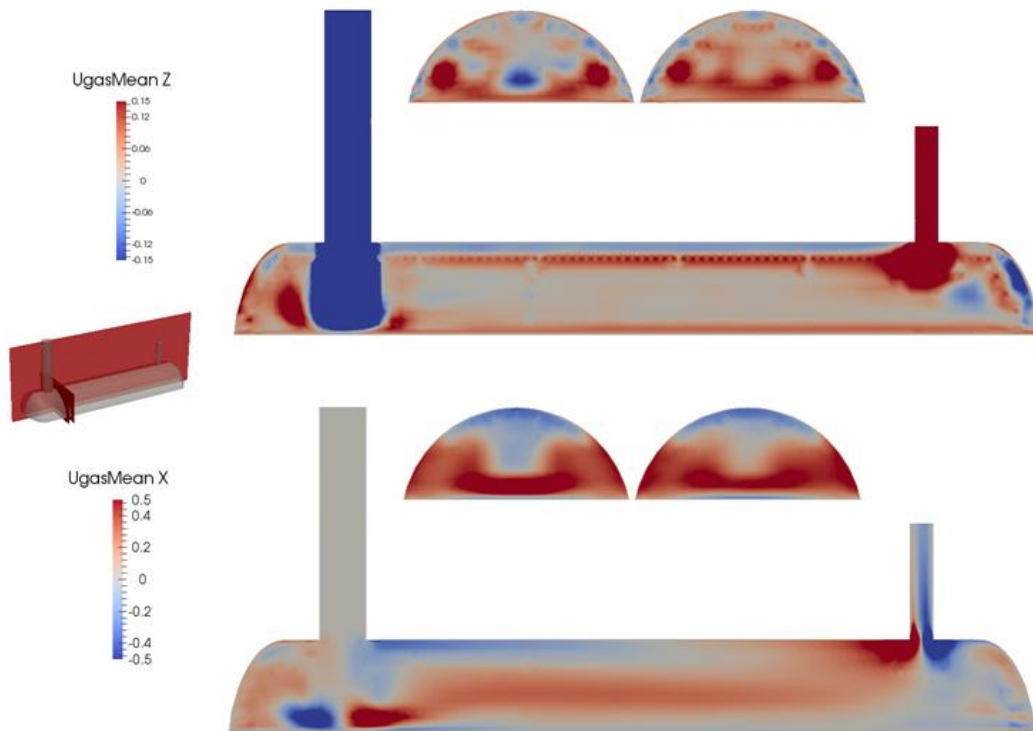


Figure 61. NOID case. Lateral and vertical velocity (m/s) near the inlet distributor.

For the other case the figures comparing lateral and vertical velocity near the distributor back end can be found from Appendix 9.

8.4 Comparison of outlet configurations

The surface reports of different outlet configuration cases were studied. In Figure 62 and Figure 63 the liquid volume fractions as a function of time for the studied cases (NOID and ID4) are presented.

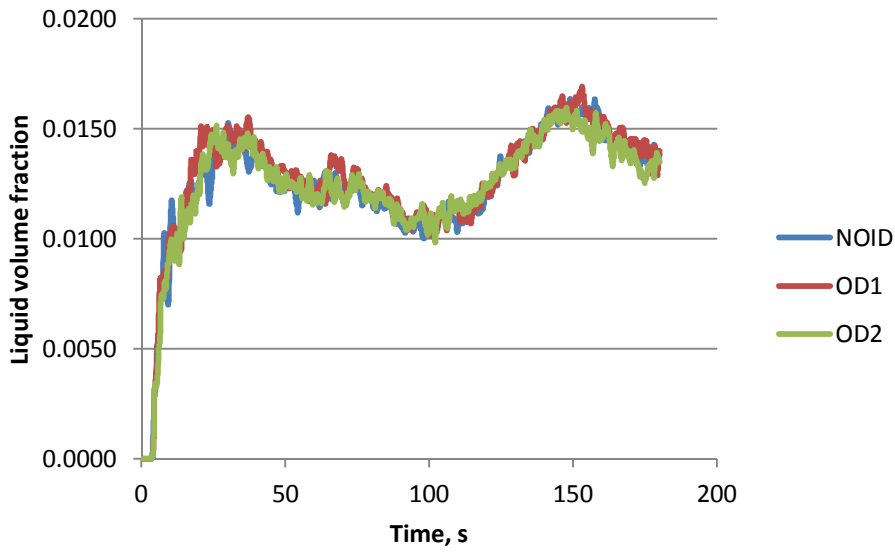


Figure 62. Effect of outlet configuration to liquid volume fraction in outlet, NOID cases with different outlet distributors.

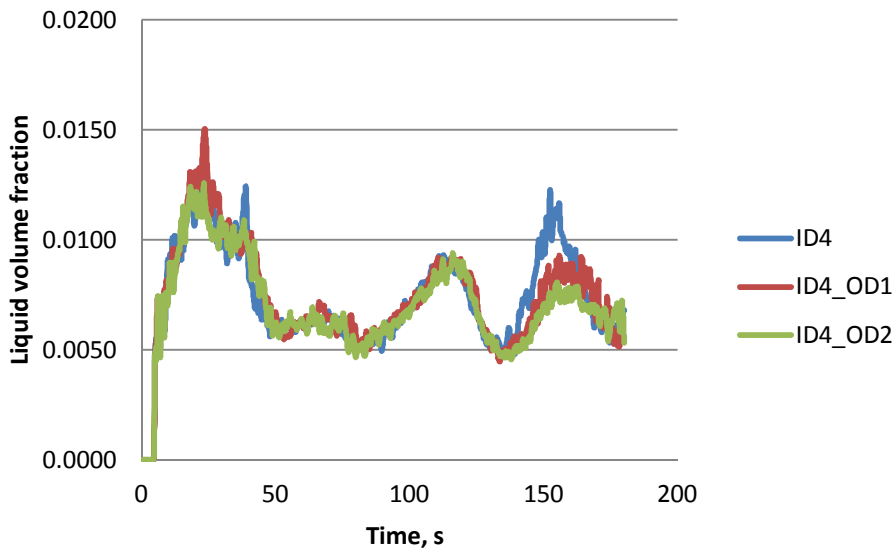


Figure 63. Effect of outlet configuration to liquid volume fraction in outlet, ID4 cases with different outlet distributors.

Outlet configurations seem to have almost no effect to the separation efficiency (Figure 62 & 63). However, with ID4 configuration the outlet configurations seem to effect the separation at later time steps ($t > 130$ s, Figure 63). This may indicate that the outlet configurations are effective, if certain liquid level is exceeded. However, the liquid level at

the later stages of the simulation is too high for gravitational separation. It is not recommended by any design guideline, and the vessels are not normally operated with that high liquid level. Surface reports also showed (Figure 62 & Figure 63) that even the transient periods were nearly similar. Therefore, the outlet distributors' effect to the separation is really small, and the usage of tested outlet configurations would not seem to be profitable.

8.5 Single phase simulations

To compare the single and two phase simulations, the case ID4 geometry was simulated as a single phase as well. In this case only gas was fed from the inlet. For the single phase simulations, an incompressible, transient solver `pisoFoam` was used. In Figure 64 the simulated ID4 geometry is shown with stream lines representing the flow orientation from the inlet.

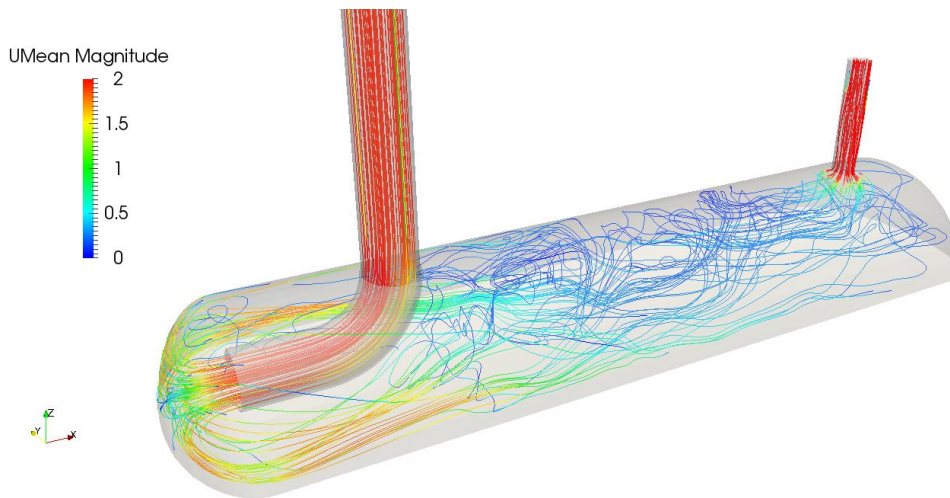


Figure 64. The single phase ID4 case with stream tracers to describe a flow orientation from inlet pipe. Coloring describes the velocity of flow in m/s.

Flow orientation in Figure 64 seems to behave similarly to the two phase when compared with the two-phase results shown in Figure 43 for ID4. The flow is guided to the vessel walls, and begins to even out when moving towards the outlet. To further compare the flow profiles between single and two-phase cases the horizontal movement of the single and two phase simulations are compared (Figure 65).

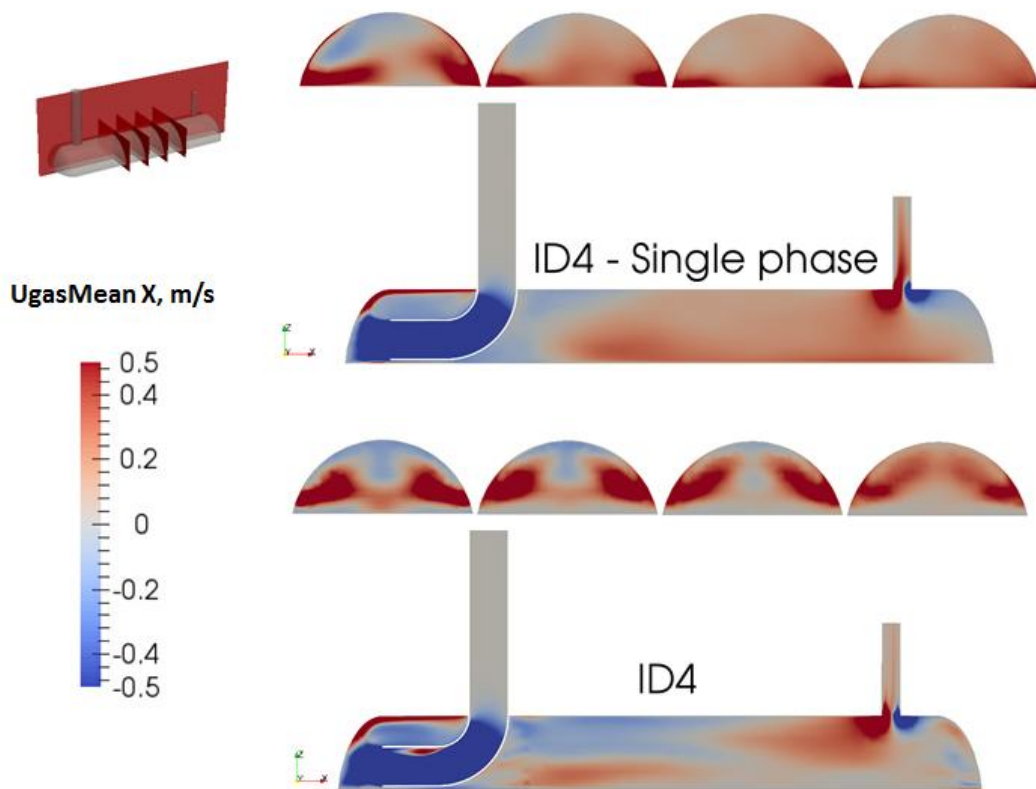


Figure 65. Horizontal velocity (m/s) profiles. Comparison between single and multiphase cases.

Figure 65 indicates single phase simulations to correlate somewhat with two phase simulations. There are two clear differences. First the single phase case seems to behave more ideally; the flow profile evens out closer to the inlet nozzle than with the two phase case. Additionally, the two-phase case seems to form much more intensive flow patterns. The second difference is the size of backward flow. In the two-phase case backward flow extends nearer to the outlet than with the single phase. There are also similarities: in both simulations the most intensive flows are focused on down and edges. The accumulation of liquid causes the intensive flow areas to be a little bit higher in the two-phase case than with the single phase.

9 Conclusions

Several model parameters and vessel internal configurations were studied in the experimental part of the thesis. The effect of droplet size, compression term and turbulence model were tested. Additionally, five different inlet configurations and two outlet configurations were simulated and evaluated. Finally, the single phase model was simulated and the results were compared to the two phase model.

9.1 Results

The used two-phase model (multiphaseEulerFoam) was found out to be sensitive to the boundary conditions. The most important parameter effecting to the simulations was liquid droplet size. Relatively small changes in the droplet size caused large effects to the liquid behavior. *E.g.* by reducing the liquid droplet size from 30 μm to 10 μm the separation efficiency dropped from 70 % to practically zero. The compression term was determined to work as expected, and when compression term was used the dispersed liquid droplets were compressed towards each other. However, with larger compression values, compressing caused problems and unphysical behavior in the simulation. The used turbulence modeling also had an effect to the two phase simulations. All of the tested turbulence models were highly dissipative, *i.e.* decreased the turbulence behavior in the simulation. The laminar model was determined to be the most suitable for two-phase simulations.

The outlet configurations were not observed to have notable difference in separation efficiency, nor a major impact towards the flow profiles. Minor effects were detected when liquid accumulation caused gas space to decrease, but further investigation is required to verify the results.

When different inlet distributors were studied, the closed curved pipes (ID3 and ID4) were found out to be the most effective when separation efficiency was considered. Overall, the curved pipe distributors were found out to be more effective than impact plate type of distributors. No clear correlation between the gas flow profile smoothness and separation efficiency in the two-phase simulations was found. It was concluded that the evenness of flow profile would not be the best indicator of the successfulness of horizontal separation.

Single phase simulations were studied, because they have multiple advantages when compared to two-phase simulations. They are simpler; the calculations can be over ten times faster. Particularly, post-processing the results, and calculating characteristic parameters to evaluate results are more straightforward. The results indicated that the gas flow profiles can be somewhat estimated by single phase calculations. Some deviations exist, but the flow orientation seems to be similar. However, correlation between the flow profile smoothness and the separation efficiency was not found. Therefore, the single phase simulations may have difficulties to forecast the separation efficiency correctly, and in the case of studying different geometries there is a risk that the single phase simulations do not give enough information to make reliable decision of which geometry performs the best.

9.2 Error sources and reliability

Overall the reliability between the studied results is good. The tested model schemes acted as expected and no major flaws, or non-physical behavior were identified within the used model. However, there is no experimental data available to validate the results.

In this work, boundary conditions (*e.g.* inlet flow composition) and physical models used were kept consistent for the all of the simulated cases. Additionally, the structure and cell size of the used mesh was kept as steady as possible. Therefore, the results are well comparable with each other.

The Euler-Euler model does not allow droplet size distribution within single phase. Eulerian solvers treat dispersed phase as a constant droplet size which is user defined. For each different droplet size, a new phase must be specified. In the real case, the droplet distribution is constantly evolving, mostly due coalescence and breakage (see Chapter 2), but modeling this would require much more computational resources or a coupled solver. This may cause errors to the simulations. Additionally, it was noted that particularly the separation efficiency results were very sensitive to the selected droplet size. The effect was shown in the model testing (Section 8.1). This must be taken into account when results are

evaluated. However, the results between different distributors and configurations are comparable, since the case setup remained the same in every case.

Additionally, almost all of the performed multiphase simulations showed checker-board instabilities within the solution at vertical direction. Checker-boarding is a numerical issue in CFD that is caused by the pressure-velocity coupling. It is a solver featured phenomenon that is caused by the used solving method for pressure and velocity fields. (Rusche, 2002)

In this thesis, the checker-board instability shows as adjacent cells having opposite directions in vertical direction. In Figure 66 checker-board phenomenon in NOID case is presented.

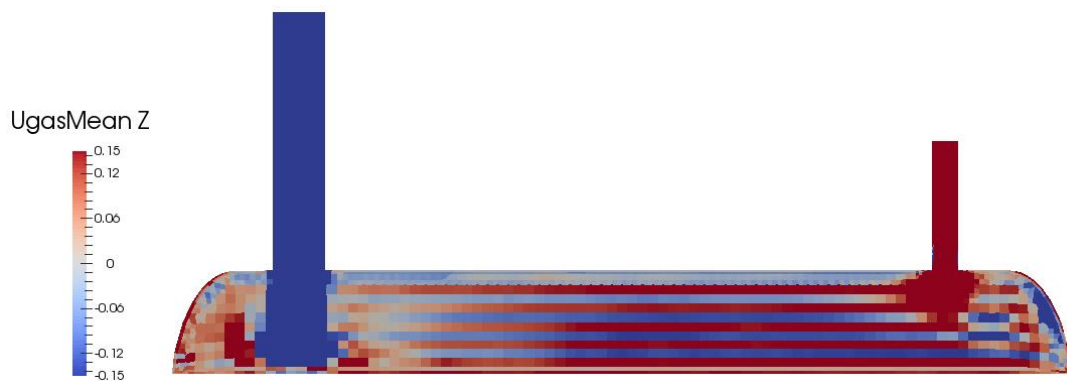


Figure 66. Checker-board instabilities in NOID case.

The checker-board instabilities caused by the solver may have an effect towards the flow velocity values, and could cause some errors in the values and interpretations. However, the tests that were conducted with denser mesh did not feature clearly observed checker-board instabilities, but otherwise had similar flow velocity profiles. Additionally, the results were consistent; clear non-physical behaviors, or peculiar reactions to the altered model specifications or boundary conditions were not found. Therefore, the results can be considered reliable and comparable to each other.

For further studies, checker-board instabilities are proposed to be avoided by using a dense enough mesh size, or by using a solver that has an implemented cure for pressure-velocity coupling. For more information regarding checker-board instabilities in two-phase CFD models see for example Rusche (2002) or Ghione (2012).

10 Further studies

This thesis studies horizontal gas-liquid separation by Euler-Euler multiphase model. It shows impact of different distributors to the flow profile. However, the lack of experimental data causes the validation of the results to be based purely to the model data with assumptions and speculations. If possible the model should be validated with experimental setup. However, with large scale vessels the experimenting is expensive. Therefore, accurate data from large scale vessels is usually very difficult to acquire, or it is not publicly available.

The comparison of the single phase models against the two-phase simulations should also be explored further. In this work there was a conflict between separation efficiency and velocity profiles. Further studies are required to analyze especially if the single phase models can predict the separation efficiency at all. The use of single phase simulations would save time and resources, when compared to the multiphase modeling. However, it needs to be validated, if the single phase simulations are accurate enough to model gravitational separation, or are the gas-liquid interactions effecting to the separation in a way that ignoring the interactions leads to unrealistic modeling.

An alternative way to study the two-phase flow would be the use of Lagrangian solvers. Lagrangian solver would enable including a droplet size distribution that could help to determine how the different droplet sizes react to the different flow phenomenon inside the vessel. This could provide more information of the separation phenomena inside the vessel. For example, it could reveal whether droplets are required to be large enough to separate, or is it only required that droplet hits the liquid surface and coalescences for separation to occur. Furthermore, this could give more reliable estimate of the behavior of the liquid.

11 Bibliography

ACS Industries, LP, 2016. *Liquid-Liquid Coalescer Design Manual*, Houston.

Arnold, K. & Stewart, M., 1999. *Surface Production Operations Volume 1 - Design of Oil-Handling Systems and Facilities*. 2nd ed. Elsevier, pp. 84-130.

Behin, J. & Azimi, S., 2015. Experimental and Computational Analysis on Influence of Water Level on Oil-Water Separator Efficiency. *Separation Science and Technology*, 50(11), pp. 1695-1700.

Buffo, A., Marchisio, D., Vanni, M. & Renze, P., 2013. Simulation of polydisperse multiphase systems using population balances and example application to bubbly flows. *Chemical engineering research and design*, 91(10), pp. 1859-1875.

Carlson, F. & Talseth, M.-A. O., 2009. *Study of mist flow inside a vane pack geometry*, Master's thesis, The Norwegian University of Science and Technology.

Chen, L. et al., 2015. Numerical Simulation and Structural Optimization of the Inclined Oil/Water Separator. *PLoS ONE*, 10(4).

Chen, P., Sanyal, J. & Dudukovic, M., 2005. Numerical simulation of bubble columns flows: effect of different breakup and coalescence closures. *Chemical Engineering Science*, Volume 60, pp. 1085-1101.

Couper, J. R., Penney, W. R., Fair, J. R. & Walas, S. M., 2012. *Chemical Process Equipment - Selection and Design*. 3rd ed. Elsevier, pp. 655-675.

Engys Ltd, 2016. *HELYX Core User Reference Guide v2.4.x*. London.

Frising, T., Noik, C. & Dalmazzone, C., 2006. The Liquid/Liquid Sedimentation Process: From Droplet Coalescence to Technologically Enhanced Water/Oil Emulsion Gravity Separators: A Review. *Journal of Dispersion Science and Technology*, 27(7), pp. 1035-1057.

Gao, Z., Li, D., Buffo, A. & Podgorska, W., 2016. Simulation of droplet breakage in turbulent liquid-liquid dispersions with CFD-PBM: Comparison of breakage kernels. *Chemical Engineering Science*, Volume 142, pp. 277-288.

Gebauer, F., Hlawitschka, M. W. & Bart, H.-J., 2015. CFD aided investigation of single droplet coalescence. *Chinese Journal of Chemical Engineering*.

Ghione, A., 2012. *Development and validation of a two-phase CFD model using OpenFOAM*, Master's Thesis. Stockholm: Royal Institute of Technology.

Hiltunen, K. et al., 2009. Multiphase Flow Dynamics Theory and Numerics. *VTT Publications* 722, p. 113.

Hlawitschka, M. W., Chen, F., Bart, H.-J. & Hamann, B., 2012. CFD Simulation of Liquid-Liquid Extraction Columns and Visualization of Eulerian Datasets. *OpenAccess Series in Informatics (OASIS)*, Volume 27, pp. 59-70.

Hooper, W. B. & Jacobs, L. J., 1996. Handbook of Separation Techniques for Chemical Engineers. In: 3rd ed. s.l.:McGraw-Hill, pp. 344-357.

Huusari, L., 2015. *Analysis of Phase Separator Design Criteria Using Computational Fluid Dynamics*, Master's Thesis, Lappeenranta: Lappeenranta University of Technology.

Jamshed, S., 2015. Using HPC for Computational Fluid Dynamics - A Guide to High Performance Computing for CFD Engineers. 1st ed. Elsevier, pp. 1-20, 81-100.

Jeelani, S., Panoussopoulos, K. & Hartland, S., 1999. Effect of Turbulence on the Separation of Liquid-Liquid Dispersions in Batch Settlers of Different Geometries. *Ind. Eng. Chem. Res.*, 38(2), pp. 493-501.

Kopriva, N., Buchbender, F., Ayesteran, J., Kalem, M., Pfennig, A., 2012. A Critical Review of the Application of Drop-Population Balances for the Design of Solvent Extraction Columns: I. Concept of Solving Drop-Population Balances and Modelling Breakage and Coalescence. *Solvent Extraction and Ion Exchange*, 30(7), pp. 683-723.

Laleh, A., 2010. *CFD Simulation of Multiphase Separators, Doctoral Thesis*. Calgary: University of Calgary.

Liao, Y. & Lucas, D., 2010. A literature review on mechanisms and models for the coalescence process of fluid particles. *Chemical Engineering Science*, Volume 65, pp. 2851-2864.

Madhavan, S., 2005. *CFD Simulation of Immiscible Liquid Dispersions, Master's thesis*, Halifax: Dalhousie University.

Oshinowo, L. M., Quintero, C. G. & Vilagines, R. D., 2016. CFD and Population Balance Modeling of Crude Oil Emulsions in Batch Gravity Separation—Comparison to Ultrasound Experiments. *Journal of Dispersion Science and Technology*, 37(5), pp. 665-675.

Perry, R., 1997. *Perry's Chemical Engineers' Handbook*. 7th ed. New York: McGraw-Hill.

Rosen, M. & Dahanayake, M., 2000. Industrial Utilization of Surfactants - Principles and Practice. In: 1st ed. s.l.:AOCS Press, pp. 15-55.

Rusche, H., 2002. *Computational Fluid Dynamics of Dispersed Two-Phase Flows At High Phase Fractions, Doctoral thesis*. London: University of London.

Saboni, A., Alexandrova, S., Gourdon, C. & Chesters, A., 2002. Interdrop coalescence with mass transfer: comparison of the approximate drainage models with numerical results. *Chemical Engineering Journal*, 88(1-3), pp. 127-139.

Shi, J., 2015. *A Study on High-Viscosity Oil-Water Two-Phase Flow in Horizontal Pipes, Doctoral Thesis*. Cranfield University: s.n.

Siikonen, T., 2014. *Virtaussimulointi, course material from Ene-39.4054* , Espoo: Aalto University School of Engineering.

Silva, L. & Lage, P., 2011. Development and implementation of a polydispersed multiphase flow model in OpenFOAM. *Computers & Chemical Engineering*, 35(12), pp. 2653-2666.

Sparks, T. & Chase, G., 2016. *Filters and Filtration Handbook*. In: 6th ed. s.l.:Elsevier, pp. 361-382.

Stewart, M. & Arnold, K., 2008. *Gas-Liquid and Liquid-Liquid Separators*. In: s.l.:Elsevier, pp. 84-130.

Stewart, M. & Arnold, K., 2009. *Emulsions and Oil Treating Equipment - Selection, Sizing and Troubleshooting*. In: 1st ed. s.l.:Elsevier, pp. 32-60.

Towler, G. & Sinnott, R., 2013. *Chemical Engineering Design - Principles, Practice and Economics of Plant and Process Design*. In: s.l.:Elsevier, pp. 563-629.

Walvekar, R. G. et al., 2009. Numerical study of dispersed oil-water turbulent flow in horizontal tube. *Journal of Petroleum Science and Engineering*, Volume 65, pp. 123-128.

Wardle, K. E. & Weller, H. G., 2013. Hybrid Multiphase CFD Solver for Coupled Dispersed/Segregated Flows in Liquid-Liquid Extraction. *International Journal of Chemical Engineering*, Volume 2013.

Wegener, M., Paul, N. & Kraume, M., 2014. Fluid dynamics and mass transfer at single droplets in liquid/liquid systems. *International Journal of Heat and Mass Transfer*, Volume 71, pp. 475-495.

Villwock, J. et al., 2014. Systematic Analysis of Single Droplet Coalescence. *Chemical Engineering Technology*, 37(7), pp. 1103-1111.

Zhou, G. & Kresta, S. M., 1997. Correlation of mean drop size and minimum drop size with the turbulence energy dissipation and the flow in an agitated tank. *Chemical Engineering Science*, 53(11), pp. 2063-2079.

12 Appendices

APPENDIX 1 - Complete case setup in HELYX® GUI

APPENDIX 2 - Mesh dependency tests, velocity profiles

APPENDIX 3 - Inlet streamlines between different inlet distributors

APPENDIX 4 - Diagonal slices with velocity profiles (magnitude) in different inlet and outlet configurations

APPENDIX 5 - Diagonal slices with lateral velocity profiles in different inlet and outlet configurations

APPENDIX 6 - Clip data analysis

APPENDIX 7 - Slice data analysis

APPENDIX 8 - Gas velocity histograms for clip data

APPENDIX 9 - Velocity profiles near the distributor

Complete case setup in HELYX® GUI

Boxes with yellow were tested and altered

Mesh	
Mesh Type	Automatic
Mesh Spacing (m)	0.04

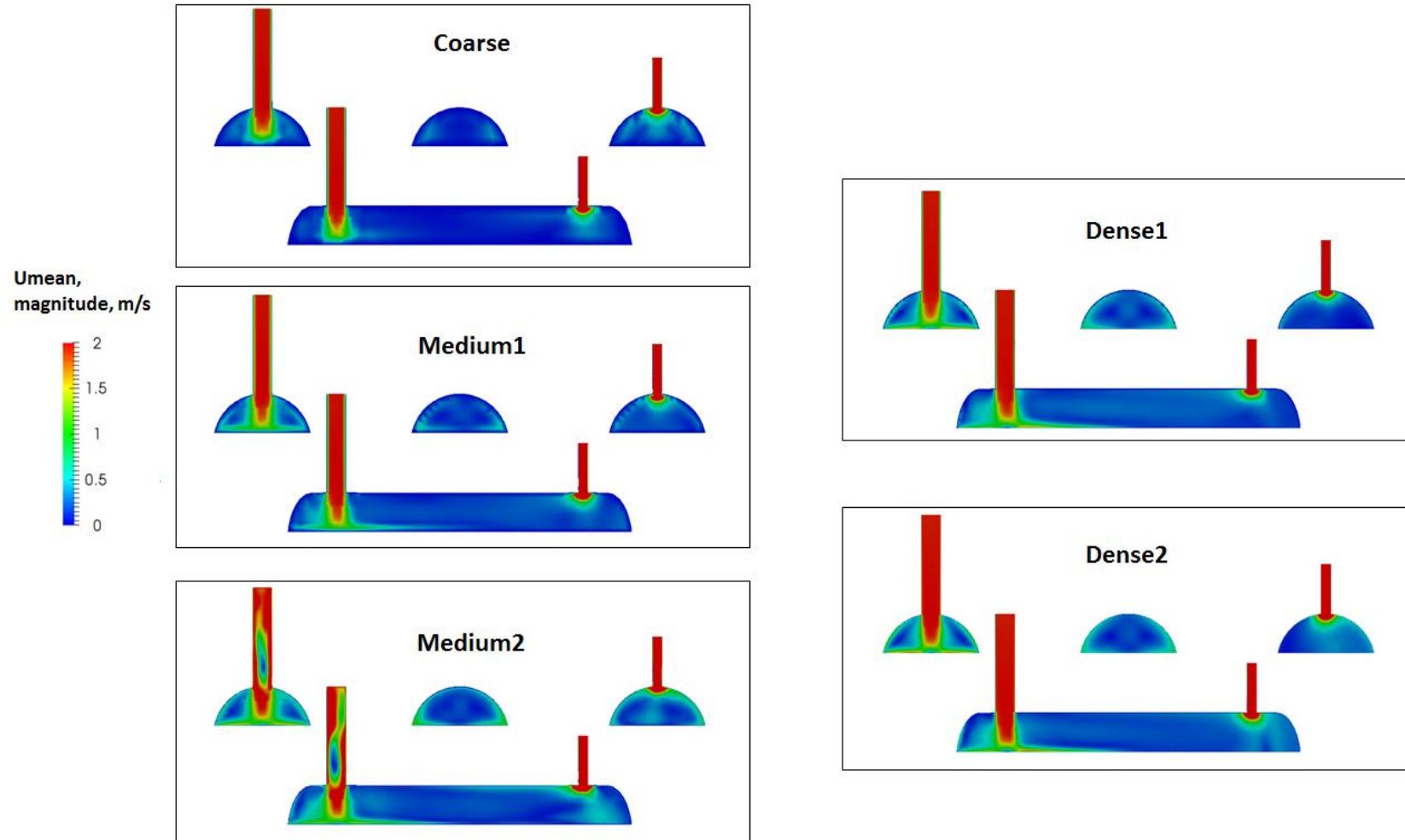
Geometry	
Vessel wall	
Refinement level	1
Number of layers	2
Layer stretching	1.25
Final layer thickness	0.4
Liquid surface	
Refinement level	0
Number of layers	2
Layer stretching	1.25
Final layer thickness	0.4
Inlet	
Refinement level	0
Number of layers	0
Outlet	
Refinement level	0
Number of layers	0
Material point	
Position	0,25 0,25

Case setup	
Solution model	
Solver type	Segregated
Time	Transient
Flow	Incompressible
Turbulence	RANS
Turbulence model	Laminar
Multiphase model	Euler-Euler
Gravity	0 0 -9,81

Phases	
Gas	
Constant diameter	
Diameter (m)	0.001
lightGasoil	
Constant diameter	
Diameter (m)	0.00003
Sigmas (N/m)	0.0097
Interface compression	-1 (OFF)
Virtual mass	0.5
Drag model	Blended
gas - lightGasoil	SchillerNaumann
lightGasoil - gas	SchillerNaumann
Residual phase fraction	0.001
Residual slip	0.001

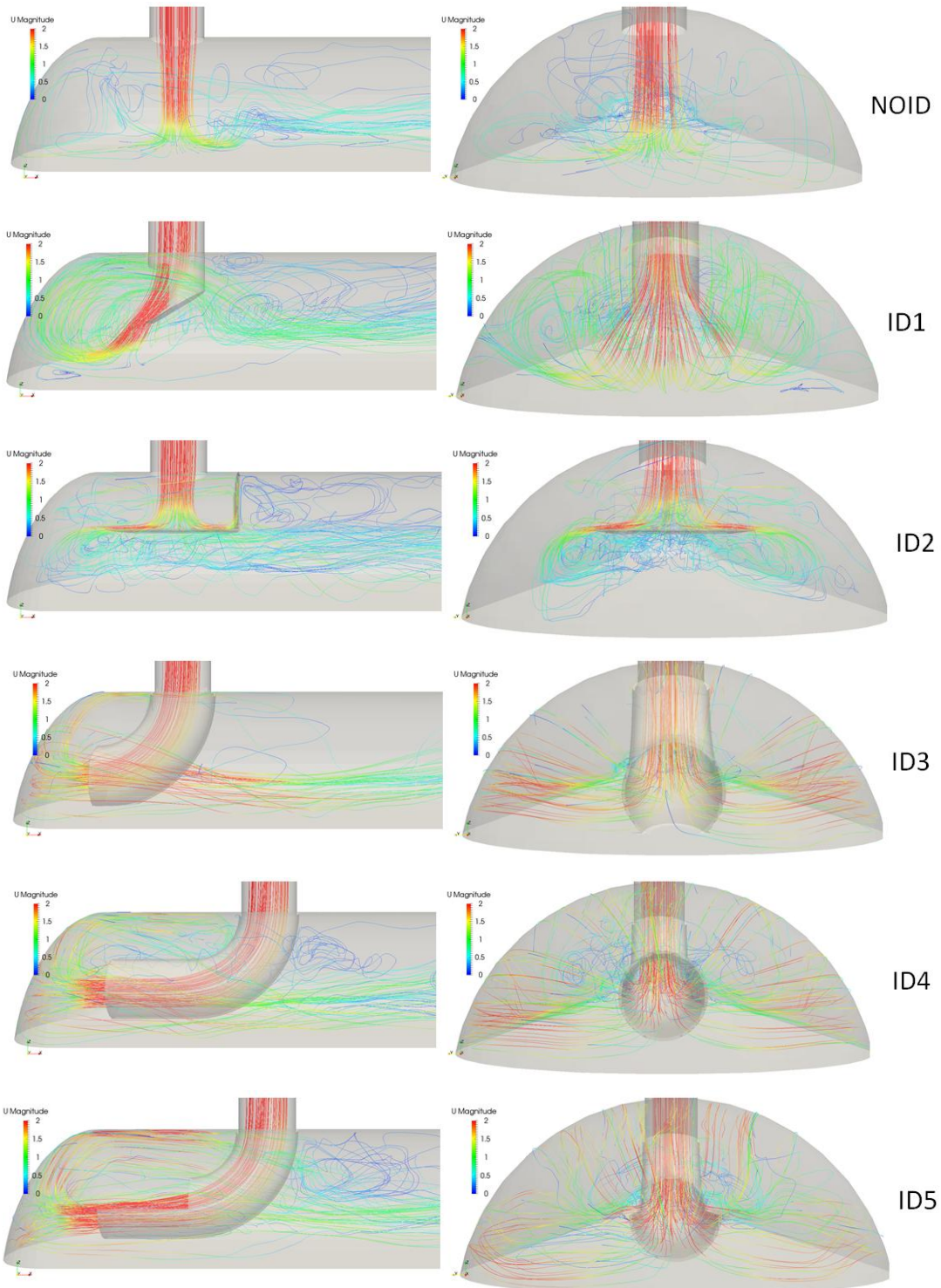
Boundary conditions			
Vessel wall		Outlet	
Type	Wall	Type	Outlet
Wall type	No-slip	Outlet type	Pressure
Liquid surface		Specification	Mean pressure
Type	Wall	Value	0
Wall type	No-slip		
Inlet			
Type	Inlet		
Inlet type	Velocity		
Specification type	Fixed flow rate		
Total flow (kg/s)	2.73		
<i>Phase fraction</i>			
Gas	0.96155		
lightGasoil	0.03845		

Mesh dependency tests, velocity profiles



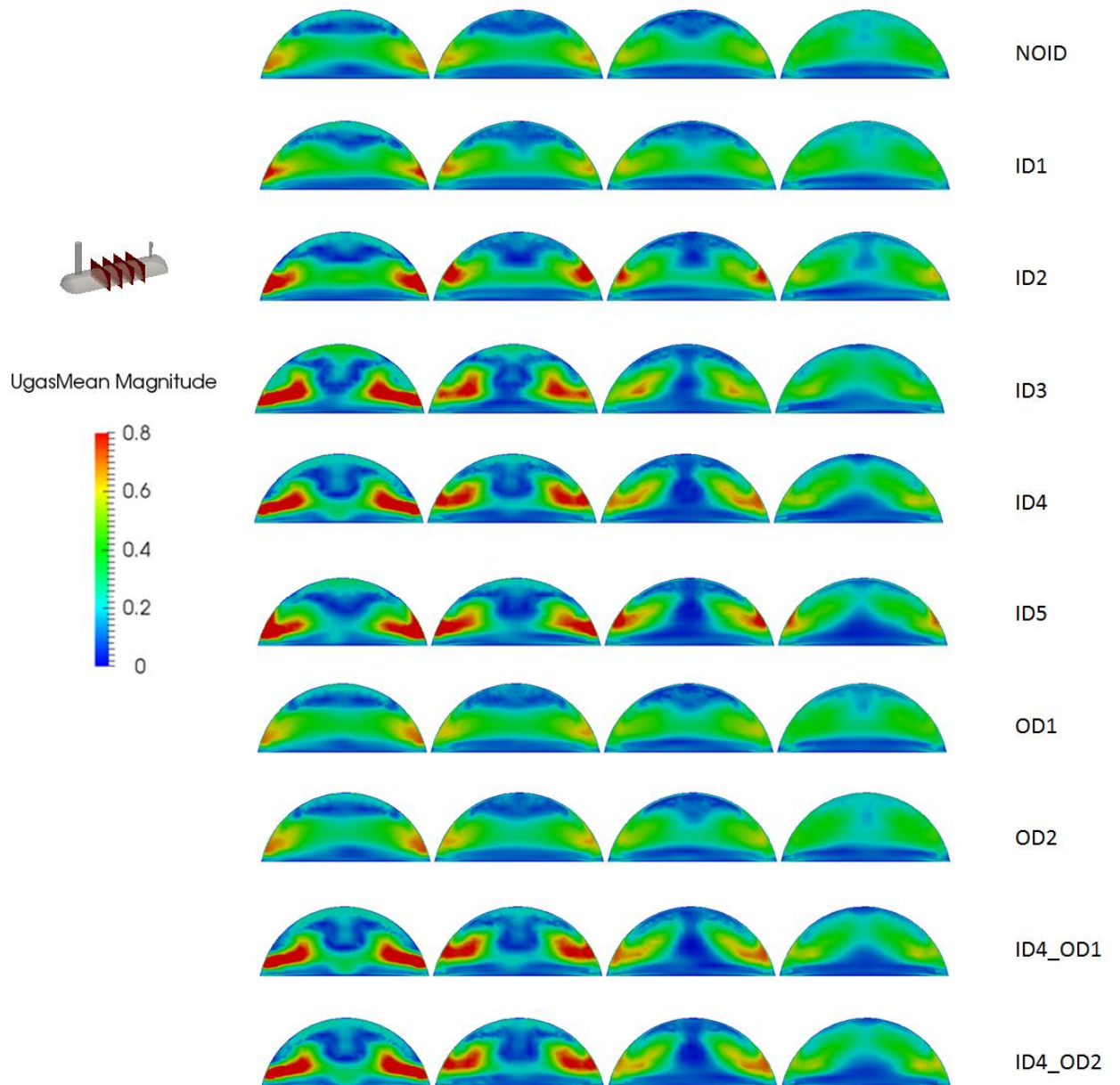
Inlet streamlines between different inlet distributors

Velocities in figures are U magnitude (m/s).



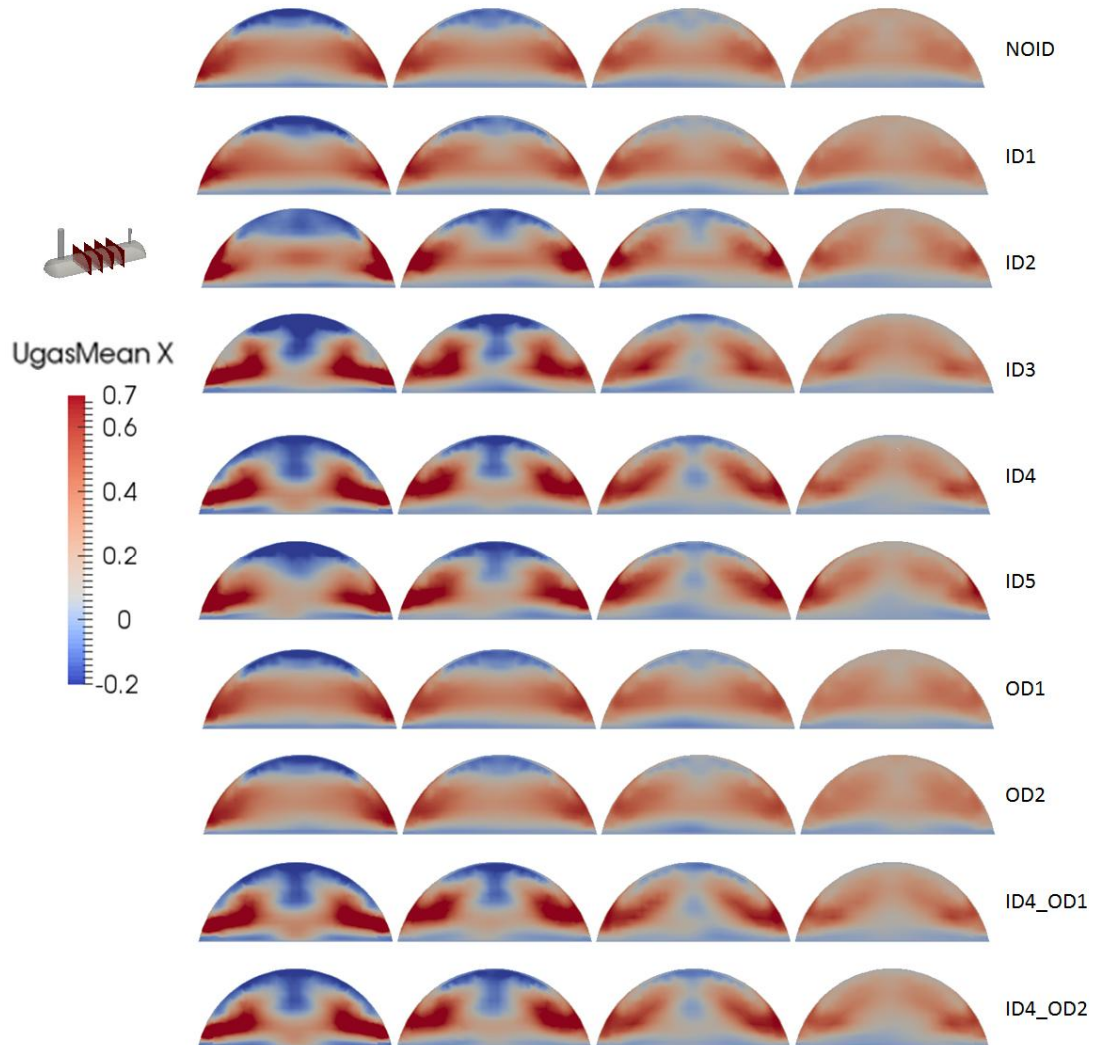
Diagonal slices with velocity profiles (magnitude) in different inlet and outlet configurations

The presented velocities are in m/s.



Diagonal slices with horizontal velocity profiles in different inlet and outlet configurations

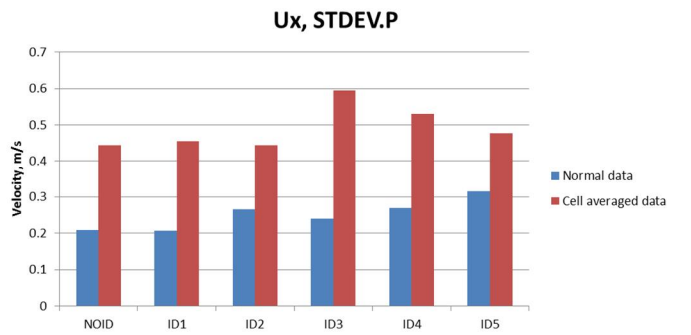
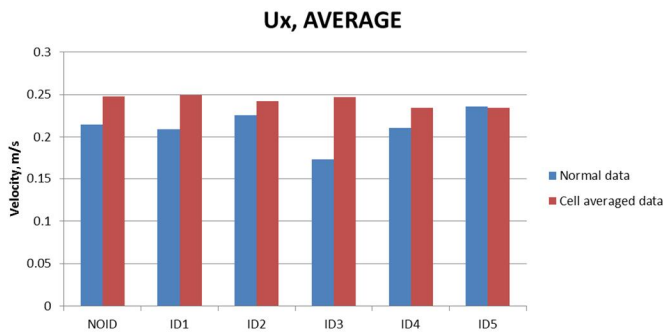
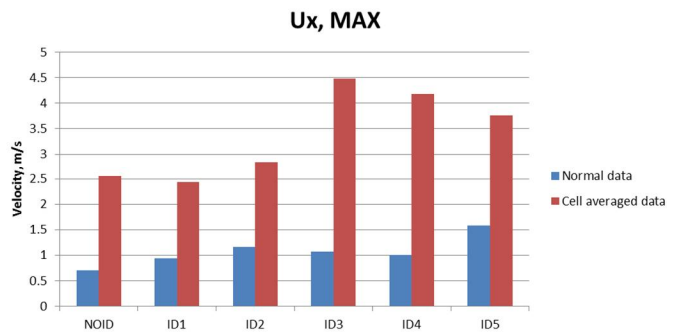
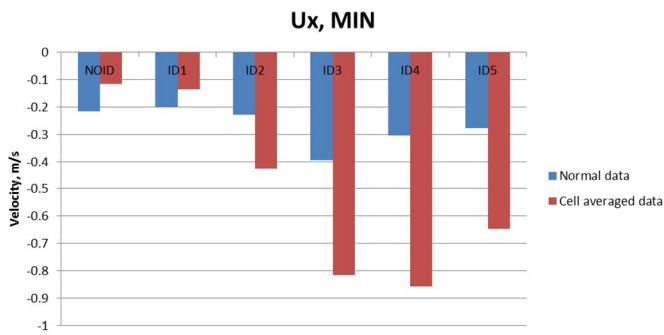
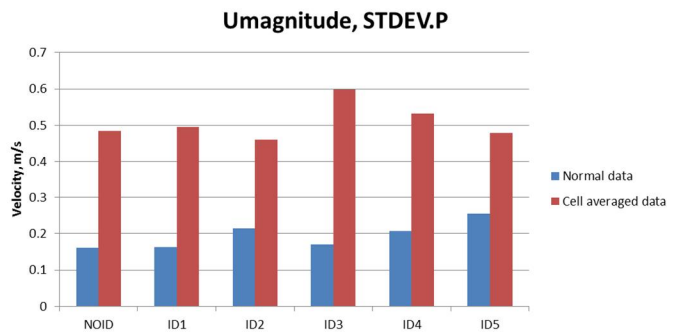
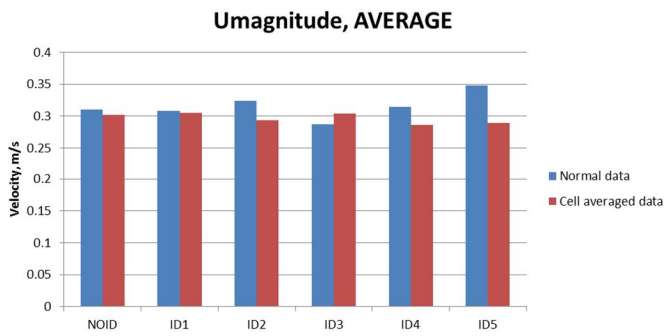
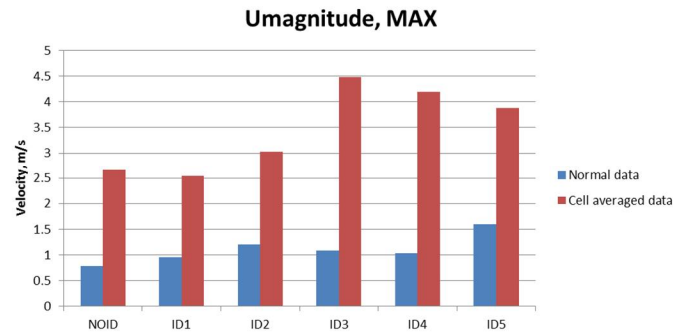
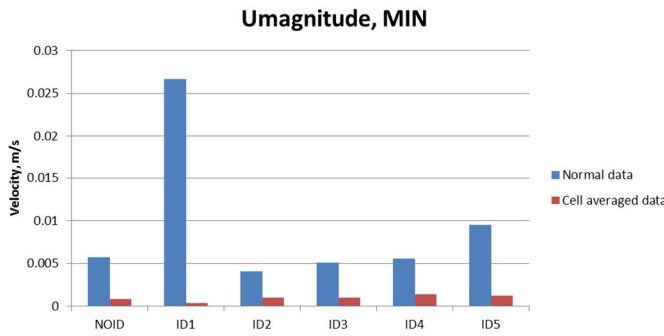
The presented velocities are in m/s.

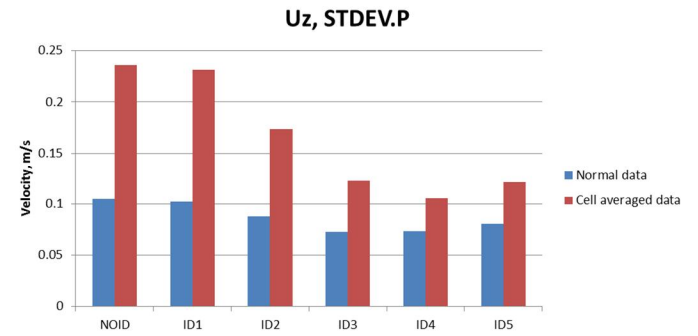
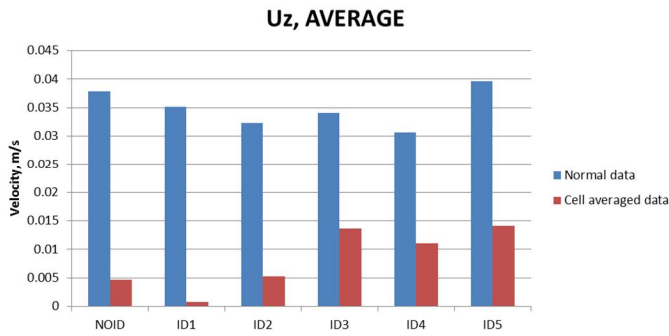
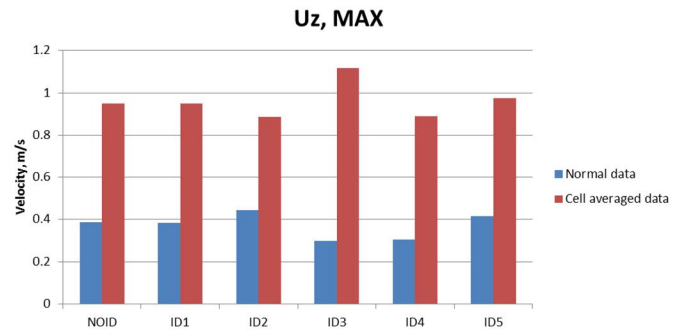
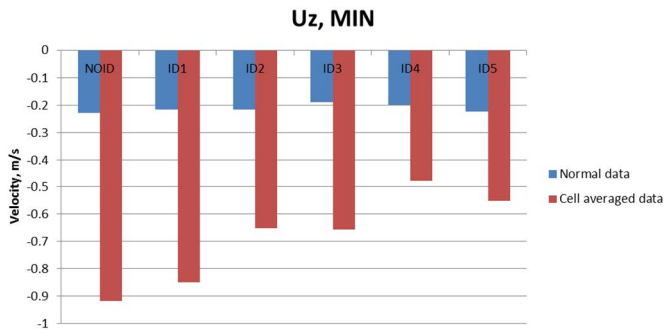


Clip data - velocity profiles

All the values presented are time averaged (60 - 90 s). All the values are m/s.

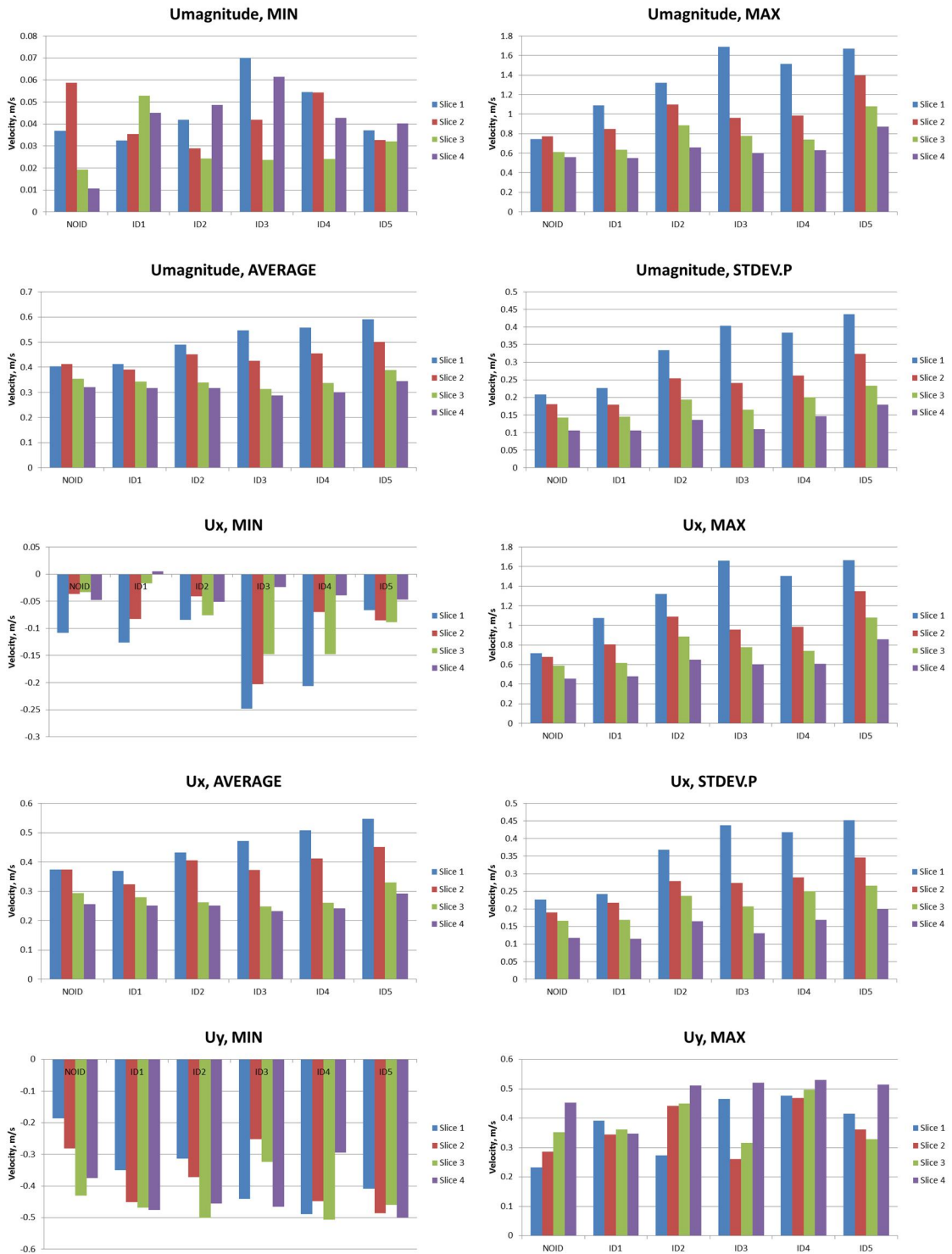
Cell averaged data values as discussed in the Section 7.2.

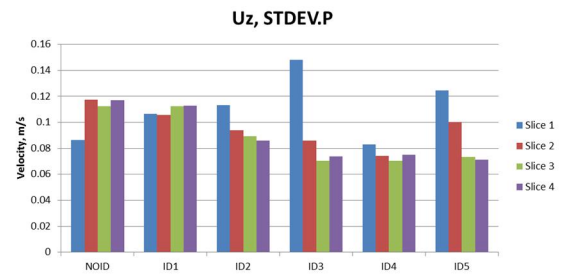
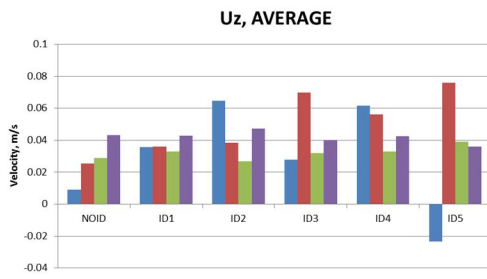
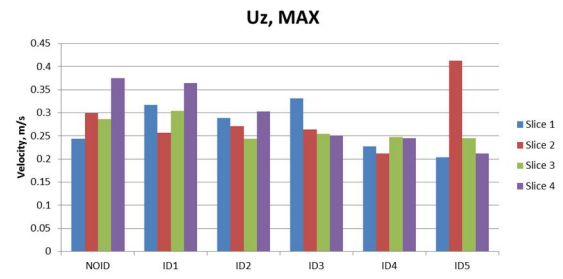
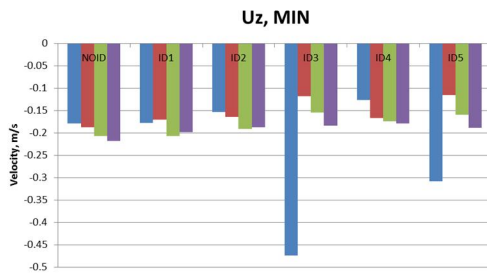
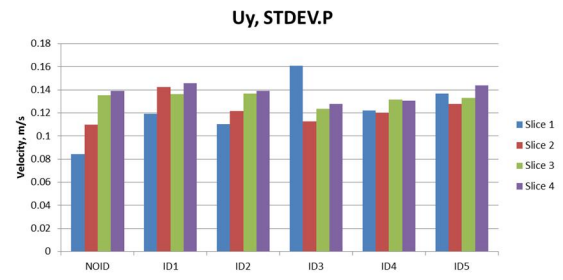
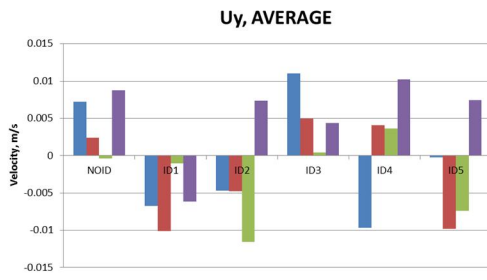




Slice data - velocity profiles

All the values presented are time averaged (between 60 - 90 s). All the values are m/s.



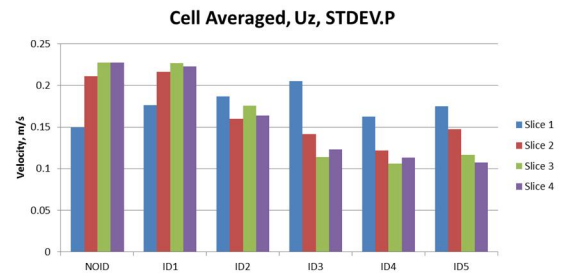
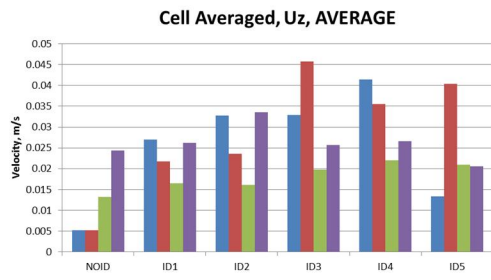


Slice data - Cell area weighted velocity profiles

All the values presented are time averaged (between 60 - 90 s). All the values are m/s.

Values are cell averaged as discussed in the Section 7.2.

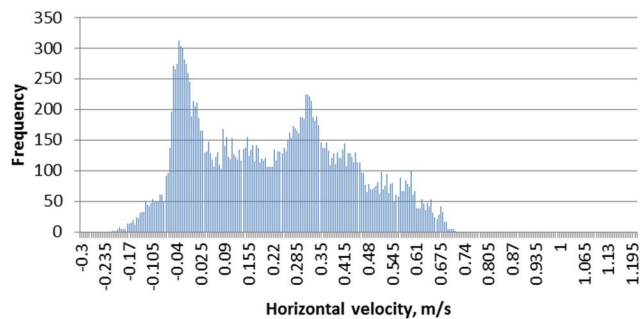




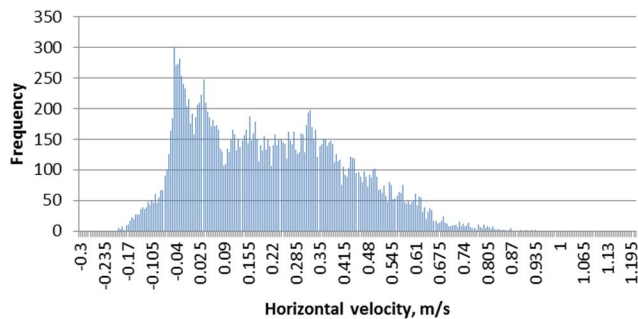
Gas velocity histograms

Clip data - Time averaged (60 - 90 s) horizontal velocities

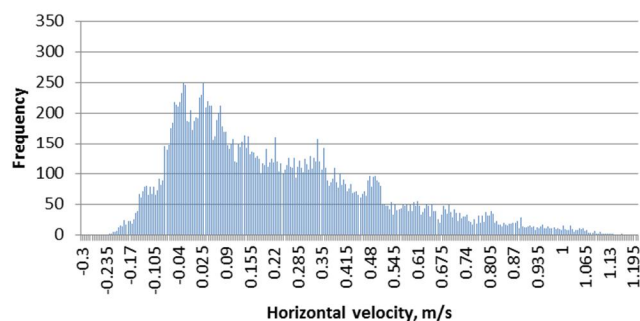
Histogram, NOID



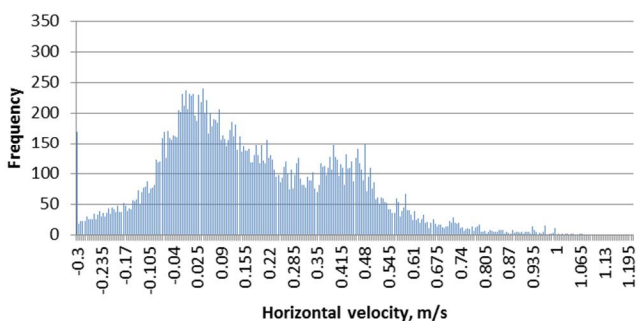
Histogram, ID1



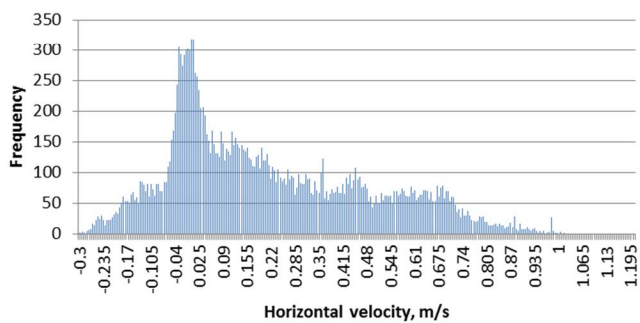
Histogram, ID2



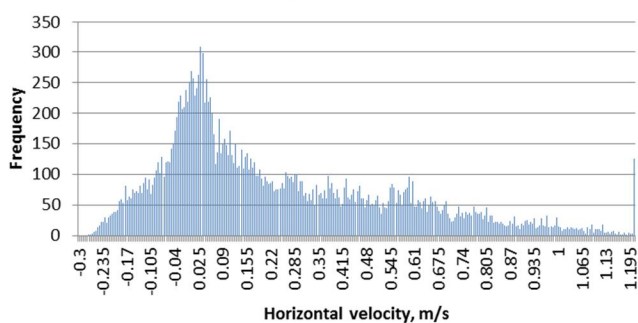
Histogram, ID3



Histogram, ID4

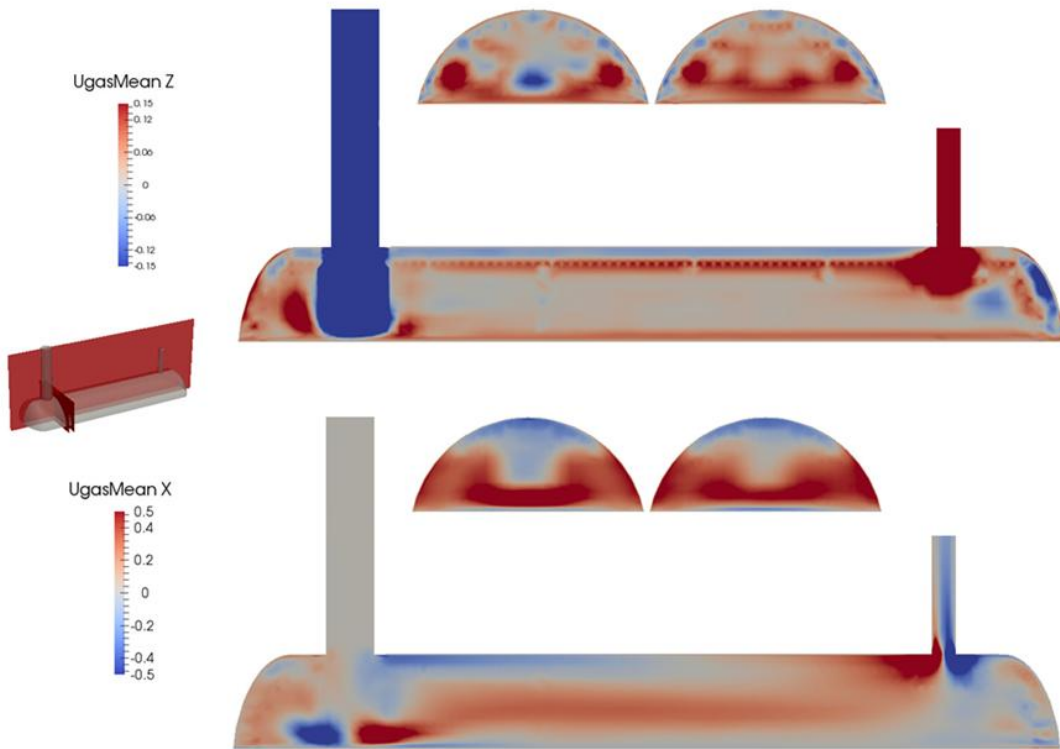


Histogram, ID5

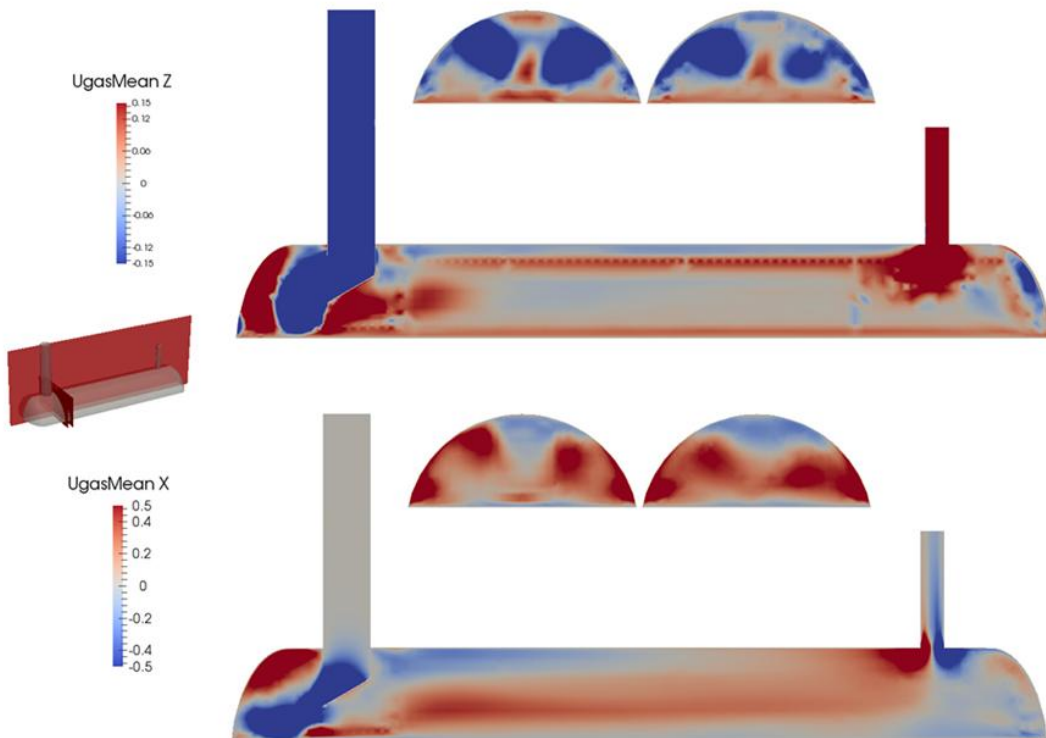


Velocity profiles near the distributor

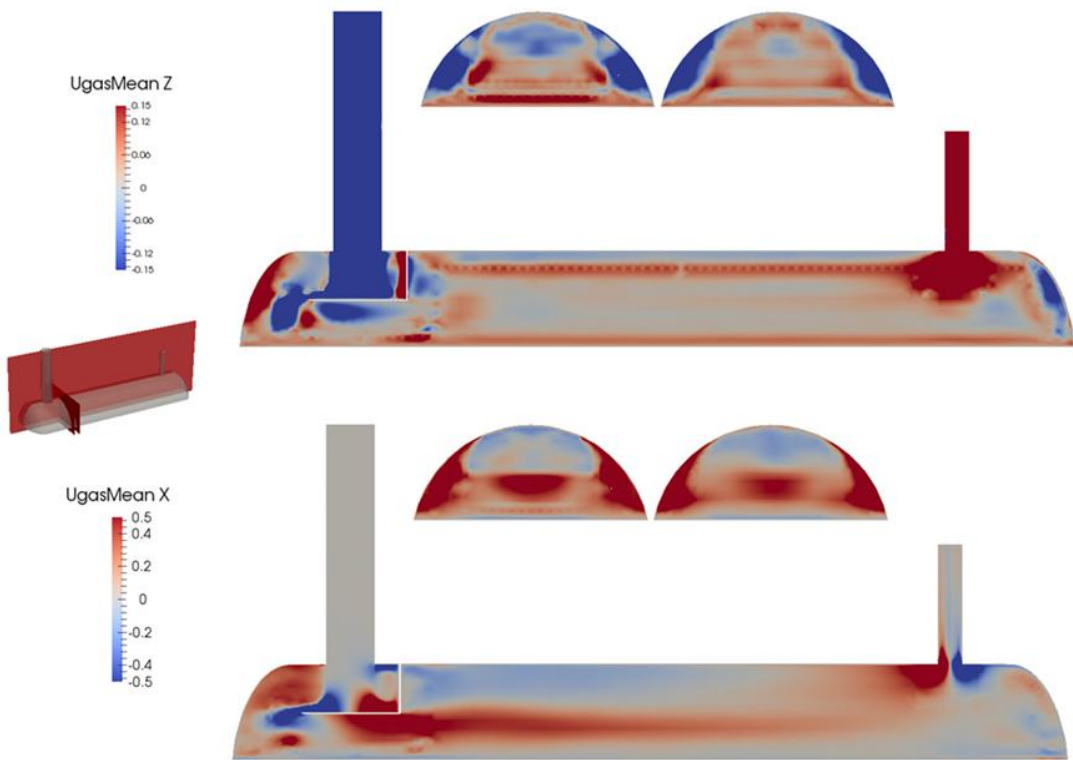
NOID



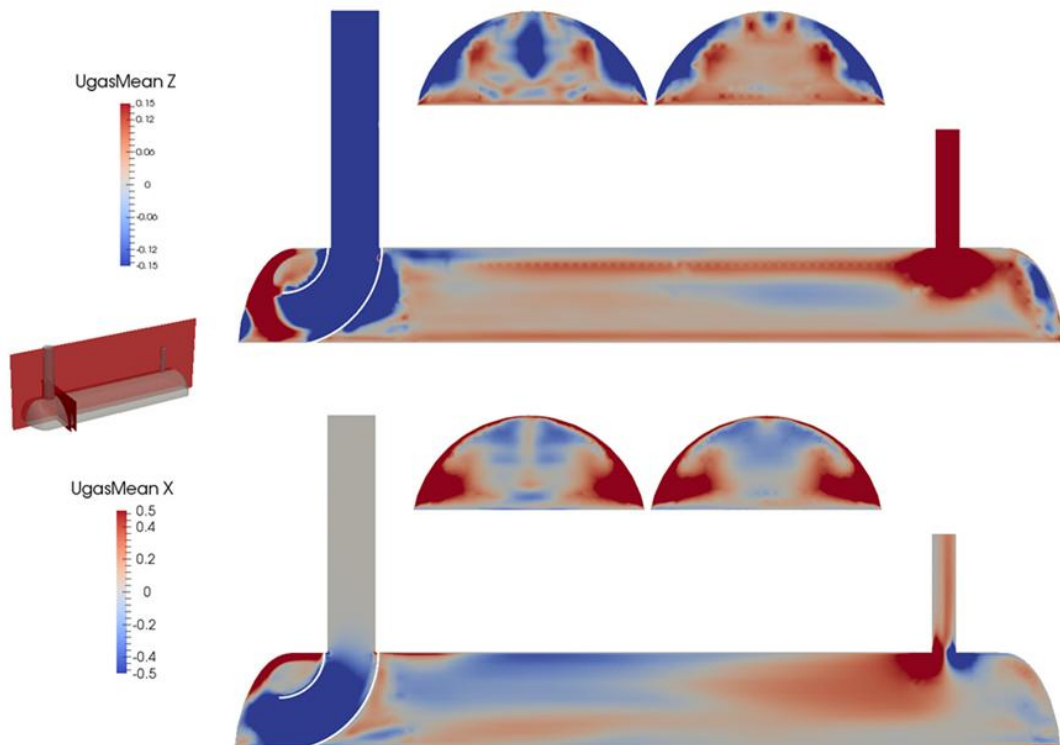
ID1



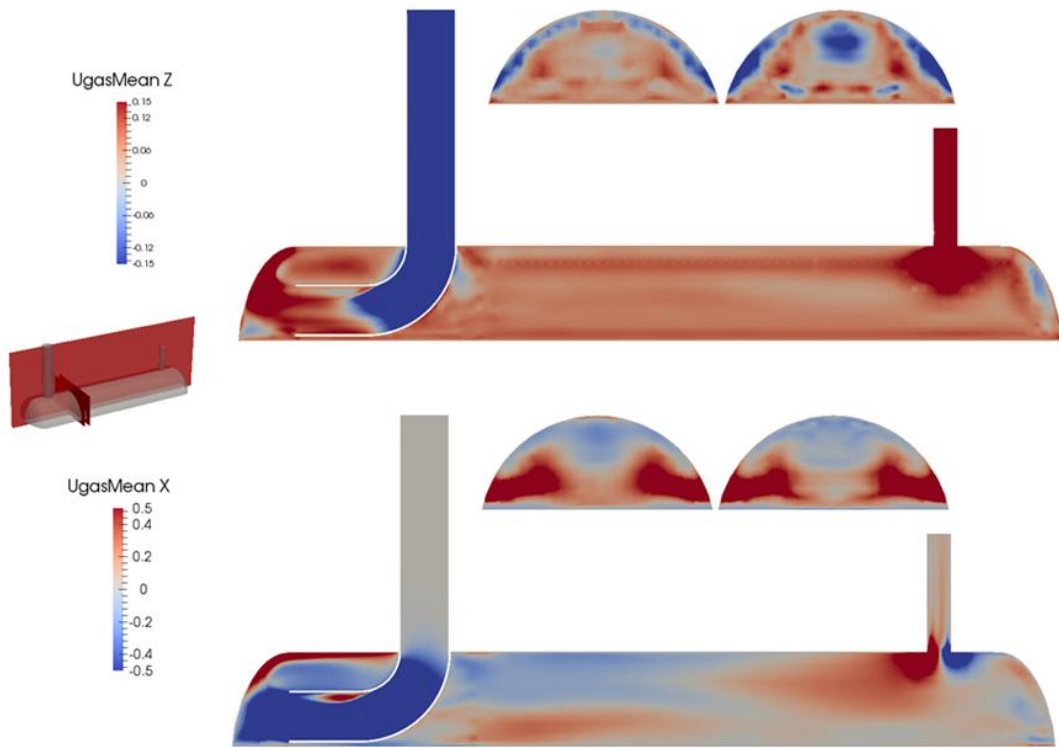
ID2



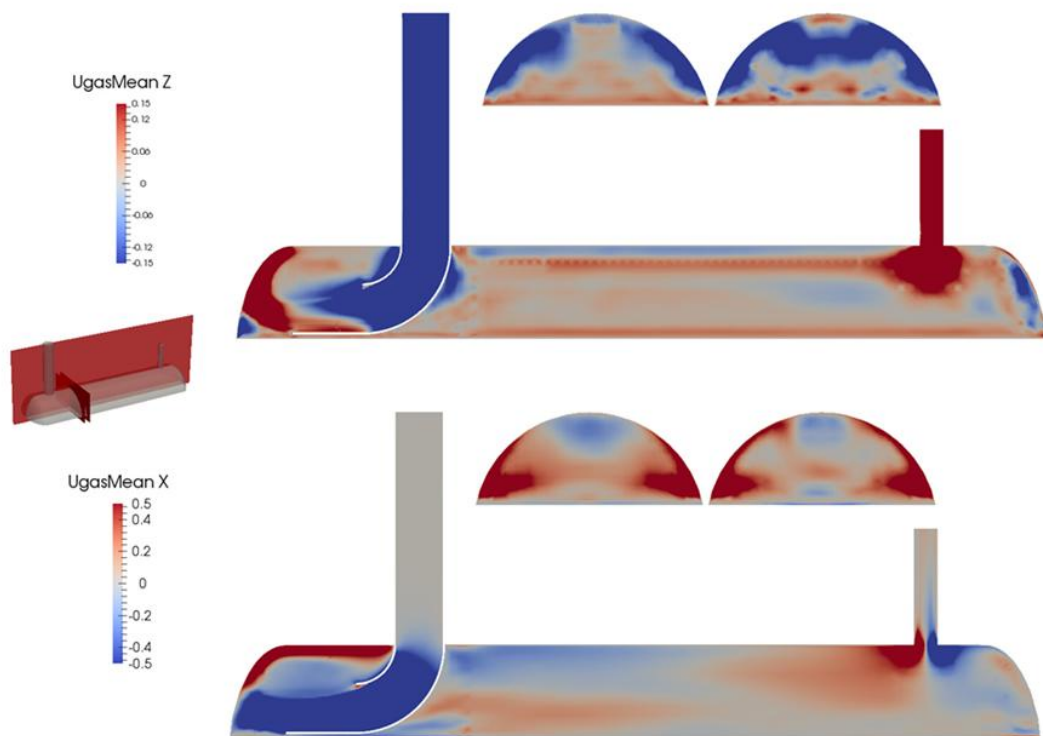
ID3



ID4



ID5



ID4 – Single phase

